The role of host heterochromatin during egress of lytic Herpes Simplex Virus 1

Hannah Claire Lewis

A dissertation

submitted in partial fulfillment of the

requirements for the degree of

Doctor of Philosophy

University of Washington

2022

Reading Committee:

Daphne Avgousti, Chair

Julie Overbaugh

Toshio Tsukiyama

Program Authorized to Offer Degree:

Molecular and Cellular Biology

University of Washington

Abstract

The role of host heterochromatin during egress of lytic Herpes Simplex Virus 1

Hannah Claire Lewis

Chair of the Supervisory Committee:

Daphne Avgousti

Department of Microbiology

The nucleus of a human cell is a crowded molecular environment full of DNA, RNA, and proteins. Viruses that replicate in the nucleus have bountiful access to host cell resources but must contend with existing host chromatin for space to replicate, assemble progeny, and exit from the nucleus. HSV-1 is one such nuclear-replicating virus that expertly manipulates host chromatin to benefit progeny production. In my dissertation studies, I found that HSV-1 lytic infection induces formation of new heterochromatin on host genomes through upregulation and re-localization of macroH2A1 and H3K27me3, marks that are frequently associated with transcriptionally repressed chromatin. Newly formed viral capsids traverse this chromatin maze to reach the nuclear periphery and ultimately exit the cell. When I reduced peripheral heterochromatin in infected cells, I found that capsid escape, or egress, from the nuclear compartment is impaired. My data suggest that HSV-1 maximizes its egress by inducing changes in nuclear architecture to allow capsids

increased access to the nuclear periphery. My work helps illuminate how humans respond to infection by revealing that pathogens use a diverse range of molecular tools within the cell to enhance their replication, even transcriptionally inert heterochromatin.

Table of Contents

Abbreviations

4sU	4-thiouridine
ac	Acetylation
ADP	Adenosine diphosphate
ADPr	ADP-ribose
ATAC-seq	Assay for transposase-accessible chromatin with high-throughput sequencing
ATP	Adenosine triphosphate
ATRX	Alpha-thalassemia X-linked disability syndrome
bp	Base pairs
cDNA	Complementary DNA
CENP-A	Histone H3-like centromeric protein A
ChHV	Panine alphaherpesvirus 3 (also known as chimpanzee herpes simplex virus)
ChIP	Chromatin immunoprecipitation
CTCF	CCCTC-Binding Factor
CUT&Tag	Cleavage under targets and tagmentation
CVSC	Capsid vertex specific component
ddPCR	Droplet digital PCR
dKO	Double knockout
DNA	Deoxyribonucleic acid
dpi	Days post infection
dsDNA	Double stranded DNA
E	HSV-1 early gene class
EBV	Epstein-Barr virus
EM	Electron microscopy
ESCRT-III	Endosomal sorting complex III required for transport
EZH1/2	Enhancer of zeste 1/2
FACT	Facilitates chromatin transcription
FC	Fold-change
FISH	Fluorescence in situ hybridization
GC-content	Guanine-cytosine content
GO	Gene ontology
gRNA	Guide RNA
HCF-1	Host cell factor 1

HCMV	Human cytomegalovirus
HFF	Human foreskin fibroblast
HFF-T	hTERT-immortalized HFFs
hg38	Genome Reference Consortium human genome build 38
HHV	Human herpesvirus
Hi-C	High-throughput chromosome conformation capture
HIRA	Histone regulator A
HIV	Human immunodeficiency virus
HP1	Heterochromatin protein 1
hpi	Hours post infection
HSV	Herpes simplex virus
HSV-1	Herpes simplex virus 1
HSV-2	Herpes simplex virus 2
hTERT	Human telomerase reverse transcriptase
HVEM	Herpesvirus entry molecule (also known as TNFRSF14)
ICP #	HSV-1 infected cell protein
IE	HSV-1 immediate early gene class
IF	Immunofluorescence
IFN	Interferon
IgG	Immunoglobulin G
IR	Internal repeats
INM	Inner nuclear membrane
JMJD2	Jumonji domain 2
kb	Kilobase
KSHV	Kaposi's sarcoma-associated herpesvirus
KO	Knockout
L	HSV-1 late gene class
LAD	Lamin associated domain
LAT	Latency associated transcript
LSD-1	Lysine-specific demethylase 1
LSH	Lymphoid specific helicase (also known as HELLS)
mb	Megabase
me	Methylation
mL	Milliliter

mH2A	macroH2A
mH2A1	macroH2A1.1 and macroH2A1.2
mH2A1.1	macroH2A1.1
mH2A1.2	macroH2A1.2
mH2A2	macroH2A2
MOI	Multiplicity of infection
MNase	Micrococcal nuclease
mRNA	Messenger RNA
µM	Micromolar
µm	Micrometer
NAD+	Nicotinamide adenine dinucleotide (oxidized form)
NADH	Nicotinamide adenine dinucleotide (reduced form)
ND10	Nuclear domain 10 (also known as PML)
NEC	Nuclear egress complex
NF-κb	Nuclear factor kappa B
NGF	Nerve growth factor
NLS	Nuclear localization sequence
nm	Nanometer
NPC	Nuclear pore complex
Oct-1	Octamer-binding protein 1
ONM	Outer nuclear membrane
PAA	Phosphonoacetic acid
PAR	Poly(ADP-ribose)
PARP1	Poly(ADP-ribose) polymerase 1
PARG	Poly(ADP-ribose) glycohydrolase
PCR	Polymerase chain reaction
PELP	Proline-, glutamic acid- and leucine-rich protein 1
PEV	Perinuclear virion
pfu	Plaque-forming units
ph	Phosphorylation
PI3K	Phosphatidylinositol-3-kinase
PKC	Protein kinase C
PML	Promyelocytic leukemia (also known as ND-10)
PolyA	Polyadenylic acid

PRC	Polycomb repressive complex
PTM	Post-translational modification
QKI	Quaking
qPCR	Quantitative PCR
RNA	Ribonucleic acid
RNA Pol II	RNA polymerase II
RNP	Ribonucleoprotein complex
RPE	Retinal pigment epithelial
rRNA	Ribosomal RNA
siRNA	Small interfering RNA
SUV39	Suppressor of variegation 39
SWI/SNF	SWItch/sucrose non-fermentable
TAD	Topologically associating domains
TBP	TATA-binding protein
TEM	Transmission electron microscopy
TET	Tetracycline
TFIID	Transcription factor II D
TNFRSF14	Tumor necrosis factor receptor superfamily member 14 (also known as HVEM)
TR	Terminal repeats
TRIM43	Tripartite motif containing 43
ub	Ubiquitination
UL	Unique long
US	Unique short
VHS	Virion host shutoff
VP #	HSV-1 viral protein
VZV	Varicella zoster virus
WT	Wild type
Xi	Inactive X chromosome
Xist	X-inactive specific transcript
XRCC4	X-Ray Repair Cross Complementing 4

List of Figures

List of Tables

Acknowledgements

This thesis would not have been possible without a metaphorical village of mentors, colleagues, friends, and family supporting me from near and far.

I'd like to start by thanking my incredible advisor, Dr. Daphne Avgousti. The work that I performed over the past 5 years was under her guidance, with her support, and, occasionally, against her advice. But seriously, I am honored to have been her first graduate student. Together, we took a project that started with 3 pieces of data (one of which was an artifact) to places neither of us expected it to go. She truly wants the best for every trainee in her lab. I know that her insight, patience, and optimism will continue to benefit the next generation of scientists.

I am also thankful for my thesis committee, which consisted of Drs. Julie Overbaugh, Toshio Tsukiyama, Keith Jerome, and Michael Lagunoff. Thank you all for contributing your excitement and training expertise to my graduate experience, and also just for being very nice. To Julie and Toshi: thank you for your insightful comments on this dissertation. To Keith: thank you for your co-sponsorship of both of my fellowship applications. And to Michael: thank you for the many letters of recommendation and your infectious passion for virology.

I would like to thank our collaborators who made this work possible. Dr. Srinivas Ramachandran's expertise in chromatin profiling changed the trajectory of the project. Thank you to the staff at the Fred Hutch core facilities, especially Drs. Steve MacFarlane, Caleigh Azumaya, and Julien Dubrulle who were exceptionally helpful.

Thank you to all the current members and alumni of the Avgousti Lab. To Laurel Kelnhofer-Millevolte: thank you for starting team HSV with me and eventually joining this project. It really would not have been possible to complete without your help. I hope you continue to #DoItforBerlin! To Dr. Kelsey Lynch: thank you for your constant support and feedback (given constructively no matter how we felt on the hedgehog cake scale that day). To Robin Kaai, Edward Arnold, Melanie Dillon, Monji Bat-Erdene, Mia Brinkley and Han Arbach; thank you for hearts-to-hearts, happy

hours, cheese spreads, cute animal videos and the self-care advice without which I could not have kept sane and semi-productive throughout the pandemic.

Thank you as well to my previous scientific mentors. To Dr. Matthew Posewitz and Dr. Robert Jinkerson: working with you was the highlight of my undergraduate studies. To Dr. Joaquin Espinosa: you not only inspired a passion for research, but also for communicating this passion to a broad audience. And to Dr. Kelly Sullivan: thank you for taking a chance on me when you hired me as a technician, for all your support getting me to graduate school, and for continuing to root for me/advise me throughout the process. To John Stillian and Dr. Paul Ogg: thank you for inspiring me to pursue this path.

The UW Program in MCB and the Fred Hutch pride themselves on being excellent training environments. This is true, largely due to the efforts of the amazing administrators and support staff. I would like to especially thank the Avgousti Lab administrator Allison Veishlow, the above-and-beyond grad student care from Maia Low (MCB), Denise Barnes (MCB), and Andrea Brocato (Fred Hutch) and give a special shout out to Luna Yu (Fred Hutch) for being a force of nature in both technical and energic support. Thank you to the remainder of the support staff at the Hutch, especially the sanitation staff who were always friendly during our late nights at the lab.

To my graduate school cohort and friends: thank you for talking science with me when I needed it and especially for *not* talking science with me when I needed not to. To Maddie Hart: thank you for inspiring me to embrace my Leo, life-of-the-party, main-character energy and for all the music we experienced together. To Vanessa Montoya: thank you for being my rotation/study/dissertation/job application buddy, always down for coffee or a cocktail (or two).To Amy Spens: thank you for introducing me to new experiences including tiny Amsterdam coffees and for taking care of the kitty and my plants. To Cassidy Danyko: thank you for listening to my million practice talks and talking me down when I was panicking. To my many roommates: thank you for loving my cat as much as I do. To 8-Bit Brass Band, Neon Brass Party, and the Seattle

Honk! community: thank you for helping me pursue that elusive work-life balance and letting me be weird.

Finally, thank you to my family for listening to me practice science communication, nodding diligently whether or not you understood what I was saying, and encouraging me throughout this process. And finally, to Tomato Soup (the cat): you are a snuggly monster and the love of my life.

Dedication

To my grandfather, Dr. Bill Snyder. You are the first academic I ever met and you showed me that the joy of learning, the joy of music, and the joy of life are not mutually exclusive.

Chapter 1. Introduction.

Preamble.

Chromatin is the complex of DNA, RNA, and proteins that winds and packages the long DNA genome of eukaryotic organisms into the nucleus. Far from being a static packaging structure, however, chromatin is a dynamic complex that has roles in many cellular processes including proper segregation of genomes during cell division (Naumova et al., 2013), maintaining genome stability (Peters et al., 2001), and regulating genome accessibility for transcription or replication (Corey L. Smith & Peterson, 2005).

Viruses are obligate intracellular parasites that rely on host factors to produce progeny. Many viruses, especially nuclear-replicating DNA viruses, take advantage of host chromatin to regulate viral gene expression or organize their genomes. Herpes simplex virus 1 (HSV-1) is a ubiquitous pathogen that uses host chromatin factors to activate gene expression during lytic replication or to repress viral transcription during latency. It is crucial to understand how viruses such as HSV-1 commandeer host chromatin to facilitate infection and persistence.

As a preamble to my thesis work on host chromatin dysregulation during lytic HSV-1 infection, I will introduce basics of host chromatin organization, HSV-1 biology, and the state of the field researching the intersections between HSV-1 and host chromatin.

A note on the term epigenetics.

A layer of genetic regulation beyond the DNA sequence is sometimes referred to as epigenetics: the Greek prefix “epi” is translated to “above”, so epi+genetics is interpreted to mean “above+genetics”. However, the implicit meaning of epigenetics is context-dependent. Historically, epigenetics was used to conceptualize cell fate during development (“epigenesis,” which is where the term originates (Waddington, 2012)) or to describe traits that are heritable across cell divisions (Holliday, 1987) summarized in (Greally, 2018). For clarity, I will avoid the term epigenetic entirely.

1.1 Host chromatin organization.

1.1.a The nucleosome: the essential unit of chromatin.

1.1.a.1 Structure of the nucleosome.

The fundamental repeating unit of chromatin is the nucleosome, which consists of a ~147 base pair-long helix of DNA wound 1.65 times around an octamer of histone proteins (Figure 1.1A) (Luger et al., 1997). The four canonical histones are H2A, H2B, H3, and H4, which are highly basic proteins which assemble into a nucleosome core particle that strongly binds negatively charged DNA. Specifically, the nucleosome is formed by tetrameter of two H3 and H4 heterodimers bracketed on each side by two H2A-H2B dimers (Figure 1.1B) (Luger et al., 1997).

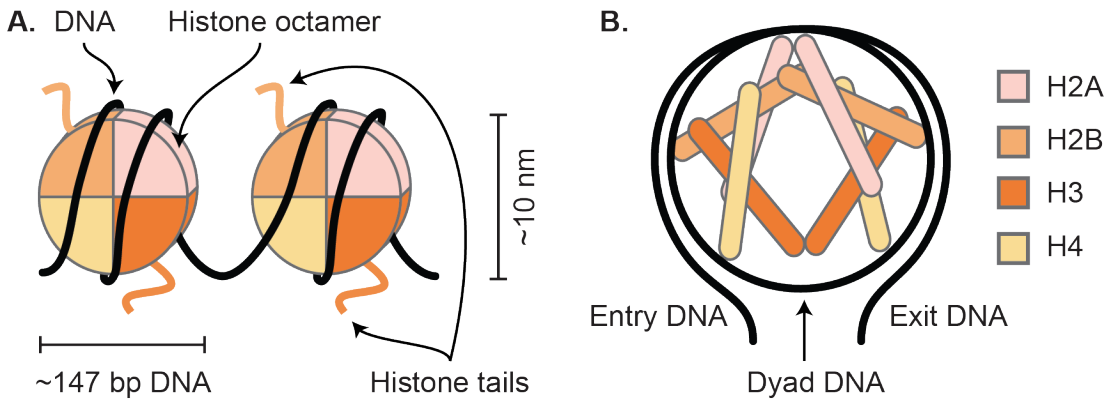

Figure 1.1 Illustrations of the nucleosome core particle.
A. 147 bp of DNA (black line) is wound around two of each histone H2A (pink), H2B (light orange), H3 (dark orange), and H4 (yellow), forming a squat disk-like structure termed the nucleosome. Longer lengths of DNA are organized by repeating nucleosome units, forming a fiber of ~10 nm. Histone tails protrude out of the nucleosome. **B.** Simplified schematic of the nucleosome core structure. Histones are represented as colored bars that show the position of their relative histone fold region. Histone tails are not depicted.

The crucial element of histones that allows for nucleosome assembly is a region called the histone-fold domain: three alpha helices designated α1, α2, and α3 are connected by two loops termed L1 and L2. Histone heterodimers form through a “handshake motif” whereby the L1 loop of one histone aligns with the L2 loop of the other, facilitating strong interactions between the helices (Arents et al., 1991). The histone heterodimer then interacts with host DNA at both two

L1/L2 interfaces and one α1/α1 pair. The histone fold domain is highly conserved across all eukaryotes at the level of tertiary structure (Arents & Moudrianakis, 1995). In addition to the histone fold domain, histones possess highly unstructured N-terminal basic tails that protrude from the nucleosome to interact with other nucleosomes and additional proteins to mediate higher-order folding. Nucleosomes and their tails are subject to a large number of covalent modifications, which I will discuss in section **1.1.a.2**.

During the S phase of cell division, nucleosomes are displaced to allow for DNA replication. After the DNA is copied, both newly synthesized and template strands must be re-packaged into chromatin. As such, the highest demand for histones occurs during replication, and expression of histone genes is tightly coordinated with the cell cycle. Animals possess multiple copies of the four canonical histones in gene clusters that are only transcribed during S phase. In humans, there are 16 genes that encode for histone H2A, 22 genes for H2B, 14 genes for H3, 15 genes for H4, and 6 genes for H1 (Amatori 2021 33827674). Their mRNAs are intron-less and regulated through a unique stem-loop structure at the 3' end rather than a polyadenylated (polyA) tail; this further allows tight expression control at the level of translation (Talbert & Henikoff, 2017). While these genes differ slightly in sequence, the isoforms they encode generally have minimal structural changes (Amatori 2021 33827674). Histones that are incorporated into DNA in a cell cycle-dependent manner are termed canonical histones to differ from those incorporated in a replication-independent manner, or histone variants. I will introduce histone variants in section **1.1.a.3**, focusing on variants found in humans.

Nucleosomes repeat along the DNA strands in fibers described as "beads on a string," where each nucleosome is connected by ~60 base pairs (bp) of DNA (Maeshima et al., 2019; Olins & Olins, 1974). For the genome to fit within the nucleus, higher-order chromatin structures form through folding of these fibers. A fifth histone family, the linker histone H1 and its variants, is one of the factors that facilitates chromatin folding. I will briefly review linker histone H1 and introduce

principles of higher-order chromatin folding in section **1.1.a.4** and will use section **1.1.b** to discuss the biological significance of chromatin architecture.

1.1.a.2 Histone post-translational modifications.

The structure and function of the nucleosome can be profoundly impacted by covalent modifications of histones. Post-translational modifications (PTMs) of many proteins influence structure, function, and stability. In the case of histones, these modifications have far-reaching impacts on DNA compaction and gene expression.

Histone PTMs are often dynamic; they are deposited by “writer” proteins and removed by “eraser” enzymes. Many PTMs have been described including acetylation, methylation, ubiquitylation, phosphorylation, and ADP ribosylation. Short names for modifications follow the convention: histone + residue + modification. For example, trimethylation of histone H3 at lysine (K) 27 is shortened to H3K27me3.

The histone’s most accessible regions to modifying enzymes are their N-terminal tails which protrude out of the nucleosome. Residues within the nucleosome can also be modified (Millán-Zambrano et al., 2022). Modifications can alter interactions of the histones with each other and with the bound DNA to influence local chromatin structure. An example of this is histone acetylation, which was one of the first PTMs discovered (Allfrey et al., 1964). While nucleosomes incorporated into DNA reduce RNA synthesis by 60-75%, Allfrey et al found synthesis decreases to 0-30% when histones are acetylated. This effect occurs due to acetylation decreasing the histone’s positive charge, which electrostatically repels the negative DNA molecule in a process termed DNA breathing (Millán-Zambrano et al., 2022). Hence, histone acetylation is often enriched at active promoters or other accessible genomic regions.

Importantly, histone modifications can impact chromatin structure indirectly. Some PTMs provide a scaffold to effector proteins or chromatin remodelers, termed “readers”. Others prevent binding of specific effector proteins. For example, HP1 (heterochromatin protein 1) binds

H3K9me3 and interacts with the H3K9me3 writer, methyltransferase SUV39 (suppressor of variegation 39), to positively influence H3K9me3 deposition in the surrounding genomic region. During mitosis, the serine adjacent to H3K9 is phosphorylated. This H3S10ph mark displaces HP1 binding and prevents additional methylation, ending the H3K9me3 deposition feedback loop (Fischle et al., 2005).

Many PTMs have been studied in isolation as either “activating” or “repressive” marks. However, PTM combinations in the same region can alter the properties of each mark, as evidenced by the methylation-phosphorylation (methyl-phospho) switch described above. Termed the “histone code”, the combinatorial impact of histone modifications expands the functional repertoire of the genome beyond the DNA sequence (Jenuwein & Allis, 2001).

1.1.a.3 Histone variants.

Histone variants are defined as proteins with high degree of homology to canonical histones that incorporate into chromatin independent of DNA replication. Replacement of canonical histones by histone variants can alter nucleosome properties as well as interactions with chromatin-modifying enzymes. Ultimately, this has profound consequences for gene expression, DNA compaction, and replication.

Regulation of histone variant expression is different than from the cell-cycle dependent canonical histones. Most histone variants are encoded separately from the clusters of canonical histone genes and incorporated into the genome by specialized proteins. Many are polyadenylated and some contain introns, which further increases variant diversity through splice isoforms (Buschbeck & Hake, 2017). While many histone variants are expressed to some degree in somatic tissues, others are germline-specific (Talbert & Henikoff, 2021). Tissue- and temporally-specific expression of histone variants allows for each variant to have a specialized function and impact on the chromatin landscape.

In humans, H2A and H3 have the largest numbers of variants. Some testis-specific H2B variants and one H4 variant, which is typically expressed at low levels but overexpressed in cancer, have also been discovered (Talbert & Henikoff, 2021). While some are highly similar to canonical histones, others are highly divergent; for example, variant H3.3 differs from canonical H3.1 by 4 amino acids while CENP-A (histone H3-like centromeric protein A) only has 48% homology to canonical H3.1 (Sullivan et al., 1994).

Many histone variants are enriched in specific genomic regions according to their function. For example, CENP-A localizes to highly repetitive DNA where it nucleates the formation of centromeres (Sullivan et al., 1994). Exchange of canonical histones for histone variants is mediated by chaperone proteins, whereas general chromatin remodelers can either promote incorporation of or evict histone variants. Histone chaperone HIRA (histone regulator A) deposits H3.3 on naked DNA as part of a nucleosome “gap filling” mechanism (Ray-Gallet et al., 2011). Chromatin remodeler ATRX (Alpha-thalassemia X-linked disability syndrome) also promotes H3.3 incorporation into heterochromatin (Buschbeck & Hake, 2017) but negatively regulates H2A variant macroH2A enrichment at heterochromatin regions (Jeongkyu Kim et al., 2019; Ratnakumar et al., 2012).

Histone variants can also be post-translationally modified to alter their localization and function. H2A variant H2A.X is phosphorylated at its C-terminal domain, which is a few amino acids longer than canonical H2A, in response to DNA damage. It then forms transient puncta around areas of DNA damage that can be up to several hundred kilobases (kb) long (Talbert & Henikoff, 2014).

1.1.a.4 Linker histone H1 and higher-order chromatin folding.

The beads on a string structure discussed in section **1.1.a.1** is also known as the 10 nm fiber. In this conformation, the negative charge of the DNA is not fully neutralized even though it is wound in repeating units of highly positively charged histones. Importantly, this remaining charge

results in electrostatic repulsion between 10 nm fibers. Additional factors must quench these charges; this can be mediated by contacts between linker proteins, nucleosome tails, or other positively charged molecules (Maeshima et al., 2019).

Linker histone H1 is one such factor that further condenses DNA through acting outside of the nucleosome core. The globular domain of H1 binds the dyad axis of the nucleosome and interacts with an additional 10 base pairs of DNA exiting or entering the nucleosome (Zhou et al., 2015). When H1 proteins are bound in array across multiple nucleosomes, H1 dimerizes to bring the chromatin into a condensed zig-zag arrangement (Fyodorov et al., 2018).

In vitro, 10 nm fibers in solution with linker proteins spontaneously fold into higher order structures called 30 nm fibers. However, little evidence has shown the existence of 30 nm fibers in cells. Instead, it is thought that multiple nucleosomes aggregate together in irregularly-folded structures termed “clutches” (Ricci et al., 2015).

1.1.b Histone variant macroH2A.

1.1.b.1 MacroH2A family.

By far the largest histone, macroH2A is almost three times the size of canonical H2A. The histone fold domain shares approximately 64% amino acid similarity to canonical H2A (Pehrson & Fried, 1992). A large C-terminal non-histone domain, termed the macrodomain, is connected to the histone fold domain by a flexible linker region (Figure 1.2A). Vertebrates express three different macroH2A proteins (Figure 1.2B): macroH2A1.1 and macroH2A1.2 arise from alternative splicing of the *MACROH2A1* gene (Figure 1.2C) (Pehrson & Fried, 1992), and macroH2A2 is encoded by separate gene *MACROH2A2* (Costanzi & Pehrson, 2001).

Although initially considered to be vertebrate-specific, recent identification of macroH2A in many invertebrates and even pre-metazoan single-celled protist *Capsaspora owczarzaki* indicates that macroH2As evolved earlier than previously believed (Rivera-Casas et al., 2016).

For yet-unknown reasons, macroH2As were lost from several invertebrate lineages such as *Drosophila melanogaster* and *Caenorhabditis elegans* (Guberovic et al., 2021).

The most unique feature of macroH2As is their non-histone macrodomain. Macrodomains are evolutionarily conserved globular structures that are found in proteins from all domains of life as well as some viruses (Pehrson & Fuji, 1998). Macrodomains bind NAD+ metabolites and are key players in ADP ribose signaling pathways. Humans encode at least 17 proteins that contain macrodomains (Rack et al., 2015), but macroH2As are unique as they link chromatin structure to metabolic sensing.

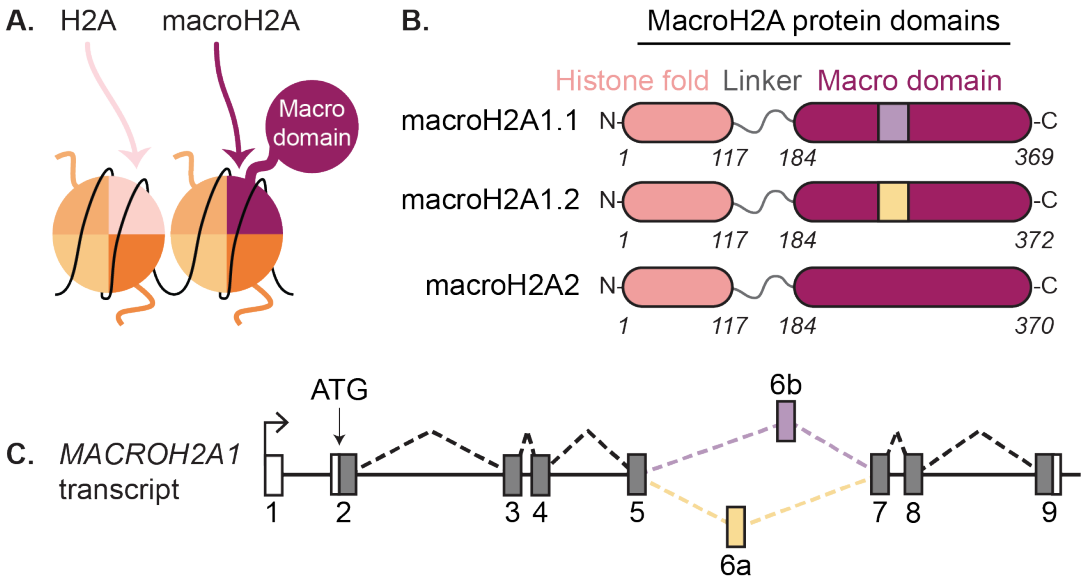

Figure 1.2 The macroH2A family of histone variants.

A. MacroH2A1 (magenta) substitutes for H2A (light pink) within nucleosomes. The macrodomain is thought to protrude from the nucleosome. **B.** Schematic representation of the three human macroH2A proteins. Each has a tripartite structure consisting of a histone-fold domain (pink), a flexible linker (grey), and a large macrodomain (magenta). The numbers refer to the amino acid number in the linear sequence. **C.** Alternative splicing of the *MACROH2A1* transcript leads to isoforms macroH2A1.1 and macroH2A1.2 through mutually exclusive exons 6b (purple) and 6a (yellow), respectively.

1.1.b.2 Properties of macroH2A-containing nucleosomes.

Despite the large size of macroH2A, the general structure of macroH2A-containing nucleosomes is similar to that of canonical nucleosomes. The macrodomain is thought to protrude from the nucleosome and is not itself wound by DNA. Evidence for this model is that macroH2A-

containing nucleosomes protect an equivalent amount of DNA from micrococcal nuclease (MNase) digestion as canonical nucleosomes (Changolkar & Pehrson, 2002). Crystallographic studies of macroH2A-containing nucleosomes confirm this observation (Chakravarthy et al., 2005).

However, differences between the sequence of the macroH2A histone fold domain and the H2A histone fold lead to differences in nucleosome stability. It is thought that nucleosomes containing macroH2A are more stable in the absence of DNA because of a 4-amino acid difference in the L1 loop of the histone fold domain that is the only place of contact between H2A-H2B dimers (Chakravarthy et al., 2005). This holds true in homotypic nucleosomes (those with two macroH2A-H2B dimers) and heterotypic (one macroH2A-H2B dimer and one H2A-H2B dimer). MacroH2A preferentially forms heterotypic nucleosomes, which are more resistant to H2A-H2B dimer exchange (Chakravarthy & Luger, 2006). Recent molecular modeling has suggested that heterotypic macroH2A/H2A nucleosomes are more stable than homotypic macroH2A/macroH2A, H2A/H2A, or H2AZ/H2Az nucleosomes (Bowerman et al., 2019; Bowerman & Wereszczynski, 2016). In addition, the linker domain of macroH2A increases compactions of mononucleosome arrays and has been suggested to function similarly to H1 to form higher-order chromatin structures (Chakravarthy et al., 2012). Although this property of the linker region is lost *in vitro* when the macrodomain is present (Chakravarthy et al., 2012), studies in cell culture have shown that full-length macroH2A causes chromatin compaction both in steady-state conditions and in response to DNA damage (Kozlowski et al., 2018).

This increased stability has the consequence of impairing nucleosome remodeling by ATP-dependent remodeling complexes. In particular, macroH2A-containing nucleosomes were initially suggested to resist efficient SWI/SNF remodeling (Angelov et al., 2003). More recent studies have contradicted this result; while SWI/SNF preferentially remodels H2A-containing nucleosomes in direct competition assays, macroH2A-containing nucleosomes are still bona fide substrates for SWI/SNF activity (Evelyn Y. Chang et al., 2008). Still, the consensus is that the increased stability

of macroH2A-containing nucleosome contributes to transcriptional repression (Doyen et al., 2006). In addition, nucleosomes containing full-length macroH2A inhibit transcription factor NF-κb binding both *in vitro* (Angelov et al., 2003) and in cells (Agelopoulos & Thanos, 2006). This may be due to steric hindrance of the macrodomain, and may further contribute to macroH2A's role in transcriptional regulation.

1.1.b.3 Transcriptional regulation and genomic localization.

MacroH2A is a marker of transcriptional repression but can positively regulate gene expression in certain contexts. In addition to its stabilization of nucleosomes, macroH2A can interact with other repressive complexes such as PRC2 (Buschbeck et al., 2009), histone deacetylases (Chakravarthy et al., 2005), and PELP (Proline-, glutamic acid- and leucine-rich protein 1) (Hussey et al., 2014). MacroH2A is often found in broad regions of the genome co-associated with marks of transcriptional repression H3K27me3 or H3K9me3 (Buschbeck et al., 2009; Douet et al., 2017; Gamble et al., 2010). MacroH2A double knockout (dKO) leads to elevated expression of retroviral elements in mice and repeat regions in human cell lines (Changolkar et al., 2008; Douet et al., 2017). In zebrafish embryos, macroH2A dKO leads to faster induction of certain developmental genes and causes developmental defects (Buschbeck et al., 2009). Two different roles of macroH2A transcriptional repression have been proposed: one to maintain constitutively silenced genes, and one to aid in temporal gene regulation.

Soon after its discovery, macroH2A was found to be concentrated on the inactive X chromosome (Xi) (Costanzi & Pehrson, 1998). Its histone fold domain and macrodomain are both sufficient for targeting to the X chromosome (Chadwick et al., 2001; Nusinow et al., 2007). This led to the idea that macroH2A is involved in transcriptional repression of the inactive X. However, several lines of evidence suggest that macroH2A is not necessary or sufficient for X inactivation. MacroH2A localizes to the X chromosome after inactivation has been initiated by long non-coding RNA Xist (Mermoud et al., 1999; Rasmussen et al., 2000). MacroH2A loss only leads to Xi re-

activation if DNA demethylases and histone deacetylatases are also inhibited (Hernández-Muñoz et al., 2005), suggesting that macroH2A is one of many redundant mechanisms for X chromosome silencing. Further evidence for this is that embryonic stem cells lacking macroH2A still have X inactivation and differentiate under normal culture conditions (Tanasijevic & Rasmussen, 2011).

It was later shown that macroH2A is found on autosomes as well as the inactive X, occupying about 10% of the genome (Gamble et al., 2010). Although largely depleted from transcriptionally active genes, macroH2A is not exclusively repressive and can protect some target genes from silencing (Changolkar et al., 2010; Changolkar & Pehrson, 2006; Gamble et al., 2010). Recent studies have revealed that macroH2A has context-specific impacts on transcription depending on its chromatin environment. When found in regions that also contain H3K27me3 or H3K9me3, macroH2A1 tends to repress gene expression (Figure 1.3) (Buschbeck et al., 2009; Douet et al., 2017). MacroH2A1 and macroH2A2 have also been found to be enriched at regions associated with the nuclear lamina, where transcription is largely silenced (Douet et al., 2017; Fu et al., 2015). However, when associated with certain H2B acetylations (K12ac, K120ac, K15ac, and K20ac), macroH2A1 can positively or negatively impact gene expression (Figure 1.3) (Hongshan Chen et al., 2014). While multiple regions of macroH2A are sufficient for targeting to H3K27me3-marked chromatin, the carboxyl-terminal half of the histone fold domain is required for macroH2A deposition into containing H2B-acetylated chromatin (Ruiz & Gamble, 2018).

Adding to this complexity are the different functions of the three macroH2A proteins: macroH2A1.1 interacts with transcription factor PARP-1 through binding metabolites that macroH2A1.2 and macroH2A2 cannot. This macroH2A1.1/PARP-1 axis has been shown to be important for oncogene-induced senescence gene expression in primary cells (Hongshan Chen et al., 2015). Recently, it was shown that macroH2A1.1 helps stimulate expression of genes where Pol II is paused (Recoules et al., 2022). A model has been proposed suggesting that macroH2A functions to suppress transcriptional “noise” in response to cellular perturbations (Lavigne et al., 2015).

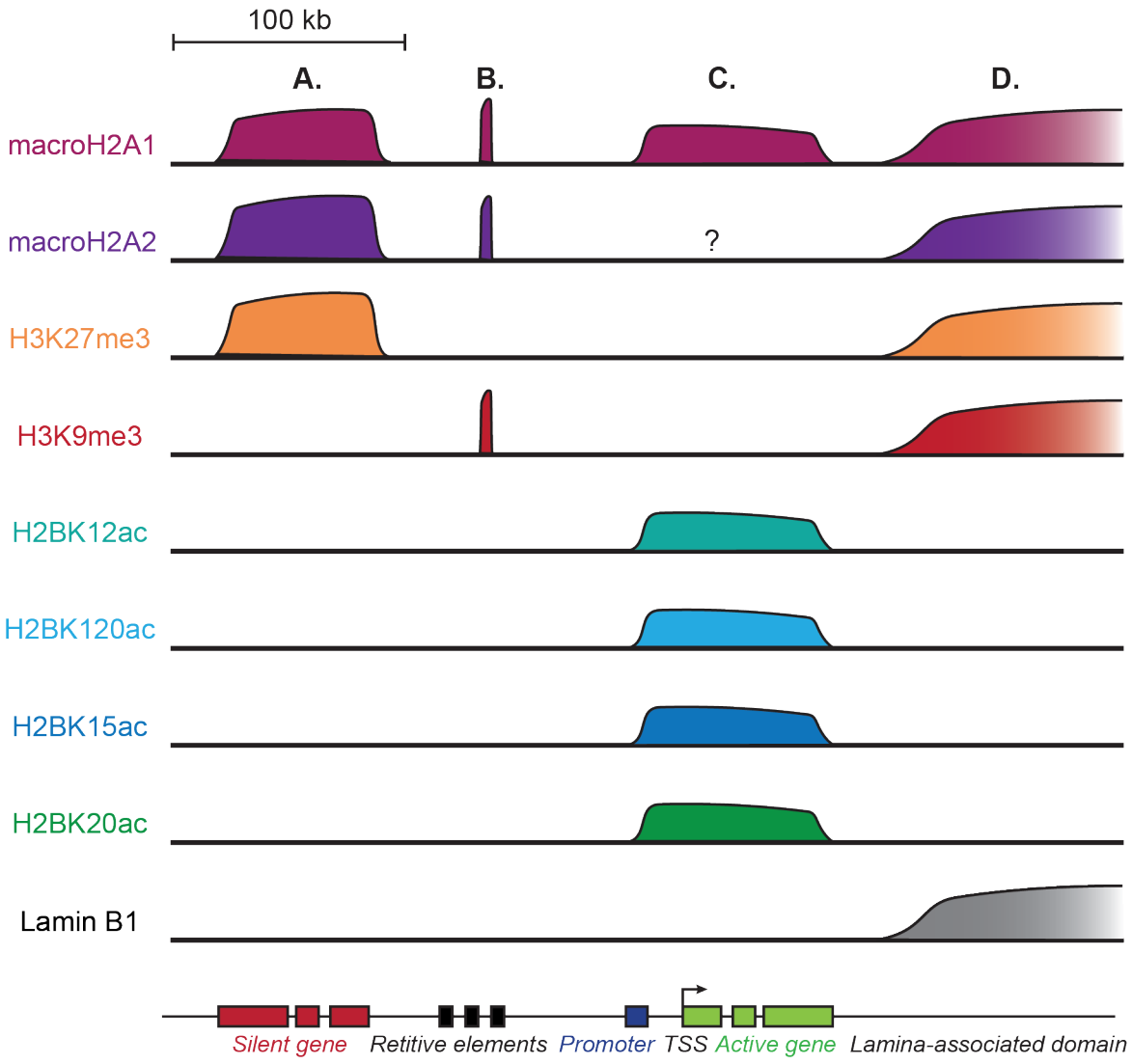

Figure 1.3 MacroH2A is enriched in different chromatin environments with context-specific roles. *Summary cartoon of ChIP-seq and DamID findings from multiple publications.* **A.** MacroH2A1 (magenta) and macroH2A2 (purple) co-localize with H3K27me3 (orange) in broad domains on the linear genome, where they contribute to gene repression. **B.** MacroH2A1 and macroH2A2 co-localization with H3K9me3 (red) but not H3K27me3 forms constitutive heterochromatin to silence repetitive elements. **C.** MacroH2A1 localizes to H2B acetylated chromatin (greens and blues), where it is associated with transcriptional activation. It is not yet known whether macroH2A2 localizes to H2B acetylated regions. **D.** Co-localization of megabase-sized domains of macroH2A1, macroH2A2, H3K27me3 and H3K9me3 occurs at lamina-associated domains (grey).

Mechanisms of macroH2A deposition. The chaperone for macroH2A was only recently discovered (Ni et al., 2020; Ni & Muegge, 2021). LSH (Lymphoid specific helicase, also known as

HELLS) belongs to the SNF2 family of ATP-dependent chromatin remodelers and has been shown to specifically induce macroH2A1.1 and macroH2A2 deposition into chromatin in an ATP-dependent manner (Ni 2021). LSH deletion reduces macroH2A incorporation at repeat sequences, which leads to increased expression of repetitive elements (Ni et al., 2020).

Multiple negative regulators of macroH2A have been identified. In particular, macroH2A is removed from regions of active transcription by FACT (FAcilitates Chromatin Transcription) in a process termed transcription-associated pruning (Sun et al., 2018). Interestingly, FACT can also promote macroH2A incorporation at fragile regions during replicative stress (Jeongkyu Kim et al., 2018). MacroH2A enrichment is negatively regulated by ATM and ATRX (Hongshan Chen et al., 2015; Ratnakumar et al., 2012)

MacroH2A position and function can also be impacted by post-translational modifications. Ubiquitination at K115 and K116 is required for its deposition at the Xi (Ogawa et al., 2005). In contrast, phosphorylation at S137 increases during cell division and leads to macroH2A exclusion from the X chromosome (Bernstein et al., 2008).

1.1.b.4 MacroH2A1 has diverse physiological functions.

MacroH2A functions during development and induced pluripotency. The expression of macroH2A1 varies between different developmental stages and tissue types. Expression of macroH2A1.1 and macroH2A1.2 is low in mouse embryonic stem cells and, in general, increases in differentiated cells (Barrero et al., 2013; Pehrson et al., 1997). Some studies have reported macroH2A loss leading to developmental defects in mouse stem cells, human stem cells, and zebrafish embryos (Barrero et al., 2013; Buschbeck et al., 2009; Creppe et al., 2012). However, mice lacking both macroH2A1 and macroH2A2 are viable and fertile, despite overall reduced size and some metabolic issues (Pehrson et al., 2014). This suggests that macroH2A is not essential for early development, although its presence has been suggested to fine-tune developmental expression programs (Buschbeck et al., 2009).

If macroH2A levels generally correspond with differentiation, then it is logical that macroH2A functions to repress pluripotency. Several studies have indicated that macroH2A loss is required to re-induce expression of pluripotency genes (Gaspar-Maia et al., 2013; Pasque et al., 2012).

MacroH2A is a tumor suppressor. Consistent with a role in differentiation and proliferation, macroH2A1 expression is dysregulated in several cancers. In melanomas, macroH2A loss is associated with malignancy and metastasis (Kapoor et al., 2010). In lung cancer, lower levels of macroH2A1.1 and macroH2A2 predict cancer recurrence (J C Sporn et al., 2009). MacroH2A1 knockdown in bladder cancer promotes stem-like activity (S. J. Park et al., 2016).

Cellular senescence is one mechanism by which organisms prevent oncogenic transformation of aged cells (Narita et al., 2003). MacroH2A localizes to large foci formed during senescence (Zhang et al., 2005). The macroH2A1.1 isoform is particularly important for a full senescence program (Hongshan Chen et al., 2015). It has been suggested that loss of specifically macroH2A1.1 allows cells to bypass senescence and become oncogenically transformed.

The ratio of macroH2A1 isoforms has also been shown to be important for oncogenesis and malignancy. MacroH2A1.2 is massively upregulated in hepatocellular carcinoma (Rappa et al., 2013). Mis-splicing of macroH2A1 leads to altered macroH2A1.1/macroH2A1.2 ratios in testicular, lung, bladder, cervical, breast, colon, ovarian, and endometrial cancers (Novikov et al., 2011; Judith C. Sporn & Jung, 2012). Splicing dysregulation promotes invasion of mouse tumors through upregulation of macroH2A1.2 and downregulation of macroH2A1.1 (Dardenne et al., 2012). Rescuing the ratio of macroH2A1.1/macroH2A1.2 through re-expression of splicing factor QKI inhibits gastric carcinoma cell proliferation, migration, and invasion in cell culture and *in vivo* (Feng Li et al., 2015). MacroH2A1.1 overexpression also attenuates prostate cancer malignancy phenotypes in cell culture (Vieira-Silva et al., 2019).

MacroH2A functions in metabolism and DNA damage. ADP-ribose (ADPr) is a derivative of NAD+ that can be added onto proteins as both as a monomer or polymer (poly-ADP ribose,

abbreviated as PAR). Proteins with macrodomains are key players in ADP ribose signaling as they can usually bind ADPr and derivatives including PAR (Rack et al., 2015). However, of the three macroH2A proteins expressed by vertebrates, only macroH2A1.1 can bind ADPr ligands (Kustatscher et al., 2005).

Protein ADP-ribosylation is perhaps most relevant to macroH2A1.1 in the context of DNA damage. Nicked DNA leads to activation of poly-ADP ribose polymerase 1 (PARP-1), which produces PAR chains to recruit DNA repair proteins. MacroH2A1.1 moves to sites of activated PARP-1, where its macrodomain binds PAR (Timinszky et al., 2009). Later during the damage response, macroH2A1.2 or macroH2A2 also move to sites of DNA damage (Kozlowski et al., 2018).

It is thought that macroH2As function to aid in DNA repair in two ways. First, macroH2A1.1 binding to PAR chains caps them to prevent their degradation and subsequent turnover by PARP-1. Preventing PARP-1 overactivation is important to promote cell survival after DNA damage (Ruiz et al., 2019). PARP-1 is a major consumer of NAD+ in the nucleus, which can ultimately lead to NAD+ deficiencies in mitochondria and decrease cellular respiration. The PAR-biding macroH2A1.1 isoform is essential for optimal mitochondrial function (Marjanović et al., 2017).

Second, the presence of any of the three macroH2A proteins compacts chromatin through the linker domain, which prevents DNA relaxation necessary for DNA repair (Kozlowski et al., 2018). MacroH2A1 accumulates at double-stranded breaks or common sites of replicative stress, such as telomeres or the late-replicating inactive X chromosome (Khurana et al., 2014; Jeongkyu Kim et al., 2018; Sebastian et al., 2020). Whereas macroH2A1.1 promotes DNA repair through end-joining mechanisms, macroH2A1.2 promotes the repair through the higher-fidelity homologous repair pathway (Sebastian et al., 2020).

1.1.c Beyond the nucleosome: Heterochromatin and nuclear organization.

The concept of genomic regions having different compaction and gene density is almost a century old. In 1928, Emil Heitz observed that different areas of chromosomes remain cytogenetically stained or become invisible depending on the cell cycle stage. He proposed the term “heterochromatin” for regions of chromosomes that remain visible until interphase or remain visible during interphase in the case of some model organisms. For regions that decondense and loose stain during telophase, he proposed the term “euchromatin”. Heitz also predicted “euchromatin is genicly active, heterochromatin genicly passive” (Trojer & Reinberg, 2007).

Remarkably, these initial observations made without molecular tools, sequencing, or advanced imaging techniques have withstood the test of time. Today, heterochromatin is characterized as regions of the genome that are replicated late during the cell cycle (Lima-de-Faria & Jaworska, 1968), resistant to MNase digestion, and generally more compact than other regions (Haws et al., 2022).

Compacted DNA can be viewed directly through transmission electron microscopy: euchromatic regions are lightly stained whereas are heterochromatic regions are electron dense and are typically found around the nuclear rim and nucleolus (Figure 1.4) (Bruni & Porter, 1965). This compacted state is proposed to exclude transcription factors, resulting in downregulation of genes found in heterochromatic regions. Studies in position effect variegation in *Drosophila melanogaster* were the first to describe a role in gene silencing; when a gene is rearranged from a euchromatic region to a heterochromatic or “inert” region, gene transcription is lost (Schultz, 1936). In addition to its role in transcriptional repression, heterochromatin guards the integrity of the genome through repressing repetitive elements and providing a crucial nuclear organization through higher-order folding.

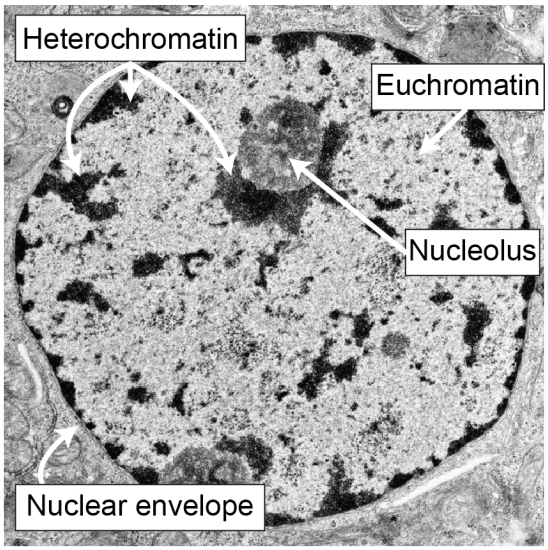

Figure 1.4 Transmission electron microscopy image of a eukaryotic nucleus.
The nuclear envelope is a double membrane structure that compartmentalizes chromatin. The nucleolus is indicated as a large, dense, circular structure. Heterochromatin stains darkly due higher electron density, where euchromatin is lighter. Heterochromatin is enriched around the periphery and nucleolus. Image adapted from the Yale Medical Studies Histology Image Gallery.

1.1.c.1 Types of heterochromatin.

Heterochromatin is molecularly classified into two subtypes according to genomic location and enrichment of factors such as histone PTMs, histone variants and DNA modifications. “Constitutive” heterochromatin refers to regions of the genomes that are almost always transcriptionally silent. The majority of constitutive heterochromatin commonly forms at highly repetitive regions such as telomeres, pericentromeres, and other elements called satellite regions. Gene-poor telomeric and pericentromeric repeat regions are critical loci to maintain genome integrity, as aberrant lengthening or recombination can lead to abnormal cell function and diseases such as cancers (Saksouk et al., 2015). Satellite regions are not structural components but can be comprised of selfish genetic elements like transposons and retrotransposons. Constitutive heterochromatin is marked by global histone hypoacetylation, DNA methylation, H3K9me2/3, and HP1 (Saksouk et al., 2015).

“Facultative” heterochromatin, in contrast, retains the potential to switch to a euchromatic state. Facultative heterochromatin can decondense and allow transcription in temporally or developmentally dependent contexts. Thus, regions of facultative heterochromatin are different between cell types and may be “poised” to respond to stimuli. The definitive marker of facultative heterochromatin is H3K27me3, which is written and read by the Polycomb repressive complexes

(PRC2 and PRC1, respectively). The canonical model is that PRC2 component protein EZH2 (Enhancer of zeste 2 Polycomb repressive complex 2 subunit) catalyzes H3K27 di- and tri-methylation. A chromodomain-containing protein in PRC1 then binds H3K27me2/3 to repress transcription through chromatin compaction and monoubiquitylation of H2AK119 (Wiles & Selker, 2017). However, H3K27me3-mediated transcriptional repression can still occur in organisms lacking PRC1, and cells knocked out for PRC2 do not have altered H2AK119ub patterns (Entrevan et al., 2016). Recently, PRC2 have been implicated in longer distance chromatin connections such as chromatin looping.

1.1.c.2 Heterochromatin and genome architecture.

It is increasingly appreciated that gene regulation does not occur only over local linear stretches of DNA but can be profoundly impacted by long-distance contacts. Consequentially, characterizing the three-dimensional (3D) genome has become a new area of intense interest. These studies have been possible due to technological advances in imaging and sequencing that have allowed visualization of how chromatin folds and forms regions of activation or repression. In particular, the combination of chromosome conformation capture technologies, first developed in 2002 (Dekker 2002 11847345), with high-resolution sequencing has allowed for genome-wide maps of chromatin contacts to be built. This technique, termed Hi-C, has revealed many topographical features of the genome (Lieberman-Aiden et al., 2009).

Although chromosomes decondense post-mitosis, they do not randomly intermingle in the nucleus as 10 nm fibers. Instead, chromosomes tend to occupy specific regions within the nucleus, termed “chromatin territories” (Cremer & Cremer, 2010). Using chromosome painting to compare territories of gene-poor chromosome 18 and gene-rich chromosome 19, Croft et al. found that chromosome 19 is more diffuse and localizes to nuclear interior more than chromosome 18 (Croft et al., 1999). This general pattern was then found to be true for all human

chromosomes: regardless of size, gene-poor chromosomes tend to localize to the nuclear periphery and have less diffuse territories (Boyle et al., 2001).

It has since been established that heterochromatin at the nuclear periphery performs a crucial structural role by tethering the genome to the nuclear envelope. This is mediated through direct chromatin interactions with the nuclear lamina. The genomic regions that are involved in this tethering are termed lamina associated domains (LADs) and are enriched with constitutive heterochromatin elements such as H3K9me2/3 (Kind et al., 2013). Interestingly, macroH2A has also been found to be enriched in LADs, and loss of macroH2A leads to lamina disruption and global heterochromatin loss (Douet et al., 2017; Fu et al., 2015).

Hi-C experiments show that contacts preferentially form within the same chromosomes rather than between different chromosomes (Lieberman-Aiden et al., 2009). Inter-chromosomal contacts do occur, and this has been proposed to have a role in regulating gene expression. Compartmentalizing active or repressive regions could lead to areas with high concentration of regulation machinery, or “hubs”. Through imaging and recent sequencing techniques both repressive and activating hubs have been found at nuclear speckles and the nucleolus (Quinodoz et al., 2018).

At a 1-megabase (Mb) resolution, correlation matrices from Hi-C data show a plaid pattern of long-range interactions. Using these data, the nucleus is partitioned broadly into two spatial compartments: the A compartment correlates with euchromatic regions while the B compartment correlates with transcriptionally repressed heterochromatin. The A and B compartments can be further subdivided when viewed at a 1-kb resolution (Rao et al., 2014). The sub-compartments have consistent histone PTM profiles; some were enriched in euchromatin marks, others were enriched for heterochromatin marks such as H3K27me3 or H3K9me3. This result is consistent with the idea that chromatin context can impact genome organization and gene regulation.

1.2 Herpes simplex virus 1.

1.2.a HSV taxonomy.

Herpes simplex viruses belong to a large family of double stranded DNA (dsDNA) viruses called *Herpesviridae* in the order *Herpesvirales* (Davison et al., 2009). Viruses in the order *Herpesvirales* are classified by unique morphological features: a large linear dsDNA genome of 125-290 kb pairs is packaged within an icosahedral capsid, which is surrounded by a proteinaceous matrix called the tegument and enveloped by a lipid membrane with viral glycoproteins on the surface (Davison et al., 2009). Because of this classification scheme, many divergent viruses are grouped into the order *Herpesvirales* with a large range of hosts including mammals, birds, reptiles, fish, frogs, and bivalves. Viruses in this order are only tenuously genetically related and there is conservation of only one herpesvirus-specific protein across all members: the putative ATPase subunit of the terminase complex which packages virus DNA into nascent capsids, which is conserved only at the amino acid level (Davison et al., 2009; McGeoch et al., 2006; Rakus et al., 2013). Using phylogenetics, the order *Herpesvirales* was classified in 2009 into three families: *Herpesviridae* containing mammalian, avian, and reptilian viruses, *Alloherpesviridae* containing fish and amphibian viruses, and *Malacoherpesviridae* containing bivalve viruses.

The family *Herpesviridae* is divided into the three subfamilies Alphaherpesvirinae, Betaherpesvirinae, and Gammaherpesvirinae. Commonly referred to as herpesviruses, these viruses share many biological properties indicative of their relation to one another. Genetically, 43 conserved genes among these three families function in nucleotide metabolism, DNA replication and virion structure (Roizman et al., 2013). Each herpesvirus replicates and packages its genome within the nucleus of the host cell, and every herpesvirus studied to date can undergo cellular latency to establish permanent infection in its host. Active production of progeny lyses the host cell, deeming the active production stage lytic infection. As of 2021, 115 species of *Herpesviridae* have been identified (Gatherer et al., 2021). Of these, 9 are known to infect humans: herpes

simplex virus 1 (HSV-1), herpes simplex virus 2 (HSV-2), human cytomegalovirus (HCMV), varicella-zoster virus (VZV), Epstein-Barr virus (EBV), and Human herpesviruses 6A, 6B, and 7 (HHV-6A, HHV-6B, HHV-7), and Kaposi's sarcoma–associated herpesvirus (KSHV, also known as HHV-8) (Roizman et al., 2013). Although many of facets of infection that I will discuss in following sections are shared among the human herpesviruses, I will focus primarily on HSV-1, the topic of my thesis, for the remainder of this introduction.

Herpes simplex virus 1 is also known by its official ICTV classification Human alphaherpes virus 1. HSV-1 and HSV-2 (also known as Human alphaherpesvirus 2) belongs to the genus *Simplexvirus* in the subfamily *Alphaherpesvirinae*. In the next section, I will discuss the origins of HSV-1 and HSV-2 and discuss their current prevalence around the globe.

1.2.b HSV origin and epidemiology.

Herpes simplex viruses 1 and 2 are highly successful pathogens that have been infecting and co-evolving with primates for millions of years. It is thought that HSV-1 infected hominids before their evolutionary split with chimpanzees 6 million years ago based on phylogenetic analysis of HSV glycoprotein gB (Wertheim et al., 2014). This split caused divergence of HSV-1 with chimpanzee herpes simplex virus (ChHV, also known as Panine alpha herpesvirus 3) (Gatherer et al., 2021). Molecular clock analysis then revealed that ChHV was transmitted to another hominid ancestor – *Homo erectus* – 1.6 million years ago (Wertheim et al., 2014).

While HSV-2 is predominantly sexually transmitted, HSV-1 can spread through both oral-to-oral or oral-to-genital contact. In addition to orolabial herpes (cold sores), HSV-1 can more rarely cause serious diseases such as keratitis and encephalitis. Seroconversion to HSV-1 typically occurs in childhood while seroconversion to HSV-2 mostly occurs after onset of sexual activity (McQuillan et al., 2018).

As of 2016, the World Health Organization estimated that 3.752 billion people (67%) are living with HSV-1 and 491.5 million people (11.3%) are living with HSV-2 (James et al., 2020). Both

HSV-1 and HSV-2 cause genital sores, although genital HSV-1 is far more rare than oral HSV-1; genital HSV-1 infection is estimated to impact 192.0 million people compared to 5.633 billion people with oral HSV-1 (James et al., 2020). Genital HSV-2 infection regardless of symptoms can almost triple the risk of contracting HIV (Looker et al., 2017); unfortunately, HSV-2 disproportionately impacts women aged 25-34 years in regions of Africa where HIV is a large driver of morbidity and mortality (James et al., 2020).

In the United States from 2015-2016, prevalence of HSV-1 was 47.8%, and prevalence of HSV-2 was 11.9% (McQuillan et al., 2018). Due to overall decreasing prevalence of HSV-1 in the United States (59.4% in 2000 compared to 47.8% in 2016), fewer infections are acquired during childhood. Adolescents entering sexual maturity consequently lack protective antibodies against HSV-1, which may explain why genital HSV-1 is specifically increasing among adolescents (Ayoub et al., 2019).

Some of the most vulnerable to severe HSV infection are neonates; over 14,000 children worldwide are affected each year (Akhtar & Kimberlin, 2021). Between 1 in 3000 and 1 in 20,000 live births are impacted by HSV. HSV disease in neonates can be limited to the skin/eyes/mouth, the central nervous system, or disseminated. Neonatal HSV can lead to encephalitis, lung damage, and seizures, and has a 75% mortality rate. HSV transmission from a mother to a neonate often occurs in the birth canal, although it can more rarely occur postnatally through oral or other close contact transmission. The neonates most at risk from HSV acquired in the birth canal are those whose mother acquires a new genital infection near the time of delivery (Fernandes et al., 2022).

HSV-1 is spread by saliva or other bodily fluids, and initial infection is typically in mucosal epithelial cells. HSV-1 replicates actively in these cells, causing eventual cell death and skin lesions. In immunocompetent hosts, primary infections are quickly cleared by the immune system. However, sensory neurons in the trigeminal ganglia can be exposed to HSV-1 progeny produced by lytic replication in the mucosal endothelium. HSV-1 infects these neurons and establishes a

mostly transcriptionally silent infection. Undetectable by the immune system, HSV-1 in the latent state persists in these terminally differentiated cells for the lifetime of the host. Periodic reactivation can occur to cause recurrences of lytic replication, which often cause sores at the initial site of infection. Reactivation is often triggered by UV damage or physical injury to the sites enervated by the sensory neurons, by hormonal imbalances, or by physical or emotional stress.

1.2.c Viral genome organization.

Like all herpesviruses, HSV-1 and HSV-2 have long linear dsDNA linear genomes (Roizman et al., 2013). Despite having diverged 6 million years ago, the two viruses share 83% sequence identity (Dolan 9499055). Both genomes are approximately 150,000 kilobase pairs with high GC-content – 68.3% and 70.4% for HSV-1 and HSV-2, respectively (Dolan et al., 1998).

The genomes are composed of one unique long fragment (U_L) covalently linked to a unique short fragment (U_S) by internal repeats (I_R), then bracketed by terminal repeats (T_R) (Figure 1.5) (Davison, 2007).The repeat regions can vary in length depending on a variation in repetition between strains. This dual-fragment structure is typical of alphaherpesviruses (Roizman et al., 2013).

Figure 1.5 HSV-1 genome structure.
Two genome segments, unique long (U_L) and unique short (U_S) are flanked by inverted terminal and internal repeats (TR and IR, respectively). Within each repeat region is a redundant *a* or inverted *a'* sequence. Arrows above indicate direction of repeat orientation. Image adapted from Davison 2007.

HSV-1 encodes 90 transcripts and 84 viral proteins (Roizman et al., 2013). The U_L and U_S regions are gene-dense with ORFS tightly clustered together. Very few transcripts are alternatively spliced, although there are instances of short transcriptional units embedded in the

coding sequence of a larger transcript. Most transcripts produce one protein, although some are noncoding. The most important of the noncoding RNAs are the latency associated transcripts (LATs), which I will discuss in section **1.2.e**.

1.2.d Lytic infection.

1.2.d.1 Viral entry into the cell and genome delivery to the nucleus.

The first stage of HSV-1 infection is invasion of the cell and delivery of the viral genome into the nucleus. Viral entry occurs in two fashions: fusion of the viral envelope with the cell membrane or through endocytosis. Both methods are mediated by viral glycoproteins. First, gC and gB attach to glycosaminoglycans at the cell surface. gD then interacts with one of three classes of receptors: Nectins-1 and -2, Herpesvirus Entry Molecule (HVEM, also known as TNFRSF14), or 3-*O*-heparin sulfate (Geraghty et al., 1998; Montgomery et al., 1996; Shukla et al., 1999). Nectins are cell adhesion molecules that are expressed on many types including neurons. HVEM is a member of the Tumor Necrosis Factor receptor family that is expressed in many tissues and has been studied extensively for its role in immune signaling. The interaction between gD and its receptors is thought to cause conformational changes in the gH/gL heterodimer that then prompts gB to fuse with the plasma membrane or endocytotic vesicle (Nicola et al., 2003).

Once the viral envelope has fused with cellular membranes, both the capsid and the associated tegument proteins are released into the cytoplasm. Some tegument proteins remain in the cytoplasm to perform important pro-viral functions, like the virion host shutoff (VHS) RNase that swiftly degrades host mRNAs (Kwong et al., 1988). Others are transported to the nucleus; this includes VP16, which lacks its own nuclear localization sequence but is transported to the nucleus by its interactions with HCF-1 (host cell factor 1) (Boissière et al., 1999). The capsid is translocated along microtubules through major capsid protein VP26 binding with motor protein dynein (Douglas et al., 2004). The capsid then docks at nuclear pores and ejects its genome into the nucleus through the force of osmotic pressure (Brandariz-Nuñez et al., 2019).

Once inside the nucleus, the viral genome swiftly circularizes through ligation. Circularization is not dependent on viral protein production, indicating that host factors mediate viral end-joining (David A. Garber et al., 1993). Indeed, knockdown of host DNA ligase VI and its co-factor XRCC4 reduces the formation of end-less genomes (Muylaert & Elias, 2007).

The viral genome also rapidly associates with host chromatin factors once inside the nucleus. Initially, silencing marks and antiviral complexes are associated with viral genomes as part of the cell's attempt to repress foreign DNA expression. However, viral proteins including VP16 and ICP0 counteract this initial silencing and promote a chromatin state on viral genomes that can promote gene expression and lytic replication. I will discuss in depth how HSV-1 manipulates chromatin on both viral and host genomes in section **1.3**.

1.2.d.2 Viral gene transcription.

Viral gene expression occurs in a tightly-regulated temporal cascade using host RNA Pol II (RNA polymerase II). First, six immediate early (IE) genes, ICP4, ICP0, ICP22, ICP27, US1.5 and ICP47, are transcribed. These then function to initiate expression of early (E) genes, which function in viral DNA replication. Transcription of some Late (L) genes begins concurrently with E genes, but is greatly enhanced by genome replication. Some L genes (early-late) are enhanced by viral replication, and some (late-late) are dependent on genome replication. An overarching theme of HSV-1 transcription is that each gene class must first be derepressed for transcription to occur (Roizman et al., 2013).

Tegument protein VP16 activates IE expression (Dalrymple et al., 1985) through formation of a complex with host co-factors Oct-1 (octamer-binding protein 1) and HCF-1 (Lai & Herr, 1997). This complex first counters the initial silencing of HSV-1 through recruitment of LSD1 (lysine-specific demethylase 1), which demethylates H3K9me3 on viral genomes, and other histone acetyltransferases to derepress IE promoters (Liang et al., 2009). Next, the complex binds at

VP16-responsive regulatory element TAATGARAT and recruits transcription factors to activate transcription of IE genes (Ace et al., 1989; Kristie, 2007).

Of the six IE proteins, only ICP4 is required for expression of almost all other viral genes (Roizman et al., 2013). It interacts with TFIID and TATA-binding protein (TBP) to form initiation complexes and activate transcription of both E and L genes (Carrozza & DeLuca, 1996). ICP4 can also directly bind DNA in a repressive manner; in this way, it represses its own expression. ICP0, ICP22, ICP47 and US1.5 are not necessary for viral gene transcription but enhance expression when present.

Although not strictly required for productive infection in cell culture or animals, ICP0 greatly enhances gene expression and genome replication. It is believed that ICP0 promotes E and L gene expression through removal of repressive marks and countering of host antiviral defenses. ICP0 is an E3 ubiquitin ligase that has been implicated in degradation of many host proteins including ubiquitinated histones, centromeric proteins, components of antiviral nuclear domain 10 (ND10 bodies), and innate host defenders (Lanfranca et al., 2014).

The next genes transcribed are E and some L genes. In the E class are seven essential proteins necessary for viral DNA synthesis: UL9 (binds HSV-1 origins), ICP8 (which binds single-strand DNA), UL30/UL42 (the DNA polymerase), and UL5/UL8/UL52 (the helicase/primase complex). ICP27 is required for maximal viral replication as mutations in this gene lead to decreased expression of many of the essential viral replication genes (Sacks et al., 1985; Uprichard & Knipe, 1996). ICP27 maximizes expression of viral genes in two ways: it promotes transport of some viral RNAs to the cytoplasm for translation (I. Hsiung Brandon Chen et al., 2002) and stimulates viral gene expression through directly binding RNA Pol II at transcribing viral genomes (Dai-Ju et al., 2006).

Finally, expression of L genes is greatly enhanced by genome replication (Godowski & Knipe, 1986). HSV-1 sequesters host and viral factors needed for replication into subnuclear structures known as viral replication compartments. In addition to replication, active viral transcription

continues; pulse-chase labeled viral RNA overlaps with stains for viral replication factors, indicating that transcription continues even as further stages of infection progress. Areas of transcription remain small even as volume of replication compartments grow to fill most of the nuclear space (Phelan et al., 1997). This suggests that many areas of viral replication compartments are dedicated solely to replication and possibly progeny assembly.

1.2.d.3 Viral genome replication and encapsulation.

Replication is initiated through UL9 binding and unwinding the dsDNA genome at an origin of replication. HSV-1 has three origins of replication: OriS is found twice within the IR *a'* repeat region and OriL is found within the U_L genome region. Once the DNA is distorted, UL9 then recruits ICP8 to the unwound ssDNA. The replication complex consisting of the polymerase and the helicase/primase then assembles at each replication fork to perform bi-directional theta replication. Eventually, the virus switches to origin-independent replication (Roizman et al., 2013).

The favored model for this second phase of replication is a rolling circle mechanism because this process intuitively creates head-to-tail concatemeric viral genomes (Roizman et al., 2013). Further, *in vitro* experiments have shown that HSV-1 replication proteins can facilitate rolling circle replication. However, complex branched replication intermediates have been detected in infected cells (Severini et al., 1996). This indicates that more complex replication mechanisms such as recombination may be at work. This is supported by the observation that homologous recombination is common during replication. Recombination has also been proposed as a method the virus uses to evade the antiviral impacts of some DNA damage repair pathways (Samantha Smith & Weller, 2015). Since the two methods are not exclusive, it is possible that both rolling circle replication and recombination are used to replicate the viral genome, or that the genome replicates using a complex rolling circle and recombination cycle.

Viral capsid genes (L) are transcribed concurrently with viral DNA replication (Roizman et al., 2013). After translation of capsid proteins, initial procapsid assembly occurs in the cytoplasm.

Evidence for this comes from immunofluorescence of exogenously expressed capsid proteins independent of infection; without concurrent expression of scaffolding protein ICP22a, major capsid protein VP5 is unable to localize to the nucleus (Nicholson et al., 1994). Final procapsid maturation into capsids occurs in the nucleus (Roizman et al., 2013). The ring-shaped portal complex (made up of pUL6) forms one of the vertices and associates with the capsid vertex specific component (CVSC) (Heming et al., 2017).

Once capsid assembly has occurred, viral genome concatemers must be cleaved and packaged. Two *cis*-acting sequences have been identified in the *a* repeat domains and termed *pacl* and *pac2*. The genome is inserted into the capsid in an ATP-dependent process and scanned for the *pac* sequences. Once these *pac* sequences are detected, the viral genome is cleaved, and the scaffolding proteins disassociate from the capsid. This process creates three types of capsids detected through sucrose gradient centrifugation (Gibson & Roizman, 1972): A capsids have lost scaffolding proteins and are thought to form as a consequence of abortive genome packaging; B capsids are empty but still associated with scaffolding proteins; C capsids contain viral genomes and have lost scaffolding proteins (Roizman et al., 2013).

1.2.d.4 Viral egress.

Infectious HSV-1 progeny can be detected in supernatants long before total cell lysis, indicating that capsids navigate through the nucleus and cytoplasm to bud from living cells. During this journey, capsids mature into infectious virions and overcome several physical barriers to exit from the cell. HSV-1 egress has two components: egress from the nucleus and egress of matured virions from the plasma membrane.

Due to the large size of the HSV-1 capsid at ~125 nm (Roizman et al., 2013), exit from the nucleus is not possible through nuclear pores, whose channels typically have diameters of ~50 nm (Lin & Hoelz, 2019). Three nuclear egress mechanisms have been proposed: 1) capsid envelopment at the inner nuclear membrane (INM) and de-envelopment at the outer nuclear

membrane (ONM), 2) enlargement of nuclear pores to allow capsid diffusion, and 3) capsid release through nuclear envelope breakdown. The first of these models, envelopment/de-envelopment, appears to be the dominant pathway, although there is evidence for the second two mechanisms occurring, albeit rarely (Roizman et al., 2013).

The envelopment/de-envelopment pathway is mediated by two conserved viral proteins: UL31 and UL34. Together, they form a nuclear egress complex (NEC), which scaffolds other host and viral proteins. Absence of either protein leads to lack of primary envelopment at the INM and capsid accumulation within the nucleus (Y. E. Chang et al., 1997; Roller et al., 2000).

The first challenge of HSV-1 nuclear egress is traversing the nucleus to reach the nuclear periphery. Initial proposals suggested that HSV-1 capsids were transported across F-actin filaments using molecular motor myosin (Feierbach et al., 2006; Forest et al., 2005). However, more recent reports contradict this conclusion; instead, they argue that HSV-1 capsids move through active diffusion, a process of Brownian motion enhanced by intracellular force fluctuations (Bosse et al., 2014, 2015). This diffusion is influenced by the structure of the marginalized and compacted host chromatin and may have profound impacts for efficient HSV-1 egress. I will discuss the interactions of HSV-1 with host chromatin in section **1.3.d**.

The second barrier is posed by the meshwork of filamentous proteins called the nuclear lamina that lines the INM (Hetzer, 2010). The lamina is important for nuclear structure, nuclear stability, and for tethering chromatin to the nuclear periphery (Solovei et al., 2013). The stability of the lamina network can be interrupted by phosphorylation. The NEC takes advantage of this property by recruiting viral kinase US3 and host kinase protein kinase C (PKC) to phosphorylate lamin proteins, which causes local disruptions of lamina structure (Bjerke & Roller, 2006; Richard Park & Baines, 2006).

The NEC then starts deforming the INM, a process known as primary envelopment. The capsid and certain tegument proteins interact with the NEC and are brought into the forming vesicle. Membrane scission aided by the host ESCRT-III complex (endosomal sorting complex III

required for transport) forms a vesicle known as a perinuclear virion (PEV). The PEV then travels the perinuclear space and fuses with the ONM to release naked capsids into the cytoplasm. Less is known about the process of de-envelopment than primary envelopment, but several glycoproteins and US3 are known to play a role in efficient membrane fusion (Roizman et al., 2013).

Once in the cytoplasm, the capsid further matures through acquiring additional tegument proteins, membranes to form the viral envelope, and glycoproteins to decorate the envelope. This maturation involves a secondary envelopment in cytoplasmic membranes. It is thought that the Golgi apparatus may be a source of some viral envelopes and may be the site of glycoprotein acquisition (Roizman et al., 2013). The newly enveloped viruses are then transported to the plasma membrane in vesicles using normal exocytosis mechanisms. The vesicle fuses with the plasma membrane and release the mature virions out of the cell.

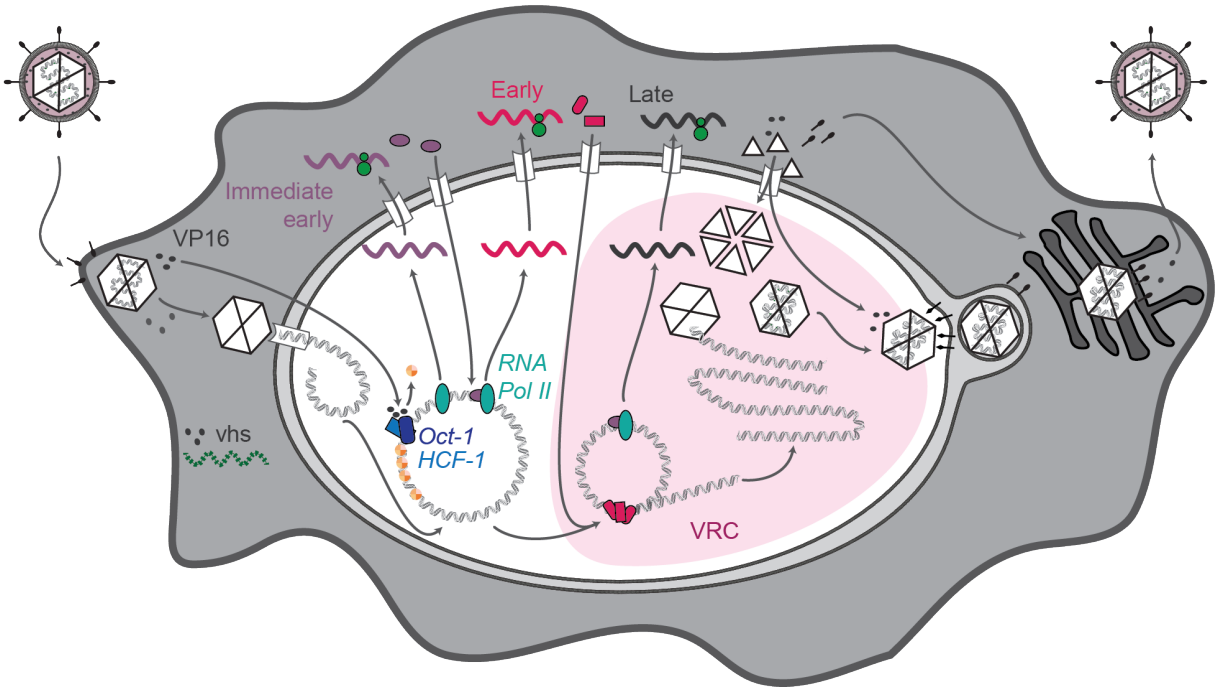

Figure 1.6 Summary of the HSV-1 lytic replication cycle.

Left to right: virions fuse with the plasma membrane to deposit capsids and tegument proteins in the cytoplasm. Capsids translocate to the nucleus where they dock at nuclear pores; after injection into the nucleus, the viral genome circularizes. Tegument protein *vhs* degrades host RNAs in the cytoplasm (green dashed line). Tegument protein *VP16* localizes independently to the nucleus, where it recruits host factors *Oct-1* and *HCF-1* (dark and light blue, respectively) to promote active chromatin states on viral genomes through eviction of repressive chromatin marks (represented by orange nucleosomes). Host *RNA Pol II* (teal) transcribes immediate early genes (purple), which further promote transcription of early genes (pink). Early genes initiate viral replication in viral replication compartments (VRC, light pink area) in a rolling circle mechanism. Late genes (black) are produced which form capsids (white hexagons) within VRCs. Long concatemeric viral genomes are cleaved and assembled into viral capsids. Capsids egress the nucleus through envelopment at the inner nuclear membrane to form a perinuclear virion and then de-envelopment at the cytoplasm. Capsids mature through the Golgi network by acquiring membranes, glycoproteins, and tegument proteins. Virions then bud out of the cell.

1.2.e Latent infection

1.2.e.1 Viral entry into the cell transport to the nucleus.

Viruses enter the neuron through pH-independent fusion at the dendritic end of the axon using nectin-1 as the receptor. Once inside the neuron, tegument proteins are released into the cytoplasm and the viral capsid associates with dynein. The capsid travels to the nucleus along chains of filamentous actin in a process known as retrograde axonal transport (Miranda-Saksena et al., 2018).

1.2.e.2 Transcriptional repression.

Once inside of the nucleus, the HSV-1 genome circularizes and persists in a non-integrated form known as an episome. The viral episome is populated with host chromatin marks, especially those associated with transcriptional repression. A few viral transcripts are expressed, but the consensus is that none are consistently translated. Genome replication is not detected during latent infection, and infectious progeny are not produced (Roizman et al., 2013).

The only transcripts made during latency are the family of latency-associated transcripts (LATs) and microRNAs (Roizman et al., 2013). The LATs are expressed from the LAT transcriptional unit via a neuron-specific promoter/enhancer (Zwaagstra et al., 1989). They are alternatively spliced to form several RNA species, the most abundant of which are 2- and 1.5-kb introns that are highly stable due to lariat structures (Roizman et al., 2013). LAT has been shown to repress IE gene expression and promote a repressive chromatin state on viral episomes (S. H. Chen et al., 1997; Cliffe et al., 2009a; D A Garber et al., 1997; Qing-Yin Wang et al., 2005). LAT deletion leads to different phenotypes in different systems; some reports indicate reduced latency establishment where others do not detect a difference in latency compared to wild-type viruses. Generally, most studies show that LAT expression protects neurons from cell death. The function of HSV-1 microRNAs during latency is currently mysterious, but the studies conducted so far point to downregulation of lytic gene expression to maintain latency (Roizman et al., 2013).

The molecular events that lead to the establishment latent infection instead of lytic replication are largely still mysterious. One possibility is that neuron-specific hormones such as nerve growth factor (NGF) repress viral gene expression. Another model is that neuronal nuclei lack several factors that the virus uses to overcome initial transcriptional silencing, e.g., the co-factor HCF-1, which transports VP16 into the nucleus during lytic infection, is primarily cytoplasmic in trigeminal ganglion neurons (Kolb & Kristie, 2008). VP16, which lacks an NLS, cannot independently enter the nucleus to initiate IE gene transcription. Without IE gene transcription at sufficient levels, the lytic cycle cannot begin (Cliffe & Wilson, 2017). It is thought that LAT then maintains latency through promotion of a repressive chromatin state on viral genomes (Roizman et al., 2013).

1.2.e.3 Reactivation.

In the absence of IE proteins, viral gene transcription is primarily dictated by host cell signaling. Most pathways to reactivation have to do with cellular stress. In latently infected mice, production of infectious virus can be triggered through heat shock (Sawtell & Thompson, 1992). In cultured neurons, neuronal stress induced by NGF deprivation or heat shock can trigger viral gene expression (Halford & Schaffer, 2001). Pharmacological inhibition of NGF pathway downstream effector PI3K also leads to this wave of viral gene expression, termed Phase I. Unlike the temporally coordinated cascade of lytic gene expression, transcripts from IE, E, and L genes are expressed concurrently during Phase I. If levels of IE gene expression are sufficient to overcome silencing at this state, another wave of gene expression will occur that resembles the lytic gene cascade, termed Phase II. This phase allows for viral DNA replication and production of infectious progeny (Ju Youn Kim et al., 2012).

As many of the mechanisms of latency and reactivation are impacted by chromatin control of viral episomes, I will discuss these processes in greater detail in sections **1.3.b** and **1.3.c**.

1.3 Chromatin regulation by HSV-1.

1.3.a Viral chromatin during lytic infection.

No host histones have been detected within HSV-1 capsids (Oh & Fraser, 2008; Pignatti & Cassai, 1980). Instead, it is thought that up to 40% of the charges on the viral DNA are neutralized with spermine to facilitate compaction and packaging (Gibson & Roizman, 1971). Consequently, the viral genome is “naked” upon entry to the nucleus and is a prime template for chromatinization.

Whereas MNase digest of latently infected cells shows a banding pattern of viral genomes similar to regularly chromatinized host genomes, digestion of lytically infected cells produces a range of fragment sizes, only a fraction of which are mono- or di-nucleosome sized (Leinbach & Summers, 1980; Oh et al., 2015; Oh & Fraser, 2008). This also holds true in mouse ganglia during acute infection (Muggeridge & Fraser, 1986). Complete MNase digestion revealed that a fraction of HSV-1 DNA is protected by nucleosomes at 1 and 6 hpi (38 and 43% of total counts, respectively), but this fraction decreases late during infection (9% at 24 hpi). These data indicate that there is some degree of nucleosome association with lytic genomes, although they do not form a regular repeating structure like host chromatin (Oh et al., 2015). More recent studies have suggested that the nucleosomes associated with HSV-1 genomes are more unstable than those associated with cellular DNA, or that HSV-1 genomes preferentially associate with ICP4 rather than host nucleosomes (Dembowski & DeLuca, 2018; Dremel & DeLuca, 2019; Hu et al., 2019; Lacasse & Schang, 2010).

Chromatin immunoprecipitation combined with qPCR (ChIP-qPCR) has identified interactions of nucleosomes with at least some viral DNA at all points during infection. By 1-2 hpi, HSV-1 genomes tend to be associated with marks of transcriptional repression such as H3K27me3 and H3K9me3 (Cliffe & Knipe, 2008; Lee et al., 2016; Liang et al., 2009; Oh & Fraser, 2008). This association consistently decreases over time, likely as viral factors remove repressive marks to facilitate gene expression and replication (Cabral et al., 2018; Kent et al., 2004; Liang et al., 2009; Oh & Fraser, 2008). Viral ubiquitin ligase ICP0 has been implicated in removal of repressive viral

heterochromatin, although this may be through indirect mechanisms of action (Cabral et al., 2018; Cliffe & Knipe, 2008; Lee et al., 2016). Chromatin dynamics, as measured by mobilization of histones, is increased by expression of ICP4 (Gibeault et al., 2016). Marks of transcriptional activation like H3K9ac, H3K14ac, and H3K4me3 are associated with viral genomes as transcription increases (Kent et al., 2004; Liang et al., 2009). The switch from H3K9me3 to H3K4me3 has been attributed to lysine demethylase LSD1 acting in conjunction with methyltransferase SET1 (Liang et al., 2009).

Importantly, the above conclusions were primarily based off ChIP-qPCR results. Recently, groups have sought to validate these ChIP-qPCR studies using ChIP sequencing. Some publications have reported similar trends to those described in the preceding paragraph: H3K9me3 and H3K27me3 bind viral genomes by 1-2 hpi and decrease over time, and H3K27ac association increases during infection (Chuan et al., 2020). Other groups have found no association of histones H1 or H3, or marks H3K27me3, H3K9me3, H3K4ac or H3K27ac, on incoming viral genomes via ChIP sequencing (Dremel & DeLuca, 2019). Additionally, no H1 or H3 was found on replicated viral genomes through iPond or immunofluorescence, which agrees with previously proposed models (Dembowski & DeLuca, 2015; Oh & Fraser, 2008).

The impact of nucleosome interactions with the HSV-1 genome is also still mysterious. One study suggested that incorporation of histone variant H3.3 onto HSV-1 coding regions is necessary for maximal gene transcription early during infection, and that replication-coupled H3.1 then becomes the dominant histone on viral genomes after replication. In this system, knockdown of H3.3 chaperone HIRA leads to decreased viral gene expression (Placek et al., 2009). Conversely, other studies showed that HIRA deposits H3.3 onto incoming HSV-1 and HCMV genomes as part of the antiviral response to invading DNA (McFarlane et al., 2019; Rai et al., 2017). Specifically, these systems found HIRA co-localizing with specific antiviral molecular structures termed ND10 (nuclear domain 10) or PML (promyelocytic leukemia) nuclear bodies. Formation of these nuclear bodies at sites of incoming HSV-1 genomes is thought to function as

part of the host's effort to silencing invading DNA; proteins are then degraded, and the complexes are dispersed through proteasomal degradation induced by ICP0 (Everett et al., 2006). In addition to their function on viral genomes, HIRA and PML have been implicated in inducing a full interferon response to HSV-1 lytic infection (McFarlane et al., 2019; Rai et al., 2017). Importantly, the study that showed HIRA acting in a pro-viral manner performed infections in cancerous HeLa cells, where the reports of HIRA acting anti-virally used diploid cell lines as a model. The different experimental systems may explain some of the variability in results.

A recently suggested model is that only a fraction of incoming viral genomes must escape silencing by the host cell to establish lytic infection, whereas a majority are transcriptionally inactivated and cannot establish infection. The genomes that escape silencing can then initiate replication and cause the changes in nucleosome dynamics observed in multiple studies (Hu et al., 2019).

Lytic HSV-1 infection also activates many DNA damage pathways (Lilley et al., 2010). For brevity, I will focus on PARP-1 signaling, which is likely activated by nicks and gaps on incoming viral genomes (Samantha Smith & Weller, 2015). HSV-1 infection causes a precipitous drop in cellular reserves of NAD+ (Grady et al., 2012; Vastag et al., 2011). This is a result of PARP-1 overactivation, which increases total levels of protein PARylation. In cultured fibroblast cells, PARP-1 remains primarily nuclear during infection (Grady et al., 2012). However, a recent study in HeLa cells showed that PARP-1 can translocate to the cytoplasm, where it PARylates effectors of antiviral immunity to suppress an innate immune response (Fei Wang et al., 2022). Broad-spectrum inhibition of all PARP enzymes in the cell or targeted inhibition of PARP-1 reduces HSV-1 yields both in cultured cells and in mice (Grady et al., 2012; Zhuan Li et al., 2012; Fei Wang et al., 2022). Certain isoforms of PARG (poly(ADP-ribose) glycohydrolase), which remove PAR chains to aid in ADPr turnover, are degraded during HSV-1 infection. However, short interfering RNA (siRNA) knockdown of all PARG isoforms leads to a 30% reduction in viral titers (Grady et al., 2012).

1.3.b Host genome during lytic infection.

During late stages of lytic infection, viral replication compartments have expanded to fill most of the nuclear space. This results in host chromatin marginalization and compaction at the nuclear periphery despite nuclei increasing in size (Monier et al., 2000). This compact chromatin poses a barrier for capsids; thus, HSV-1 remodels host chromatin and the proteinaceous lamina barrier to allow for nuclear egress.

In uninfected cells, it has been calculated that the maximum diameter at which a particle can freely diffuse is ~300 nm (Görisch et al., 2004). However, compaction of chromatin at the nuclear periphery has been shown to impact the movement of the ~125 nm HSV-1 capsids (Aho et al., 2017, 2019, 2021). Rather than indiscriminately diffusing throughout all chromatin at the nuclear periphery, the capsids access the nuclear envelope through regions of less dense chromatin, termed “channels” (Myllys et al., 2016).

One of the main functions of the HSV-1 nuclear egress complex, composed of UL31 and UL34, is to re-organize the nuclear lamina. Exogenous expression of UL31 and UL34 either separately or together is sufficient to mis-localize lamins A and C from a smooth distribution around the nucleus into punctate structures either at the nuclear rim or in the cytoplasm (Reynolds et al., 2004; Simpson-Holley et al., 2004). Some lamin proteins are degraded through autophagy, which is necessary for HSV-1 egress from dendritic cells (Turan et al., 2019).

In addition to providing structure to the nucleus, the lamina is also important for organizing chromatin architecture through tethering chromatin to the nuclear envelope. Loss of lamin proteins can lead to heterochromatin dysregulation and disease (Schreiber & Kennedy, 2013). Interestingly, loss of lamina during HSV-1 infection has been reported to impact HSV-1 gene regulation. Lamin A deletion in mouse embryonic fibroblasts lead to inclusion of H1 and H3K9me3 within viral replication compartments as measured by IF and ChIP-qPCR of viral genomes (Silva et al., 2008). HSV-1 gene expression and titers were also reduced upon Lamin A deletion. In a follow-up paper, Silva et al. argued that these phenotypes occur because incoming viral genomes

tether to the nuclear periphery to efficiently interact with transactivator complex VP16 and HCF-1, which are imported from the cytoplasm (Silva et al., 2012). Interestingly, disruption of centrosomal protein TRIM43 (Tripartite motif containing 43) leads to pericentrin destabilization and subsequently loss lamina integrity loss. This also restricts a broad range of herpesviruses, although the mechanism was not fully characterized (Full et al., 2019).

The connection between lamina disruption and impact on host chromatin has been characterized extensively in uninfected cells. In general, however, the impact of host chromatin dysregulation on HSV-1 fitness is an area in need of further study.

1.3.c Viral chromatin during latent infection.

HSV-1 latency is defined as a persistent infection where infectious viral progeny is undetectable by experimental methods unless reactivated by specific stimuli. HSV-1 establishes latency in post-mitotic neurons, where it maintains its genome as an unintegrated episome decorated with regularly spaced nucleosomes. This is evidenced by MNase digestion of viral genomes producing a regular banding pattern by similar to host chromatin (Deshmane & Fraser, 1989). Although many factors may trigger latent instead of lytic infection in neurons, it is generally accepted that the chromatinization of the HSV-1 episome is important for latency establishment and maintenance while preserving the ability of the virus to reactivate.

Most studies of latency have focused on histone post-translational modifications, as there is evidence that the latent HSV-1 genome is not subject to DNA methylation (Kubat et al., 2004). Several markers of heterochromatin have been found at transcriptionally silenced lytic gene promoters by 7 days post-acute infection including macroH2A1, H3K27me3, H3K9me2 and H3K9me3 (Cliffe et al., 2009a; Kwiatkowski et al., 2009; Nicoll et al., 2016; Qing-Yin Wang et al., 2005). In contrast, the transcriptionally active LAT enhancer and promoter have been found to be marked by H3 acetylations and H3K4me3 (Cliffe et al., 2009a; Kubat et al., 2004)). There is likely heterogeneity of the chromatin structure of HSV-1 episomes, as other studies have found marks

of facultative heterochromatin, specifically macroH2A and H3K27me3, at the LAT enhancer (Kwiatkowski et al., 2009). It is unknown whether different genomes within the same neuron have heterogeneous structures or whether all genomes within a cell have similar conformations and the heterogeneity arises between different neurons.

Many studies have pointed to LAT as a key factor in maintaining latency, possibly due promoting heterochromatin maintenance at lytic genes. Deletion of either the entire LAT region or the small 1.8-kb transcript leads to less H3K9me3/H3K27me3 and increased H3K4me3 at lytic viral genes (Cliffe et al., 2009a; Qing-Yin Wang et al., 2005). However, LAT is not responsible for the initial targeting of H3K27me3 to viral genomes (Cliffe et al., 2013).

Given that HSV-1 can replicate lytically in many cell types but targets neurons for latent infection, it is likely that there are neuron-specific reasons why the HSV-1 genome becomes transcriptionally repressed to set up latency. As discussed in section **1.2.e.2**, lack of Oct-1 expression or localization of VP16 or HCF within the neuron's nucleus may contribute to a lack of lytic gene transcription. It is possible then that heterochromatin forms on latent viral genomes after latency is established and is not directly responsible for its establishment. This model is supported by the observation that the ability of the HSV-1 to reactivate decreases over time in cultured cell models of latent infection. Consistent with this, H3K27me3 presence at lytic gene promoters is low at 7 days post infection (dpi) but increased by 14 dpi in mouse trigeminal ganglion (Cliffe et al., 2013). Overall, these data suggest that increasing viral genome chromatinization occurring over time leads to increasing viral genome silencing.

In addition to a lack of lytic gene expression upon latency establishment, neurons express a different composition of PTM writers and readers. In particular, the major species of Polycomb methyltransferase in mature neurons is EZH1 rather than EZH2 (Whitford & Cliffe, 2022). It is also possible that the HSV-1 genome may form higher-order structures during latency. Chromatin insulator protein CTCF (CCCTC-binding factor), which plays a role in organizing distinct 3D

chromatin regions, has been shown to bind latent viral genomes and influence deposition of H3K27me3 (Washington et al., 2018).

1.3.c Viral chromatin during reactivation.

For latent HSV-1 to reactivate, transcriptional repression by heterochromatin must be overcome. Lack of viral proteins necessary for initiation of transcription and replication, especially VP16 or any of the essential IE genes, means that reactivation is dependent on host signaling pathways. Neuronal stress pathways activated by heat shock, hormone deprivation, or other stressors are thought to trigger reactivation. The current model is a biphasic process of reactivation. During the first stage, termed Phase I, lytic gene transcription of all classes is activated by host proteins independent of viral DNA replication; Phase II occurs after a threshold of gene expression has been reached in order to stimulate a cascade reminiscent of lytic infection (Ju Youn Kim et al., 2012).

It's thought that removal of repressive histone methylation is crucial for efficient reactivation. This is evidenced by reduced reactivation in explant models and animal models when histone demethylases LSD1 and JMJD2 are inhibited (Hill et al., 2014; Liang et al., 2009; Liang, Quenelle, et al., 2013; Liang, Vogel, et al., 2013; Messer et al., 2015). Paradoxically, Phase I gene expression has been shown to be independent of demethylase activity depending on the reactivation stimuli and experimental system used (Cliffe et al., 2015; Whitford et al., 2022). This ability of the virus to express lytic genes despite H3K9me3 presence on genomes has been attributed to a “phospho-methyl switch” that is a strategy of gradual de-repression in host genes (Fischle et al., 2005). As described in section **1.1.a.2**, phosphorylation of H3S10, the residue directly next to H3K9me3, releases binding of repressive protein HP1. This negates the H3K9me3-caused repression without requiring demethylases to remove the trimethylation (Avgousti & Weitzman, 2015; Cliffe et al., 2015).

Higher order structure of the viral genome may also influence its ability to reactivate. Interrupting CTCF interactions with latent genomes through deletion of CTCF binding sites decreases the ability of HSV-1 to reactivate (Lee et al., 2018). This is possibly because CTCF insulates heterochromatin from euchromatic regions on the viral genome; its deletion is thought to allow heterochromatin to "spread" to regions that are required for reactivation (Lee et al., 2018). However, CTCF binding is lessened during reactivation (Ertel et al., 2012), indicating that temporal control of the 3D genome is crucial to successful reactivation.

Finally, it is thought that different viral genomes may be maintained in different states either in the same neuron or between different neurons. Exposing cultured neurons to antiviral interferon (IFN) during establishment of latency leads to viral genomes co-localizing with ND10 bodies, which leads to significantly decreased ability of these genomes to reactivate (Suzich et al., 2021). Although ND10 bodies do not typically form in neurons not exposed to IFN, this may indicate that immune signaling at the onset of latent infection may make HSV-1 less prone to reactivation.

Post-amble

Despite a wealth of research, there are many unaddressed questions about how HSV-1 manipulates chromatin to promote active replication and persistent infection. For my dissertation work, I chose to focus on changes in the host genome during lytic infection. In particular, I was interested in why heterochromatin marks such as macroH2A1 and H3K27me3 increase during active viral replication. Heterochromatin marks can serve as barriers to HSV-1 gene expression when associated with viral genomes (Knipe & Cliffe, 2008; Whitford & Cliffe, 2022); an increase in density of heterochromatin at the nuclear periphery could theoretically also pose a barrier for capsid movement (Aho et al., 2017, 2019, 2021; Bosse et al., 2015; Myllys et al., 2016). In my thesis work, I determined that this increased peripheral heterochromatin is beneficial for lytic HSV-1 infection by promoting channels that capsids exploit to egress from the nucleus.

Chapter 2. Methods and Materials

2.1 Cell culture and viral infections.

2.1.a Cell culture.

Primary human foreskin fibroblasts (HFFs), hTERT-immortalized HFFs (HFF-Ts) and macroH2A1 knockout HFF-Ts were cultured using standard methods with DMEM + 10% FBS + 1% penicillin-streptomycin (pen-strep) as previously described (Lynch et al., 2021). hTERT-immortalized retinal pigment epithelial (RPE) and macroH2A1 knockout RPE cells were cultured using standard methods with DMEM/F12 + 10% FBS + 1% pen-strep + 0.01 mg/mL hygromycin. Cells were grown at 37 °C with 5% CO_2 and tested for mycoplasma contamination approximately once a month. See **Table 1** for cell line sources.

2.1.b HSV-1 infections.

The lab adapted strain HSV-1 *syn 17+* (Brown et al., 1973) was used for all experiments unless otherwise noted. Virus stock was grown by infecting Vero cells at an MOI of 0.0001. Virus was harvested ~60-80 hours post infection and titered on U2OS cells to determine stock plaque forming units per mL (pfu/mL). Monolayers of cells were infected for 1 hour at 37 °C as previously described (Lilley et al., 2005). A multiplicity of infection (MOI) 3 was used for all experiments, except for infections for electron microscopy which used MOI 10. Cells were collected at mock, 4, 8, 12, and sometimes 16 hours post infection for western blotting. Supernatant was collected at 8 and 12 hpi for plaque assays. Experimental plaque assays were performed on Vero cells through serial 10-fold dilutions in serum-free DMEM. Cells were incubated with viral dilutions for 1 hour; the viral inoculum was then removed and cells were washed with 1X PBS pH 7.46 then overlaid with 1% methylcellulose in DMEM with 2% FBS and 0.5% pen-strep. Plaques were fixed

with 0.2% crystal violet between 96-100 hours post infection and plaques were counted by hand. All plaque assays were set up with 2 technical replicates.

Clinical HSV-1 isolates were acquired in 1994 and 1995 from oral swab collections. Samples were de-identified on collection. Patients provided daily home collections of oral swabs, and qPCR was used to detect how many days HSV was detected in these swabs. Patients that had detectable HSV in only a few swabs were classified as “low-shedders” and patients that had a high percentage of days with positive swabs were classified as “high-shedders.” Stocks were a gift from the lab of Keith Jerome.

2.1.c HCMV infections.

The lab adapted strain HCMV Towne (Plotkin et al., 1975) was used for all experiments. Virus stock was grown by infecting HFF-Ts at an MOI of 0.0001. Virus was harvested approximately 14 days post infection and titered on HFF-Ts to determine stock pfu/mL. Monolayers of cells were infected for 1 hour at 37 °C, then viral inoculum was removed and cells were overlaid with fresh complete media. All HCMV experiments used MOI 1. Cells were collected at mock, 4 hour, 4 day, and 6 days post infection (dpi) for genome analysis. Supernatant was collected at 4 and 6 dpi for plaque assays. Experimental plaque assays were performed on HFF-Ts through serial 10-fold dilutions in serum-free DMEM. Cells were incubated with viral dilutions for 1 hour; the virus was then aspirated and cells were washed with 1X PBS pH 7.46 then overlaid with 1% methylcellulose in DMEM with 2% FBS and 0.5% pen-strep. Plaques were fixed with 0.2% crystal violet between 10-14 days post infection and plaques were counted by hand. All plaque assays were set up with 2 technical replicates.

2.1.d HSV-1 replication inhibition with PAA.

Phosphonoacetic acid (PAA, Thermo 284270) 100 mM stock solution was prepared in serum-free medium and adjusted to pH 7.0 with 1 N sodium hydroxide (NaOH). The stock was diluted to

400 μM in DMEM + 10% FBS and added to the cells after removing viral inoculum and washing with PBS.

2.1.e MacroH2A1 knockout, overexpression, and rescue.

2.1.e.1 MacroH2A1 knockout.

MacroH2A1 guide RNA (gRNA, see **Table 2**) was cloned into TLCv2 (Addgene plasmid: 87360), a plasmid encoding doxycycline-inducible Cas9-2A-GFP and gRNA expression. To generate lentiviral particles, $1.0x10^7$ HEK293T cells were transfected with 12 μg TLCV2_sg_mH2A1, 8 μg pMDL (Addgene plasmid: 12251), 4 μg pCMV_VSVg (Addgene plasmid: 8454), and 2.5 μg pREV (Addgene plasmid: 115989) using Attractene transfection reagent (Qiagen: 301005). Lentivirus was harvested at 24, 48, and 72 hours post-transfection, filtered through 0.2 μm filters, aliquoted, flash frozen with liquid nitrogen, and stored at -80 °C. 2 mL of thawed filtered lentivirus was used to transduce approximately $2.25x10^6$ HFF-T or $3x10^6$ RPE cells in 10 cm plates with 8 μg/mL polybrene (Millipore-Sigma: TR-1003-G). Cells were allowed to reach confluence before selection with 1 μg/mL puromycin for 3 days. Cells were then sorted by GFP positivity or counted by hemocytometer, plated at 1 cell per well into 96-well plates, and selected through serial expansion of colonies. Selected cells were screened for macroH2A1 knockout by western blotting.

2.1.e.2 MacroH2A1 overexpression.

MacroH2A1.1-FLAG or macroH2A1.2-FLAG tagged cDNA constructs in a pLVX_puro backbone (Takara Bio Cat. 632164) were a gift of M. Gamble. Expression of transgenes is driven by human cytomegalovirus immediate early promoter. To generate lentiviral particles, $1.0x10^7$ HEK293T cells were transfected with 2.66 μg pLVX_mH2A1.1-FLAG or pLVX_mH2A1.2-FLAG, 10 μg psPAX2 (Addgene plasmid: 12260) and 6.66 μg pCMV_VSVg (Addgene plasmid: 8454) using Attractene transfection reagent (Qiagen: 301005). Lentivirus was harvested and WT HFF-

T cells were transduced as above, then selected with 1 μg/mL puromycin for 3 days. Protein expression was confirmed by western blotting (see Figure 3.19), and infections were performed immediately after conclusion of selection to normalize protein expression between replicates.

2.1.e.3 MacroH2A1 rescue.

Overexpression constructs described above were modified to 1) mutate the gRNA binding site, 2) change the FLAG tag to an HA tag, and 3) change the antibiotic resistance to blasticidin (macroH2A1.1-HA rescue) or hygromycin (macroH2A1.2-HA rescue). To accomplish this mutation to disrupt gRNA interaction with re-introduced cDNA, plasmids were amplified with PCR primers containing a mutation in the gRNA binding site. To change the FLAG tag to HA, plasmids were amplified with primers containing HA tags and re-ligated using Gibson assembly (Gibson 2009 19363495). To change resistance, donor plasmids containing genes encoding blasticidin or hygromycin resistance were amplified with primers containing homology to pLVX_puro. pLVX_puro was then amplified with primers containing homology to either of the two resistance genes and the constructs were assembled using Gibson assembly. See **Table 2** for sequences of all primers used in mutagenesis and Gibson assembly. Lentiviral particles were generated as described in section **2.1.e.2** and macroH2A1 KO HFF-T were transduced and selected with antibiotic for 3-7 days. Exogenous protein expression was confirmed by western blotting (see **Figure 3.17**).

2.1.f H3K217me3 reduction through EZH2 inhibition with Tazemetostat.

HFF-Ts and macroH2A1 KO HFF-Ts were treated with DMSO or 10 μM of Tazemetostat (MedChem: HY-13803) in DMSO for 3 days prior to infection. Cells were then infected at MOI of 3 and, after 1 hour of incubation with virus, fresh media with 10 μM Tazemetostat was added to previously treated cells. Control samples were treated with equivalent volumes of DMSO. Samples were harvested as above.

2.2 Western blotting

Western blotting was performed as previously described (Lynch et al., 2021). Briefly, cells were counted, pelleted, resuspended in 1x NuPAGE lithium dodecyl sulfate (LDS) sample buffer (Fisher Scientific: NP007) + 5% 2-betamercaptoethanol, and boiled for 15 minutes. Protein lysates were separated by 13.5% SDS-PAGE gels using NuPAGE MOPS buffer (Fisher Scientific: NP0001) at 75 volts for 30 minutes then 110 volts for 100 minutes, then transferred to a nitrocellulose membrane (Bio-Rad) at 100 volts for 70 minutes using Transfer Buffer (25 mM Tris Base, 100 mM glycine, 20% methanol). Membranes were ponceau stained and imaged. Membranes were blocked in 5% milk in Tris-buffered saline with Tween (TBST) for 1 hour, then probed with primary antibody overnight. Membranes were washed with TBST for thirty minutes, incubated with secondary antibodies conjugated to horseradish peroxidase (α-mouse or α-rabbit; 1:5000) at room temperature for 1 hour, washed with TBST for thirty minutes, and detected using Clarity Western ECL Substrate (Bio-Rad: 1705061) and Chemidoc MP Imaging System (Bio-Rad). Images were formatted using Adobe Photoshop and Illustrator. See **Table 3** for antibody sources and concentrations.

2.3 Immunofluorescence (IF).

Cells were grown on glass coverslips in 24-well plates. Cells were harvested for IF at the indicated time points, fixed in 4% paraformaldehyde (Fisher Scientific: 50-980-487) for 5-15 min, and washed three times with PBS post-fixation. Fixed cells were permeabilized with 0.5% Triton-X in PBS for 10 minutes and blocked with 3% goat serum (Sigma Aldrich: G9023) for 1 hour at room temperature. Cells were incubated with primary antibodies diluted in 3% bovine serum albumin (BSA, Sigma Aldrich: A7906) for 1 hour each at room temperature, then incubated with secondary antibodies and DAPI (4′,6-diamidino-2-phenylindole, Fisher Scientific: 50-874-10001, used at 1:10,000) in 3% BSA. Cells were washed three times with 3% BSA in PBS between each antibody incubation, and three times with PBS prior to mounting. Coverslips were mounted using

ProLong Gold Antifade Reagent (Fisher Scientific: P36934). Immunofluorescence was visualized using a Leica Stelaris using a 63X oil objective. Images were processed using ImageJ and assembled with Adobe.

2.4 HSV-1 genome quantification.

2.4.a HSV-1 genome isolation from cells or supernatants.

Cells were harvested at the indicated times post infection by trypsinization, washed with 1X PBS and centrifuged at 5000 xg for 2 minutes. Pellets were flash-frozen in liquid nitrogen and stored at -80 °C until processed. HSV-1 DNA within cells was isolated from frozen pellets using the QIAamp DNAMini Kit (Qiagen: 51304).

Supernatants were harvested at the indicated times post infection, centrifuged at > 3500 xg and filtered through 40 micron sterile syringe filters. DNA on the exterior of filtered capsids was digested for 1 hour at 25 °C with 20.3 units DNase (Qiagen: 79254) supplemented with 10 mM $MgCl_2$. DNase was inactivated at 75 °C for 10 minutes followed by vortexing. Capsids were digested with 3 mg/mL proteinase K (Fisher Scientific: BP1700) in 100 mM KCl, 25 mM EDTA, 10 mM Tris-HCl pH 7.4 and 1% Igepal for 1 hour at 50 °C. HSV-1 genomes from digested capsids were isolated using the QIAamp DNAMini Kit (Qiagen: 51304).

2.4.b Droplet digital PCR (ddPCR)

A duplexed ddPCR reaction was performed to measure the levels of cellular or supernatant HSV-1 or HCMV genomes on the QX100 droplet digital PCR system (Bio-Rad Laboratories, Hercules, CA) using a primer/probe set specific to HSV-1 gB or HCMV UL55. Cell numbers were determined using a primer/probe set specific to human Beta-globin, a reference gene that exists at two copies per cell. See **Table 2** for oligonucleotide sequences, which have been previously established for ddPCR of HSV-1 (Aubert et al., 2014) or HCMV (Sedlak et al., 2014). The ddPCR reaction mixture consisted of 12.5 µL of a 2X ddPCR Supermix for Probes no dUTP (Bio-Rad:

1863024), 1.25 µL of each 20X primer-probe mix, and 10 µL of template DNA. 20 µL of each reaction mixture was loaded onto a disposable plastic cartridge (Bio-Rad: 1864008) with 70 µL of droplet generation oil (Bio-Rad: 1863005) and placed in the droplet generator (Bio-Rad). Droplets generated were transferred to a 96-well PCR plate (Bio-Rad 12001925), and PCR amplification was performed on a Bio-Rad C1000 Touch Thermal Cycler with the following conditions: 95 °C for 10 minutes, 40 cycles of 94 °C for 30 seconds, and 60 °C for 1 minute, followed by 98 °C for 10 minutes and ending at 4 °C. After amplification, the plate was loaded onto the droplet reader (Bio-Rad: QX200), and the droplets from each well of the plate were automatically read with droplet reader oil (Bio-Rad: 186-3004) at a rate of 32 wells per hour. Data were analyzed with QuantaSoft analysis software and quantitation of target molecules presented as copies per µL of PCR reaction. HSV-1 genome values were standardized to cellular β-globin levels. Experiments were completed in biological triplicate and statistical analysis was performed using Prism v10 (GraphPad Software).

2.4.c qPCR.

For viral DNA quantification during infection, cells were recovered at indicated time points as described above and genomic DNA was isolated using the QIAamp DNA Mini Kit (Qiagen: 51304). Quantitative PCR was performed on 50 µg gDNA using primers specific for HSV-1 gB and cellular tubulin and analyzed using the BioRad CFX384 Real-Time System. Ct values for gB were normalized internally to tubulin and to then to the 1 hpi viral input sample. Experiments were completed in biological triplicate and statistical analysis was performed using Prism v10 (GraphPad Software). See **Table 2** for oligonucleotide sequences.

2.5 CUT&Tag.

2.5.a CUT&Tag library generation.

Two biological replicates per time point were obtained from independent infections. Protocol was adapted from the established CUT&Tag methods (Kaya-Okur et al., 2019). Cells were harvested using trypsin, washed three times with ice-cold phosphate-buffered saline (PBS) via centrifugation at 600 xg for 3 minutes and counted using a hemocytometer. Nuclei from 600,000 cells were isolated by hypotonic lysis in 1 mL buffer NE1 (20 mM HEPES-KOH pH 7.9; 10 mM KCl; 0.5 mM spermidine; 0.1% Triton X-100; 20% Glycerol; Roche EDTA-free protease inhibitor) for 10 minutes on ice followed by centrifugation at 1300 xg for 4 minutes. Nuclei were resuspended in Wash buffer (20 mM HEPES-NaOH pH 7.5; 150 mM NaCl; 0.5 mM spermidine; Roche EDTA-free protease inhibitor) and counted using a hemocytometer. BioMag Plus Concanavalin A coated beads (Polysciences: 86057-3) were equilibrated with Binding buffer (20 mM HEPES-KOH pH 7.9; 10 mM KCL; 1 mM $CaCl_2$; 1 mM $MnCl_2$). Beads (5 µL) were mixed with aliquots of 75,000 nuclei and incubated at 25 °C for 10 minutes followed by magnetic separation of beads. Beads were resuspended in 50 µL primary antibody (anti-macroH2A1 or anti-H3K27me3) or anti-mouse IgG in Wash buffer supplemented with 2 mM EDTA and 0.1% bovine serum albumin (BSA) and incubated on a nutator at 4 °C overnight. The beads were decanted on a magnet stand then resuspended in 50 µL secondary antibody in Wash buffer supplemented with 2 mM EDTA and 0.1% BSA and incubated on a nutator at room temperature for 1 hour. See **Table 3** for antibody sources and concentrations.

The beads were decanted on a magnet stand and washed with 200 µL Wash buffer, then were resuspended in 50 µL pA-Tn5 (1:200) in 300-Wash buffer (Wash buffer containing 300 mM NaCl) and incubated on a nutator at room temperature for 1 hour. The beads were washed twice with 200 µL 300-Wash buffer, then resuspended in 50 µL Tagmentation buffer (300-Wash buffer supplemented with 10 mM $MgCl_2$) and incubated at 37 °C for 1 hour. Beads were then washed with 50 µL TAPS wash buffer (10 mM TAPS pH 8.5, 0.2 mM EDTA), then resuspended in 5 µL

TAPS wash buffer supplemented with 0.1% SDS and incubated at 58 °C for 1 hour. SDS was neutralized on ice with 15 µL 0.67% Triton-X100. 2 µL of 10 mM indexed P5 and P7 primer solutions and 25 µL NEBnext High-Fidelity 2X Master Mix (New England BioLabs: ME541L) were added. Gap-filling and 15 cycles of PCR were performed using an MJ PTC-200 Thermocycler.

Library clean-up was performed by incubating beads with 65 µL SPRI bead slurry for 5-10 minutes, then magnetization and two washes with 200 µL 80% ethanol. Libraries were eluted with 22 µL Tris-HCl pH 8.0 and 2 µL was used for Agilent 4200 Tapestation analysis. The barcoded libraries were mixed to achieve equimolar representation as desired aiming for a final concentration as recommended by the manufacturer for sequencing on an Illumina HiSeq 2500 2-lane Turbo flow cell.

2.5.b CUT&Tag data processing.

CUT&Tag raw sequencing data were aligned to a custom genome made by concatenating human (hg38), HSV (JN555585.1), and E. coli (U00096.3 Escherichia coli str. K-12 substr. MG1655, complete genome). We performed alignments using bowtie2.

2.5.b.1 Domain calling.

Coverage at 100 bp windows of the human hg38 reference genome was calculated as number of reads of given length (120-1000 bp for the analyses presented here) that mapped at that window normalized by the factor N:

N=10,000/(Total number of reads that mapped to E. coli genome).

Here 10,000 is an arbitrarily chosen number. We used *E. coli* DNA as a spike-in to normalize all datasets. We partitioned all chromosomes into domains of macroH2A1: domains had an enrichment that was two times the genome-wide median and at least four-fold higher than the IgG control. The normalized coverage at each base-pair from each replicate was averaged when combining multiple replicates. The normalized read density in 100 bp bins were then smoothed

with a running average over the bins spanning +/- 1000 bp around each bin. We then calculated the genome-wide distribution of normalized read density and medians that were plotted in Figure S1. We averaged medians across WT macroH2A1 datasets (mock, 4 hpi, 8 hpi, and 12 hpi), and multiplied the average by 2, to set the cutoff for domain definition for macroH2A1 datasets. We defined a similar cutoff for H3K27me3 datasets using H3K27me3 WT datasets.

2.5.b.2 Identifying domain level dynamics of macroH2A1 over time course of infection.

To measure changes in macroH2A1 across time points where the domain boundaries are not the same, we first concatenated domain definitions from all macroH2A1 datasets and then defined a set of non-overlapping intervals using the “disjoin” method of GenomicRanges R package (Lawrence et al., 2013). We then calculated the log2 ratio of macroH2A1 enrichment over IgG for the non-overlapping regions for the mock, 4, 8, and 12hpi. The 4, 8, and 12hpi enrichments were then divided by the enrichment of the mock dataset to obtain change in macroH2A1 over time course at the non-overlapping regions. k-means clustering (k=6) using R (CiteR) was performed on the matrix where the rows are the non-overlapping regions and the columns are change in macroH2A1 over mock at 4, 8, and 12hpi. We extended the non-overlapping regions by 5 bp on each end and then merged regions within each cluster using “reduce” method of GenomicRanges, to obtain domains in each cluster. We recalculated change in macroH2A1 at 4, 8, and 12hpi over mock, which was used to plot heatmaps and boxplots shown in Figure 1 and Figure S1. H3K27me3 enrichment for WT and macroH2A1 KO cells was calculated at clustered macroH2A1 domains. The unique code for this work can be found here: https://doi.org/10.5281/zenodo.6783949

2.6 RNA sequencing.

2.6.a RNAseq library generation.

Three biological replicates per time point were obtained from independent infections. Cells were harvested at the indicated times post infection by trypsinization, washed with PBS and centrifuged at 5000 xg for 2 minutes. Pellets were lysed with TRIzol (Thermo Fisher: 15-596-026) and total RNA was harvested according to manufacturer's instructions. The RNA was then treated with DNase (Qiagen: 79254) on RNeasy columns (Qiagen: 74104) per manufacturer's instructions. RNA was precipitated with 3 volumes ice-cold 96% ethanol, 1 volume 3 M sodium acetate pH 5.5, and 1 µL glycogen (Thermo Fischer: R055) overnight at -80 °C. Precipitated RNA was pelleted at 15,000 xg and 4 °C for 30 minutes, washed with ice-cold 75% ethanol and spun as above for 10 min. Purified RNA was resuspended in nuclease-free water.

RNA was quantified by Nanodrop and integrity analyzed with the 4200 Tapestation Bioanalyzer system (Agilent). 500 ng of total RNA with an RNA Integrity Number (RIN) greater than 9.5 were used to prepare sequencing libraries with the TruSeq® Stranded mRNA Library Prep Kit (Illumina: 20020594). Library concentrations were measured with Qubit dsDNA HS Assay Kit (Thermo Fisher: Q32854) then analyzed with Agilent High Sensitivity D5000 ScreenTape System and pooled. Libraries were sequenced with 100-bp paired-end reads on an Illumina NovaSeq 6000 SP sequencer at the Fred Hutch Genomics Core Facility.

2.6.b RNAseq, 4sU-RNA and Hi-C data analysis.

Fastq files were filtered to exclude reads that didn't pass Illumina's base call quality threshold. STAR v2.7.1 (Dobin 2013 23104886) with 2-pass mapping was used to align paired-end reads to a combined reference of human genome build hg38 and HSV1 genome JN555585.1 (https://www.ncbi.nlm.nih.gov/nuccore/JN555585.1/).

FastQC 0.11.9 (https://www.bioinformatics.babraham.ac.uk/projects/fastqc/) and RSeQC 4.0.0 (Liguo Wang et al., 2012) were used for QC including insert fragment size, read quality, read

duplication rates, gene body coverage and read distribution in different genomic regions. FeatureCounts (Liao 2014 24227677) in Subread 1.6.5 was used to quantify gene-level expression by strand-specific paired-end read counting.

Gene annotation were based on GENCODE V31 (https://www.gencodegenes.org/human/) and GCA_000859985.2_ViralProj15217 (https://www.ncbi.nlm.nih.gov/data-hub/genome/GCF_000859985.2/). For HSV1, annotated genes were collapsed into non-overlapping transcribed regions, e.g. X indicating a transcribed region unique to gene X, X:Y indicating an overlapping transcribed region for genes X and Y, and so on.

Bioconductor package edgeR 3.26.8 (Robinson et al., 2010) was used to detect differential gene expression between sample groups. Genes with low expression were excluded by requiring at least one count per million in at least N samples (N is equal to the number of samples in the smaller group). The filtered expression matrix was normalized by TMM method (https://genomebiology.biomedcentral.com/articles/10.1186/gb-2010-11-3-r25) and subject to significance testing using quasi-likelihood pipeline implemented in edgeR. Genes were deemed differentially expressed if fold changes were greater than 2 in either direction and Benjamini-Hochberg adjusted p-values were less than 0.01.

The intervals representing start and end of each gene were intersected with clustered macroH2A1 domains to obtain cluster assignments for genes. Intersection was performed using “intersect” function of bedtools (Quinlan & Hall, 2010). Genes that did not uniquely intersect with domains in a single cluster were discarded. The cluster assignments for genes were used for plotting total RNA fold changes in Figure 3.6. Reads per kilobase of transcript per million reads mapped (RPKM) values for 4sU-RNA was obtained from GEO (GSE59717) and converted to transcripts per million (TPM). The TPM values across two 4sU-RNA replicates for each condition was averaged and box plots were generated similarly to total RNA.

For calculating eigenvector distributions, compartment wig file was downloaded from the following link: https://4dn-open-data-public.s3.amazonaws.com/fourfront-webprod/wfoutput/b543cbf4-ce54-4d2d-8960-281528ff18a6/4DNFI342UZP1.bw

Regions from compartment file intersecting with each domain cluster were extracted and the values were used for generating box plots shown in Figure 2D.

The CUT&Tag and RNA-seq data can be found here: **Series GSE209820**

2.7 Electron microscopy.

2.7.a Sample fixation and imaging.

Cells were fixed in 2% paraformaldehyde and 2.5% glutaraldehyde in 0.1M sodium cacodylate buffer (pH 7.3) at 4 °C. Fixed cells were rinsed briefly in 1% sucrose in 50mM cacodylate (pH 7.2), then postfixed on ice for 30 mins in a solution of 1% osmium (EM Sciences: RT19152) and 0.8% potassium ferricyanide in 50mM cacodylate (pH 7.2). Cell pellets were washed twice briefly at 25 °C in 1% sucrose in 50mM cacodylate (pH 7.2), then washed in three changes of 50mM cacodylate (pH 7.2) for 5 min each. Cell pellets were treated with 0.2% tannic acid (Sigma-Aldrich: 1401-55-4) in 50 mM cacodylate (pH 7.2) for 15 minutes at 25 °C, then rinsed several times in water. Cells were dehydrated through a graded ethanol series and embedded in Epon 12 resin (Ted Pella: 18010). 70 nm thin sections were cut using an Ultracut UC7 ultramicrotome (Leica Mikrosysteme) and collected on 200 mesh formvar/carbon copper grids (Ted Pella: 01800). Sections were stained with 2% aqueous uranyl acetate and Reynolds lead citrate. Cell pellet sections were imaged using a Talos L120C microscope operated at 120kV with a Ceta-16M (4096 x 4096) camera (Thermo Fisher Scientific).

All data were collected at spot size 5 with a 100um C2 aperture and 70um objective aperture. For quantification, nuclei were targeted at 1250x and manually circled. Autofocus was set to 2.0 µm. Nuclei were then imaged at 11000x as a montage and stitched together automatically using SerialEM (Nexperion Inc). Stitched maps were exported as uncompressed 16-bit .tif files for

further analysis. For qualitative analysis, images were manually focused to -2.0 µm defocus and then 20 1-second frames were collected and drift-corrected using Velox software (Thermo Fisher Scientific, Eindhoven, NL). Final summed images were exported as 16-bit .tif files and cropped using ImageJ.

2.7.b EM image analysis.

Image analysis pipelines for counting capsids and for measuring chromatin density at the nuclear envelope were deployed in MATLAB R2020b. Scripts are available on the Fred Hutch GitHub repository. Capsid pipeline follows three steps: 1) nuclear boundaries identification, 2) capsid detection, 3) capsid classification. Nuclear boundaries were identified with user input, by outlining a freehand contour of the nucleus of interest, from which a binary mask is extracted. Capsid detection was performed on the median-filtered complement of the original image, using a Circular Hough Transform based algorithm, with phase coding for radii estimation (Atherton & Kerbyson, 1999), and search radius ranging from 10.6 to 31.7 nm. Capsids residing within the nuclear mask were then counted and classified. Detected capsids were classified in three categories (Empty, Intermediate and Full), depending on the distribution of the pixel grayscale intensities within the capsids relative to a normal distribution.

Width of heterochromatin abutting the nuclear envelope was quantified by measuring the length of the binarized chromatin from 1D intensity profiles along the normal of the nuclear perimeter, sampled at every 10 perimeter pixels. Dense heterochromatin was binarized using global Otsu's thresholding method applied to the background-corrected complement of the contrast-adjusted original image. Noise from the binarized image was further reduced by applying a 2D order statistic filter using the minimum value of a varying domain interactively defined by the user, with default value of 8-by-8 pixels. The resulting heterochromatin density distribution was normalized to the total length of the nucleus' perimeter.

Table 1: Cell line sources.

Cell Line	**Source**
Human: RPE (hTERT-immortalized)	Gift of E. Hatch Lab (Hatch et al., 2010) (Invitrogen)
Human: Primary HFF	Gift of D. Galloway Lab
Human: HFF (hTERT-immortalized)	Gift of J. Kamil Lab (Gang Li et al., 2015)
African Green Monkey: Vero	Gift of A. Geballe Lab (Child et al., 2021)

Table 2: Primers used for macroH2A1 knockout, overexpression, rescue, and for ddPCR or qPCR of viral genomes.

Application	Name	Sequence
CRISPR/Cas9 knockout of macroH2A1	MacroH2A1 gRNA	CCTCAATAGCAAGCCATCCTGT
qPCR and ddPCR	HSV1_gB_qPCR_F1	CCGTCAGCACCTTCATCGA
	HSV1_gB_qPCR_R1	CGCTGGACCTCCGTGTAGTC
ddPCR	HSV1_gB_probe1	6FAM-CCACGAGATCAAGGACAGCGGCC-BHQ1
	beta-globin_qPCR_F1	TGAAGGCTCATGGCAAGAAA
	beta-globin_qPCR_R1	GCTCACTCAGTGTGGCAAAGG
	beta-globin_probe2_hex	/5HEX/TC CAG GTG AGC CAG GCC ATC ACT A/3BHQ_1/
qPCR	H_TUBB_gDNA_pPCR_F2	ACCAACCTACGGGGATCTGAA
	H_TUBB_gDNA_pPCR_R2	TTGACTGCCAACTTGCGGA
Mutagenesis of gRNA binding site in gDNA	mH2A1_mut-for-cas9-resistance_F1	GGGACGGGTCACACCCAGACATATCTT GCTGGCTGTGGCCAATGATG
	mH2A1_mut-for-cas9-resistance_R1	CATCATTGGCCACAGCCAGCAAGATAT GTCTGGGTGTGACCCGTCCC
Swap FLAG tag for HA tag	mH2A1-flag-to-HA_F1	TACCCATACGATGTTCCAGATTACGCTT AGTAGCCCGGGATCCCGCGACTCTAG
	mH2A1-flag-to-HA_R1	AGCGTAATCTGGAACATCGTATGGGTA GTTGGCGTCCAGCTTGGCCATTT

Swap pLVX puromycin resistance to hygromycin resistance	PuroToHygro_Insert_pLVX_F1	CCTGCAGCCCAAGCTTACCATGAAAAAGCCTGAACTCA
	PuroToHygro_Insert_pLVX_R1	GGTTGATTGTTCCAGACGCGGCTATTCCTTTGCCCTCG
	PuroToHygro_Vector_pLVX_F1	TGAGTTCAGGCTTTTTCATGGTAAGCTTGGGCTGCAGG
	PuroToHygro_Vector_pLVX_R1	CCGAGGGCAAAGGAATAGCCGCGTCTGGAACAATCAAC
Swap pLVX puromycin resistance for blasticidin resistance	PuroToBlast_Vector_pLVX_F1	tcttgagacaaaggcttggccaTGGTAAGCTTGGGCTGC
	PurotoBlast_Vector_pLVX_R1	ggttatgtgtgggagggctgaCCGCGTCTGGAACAATCAAC
	PuroToBlast_Insert_pLVX_F1	CCTGCAGCCCAAGCTTACCatggccaagcctttgtctcaaga
	PuroToBlast_Insert_pLVX_R1	GTTGATTGTTCCAGACGCGGtcagccctccacacataaccaga

Table 3: Sources and conditions of antibodies used.

Antibody	Source	Catalog #	Concentration
Mouse anti-actin	Abcam	5441	WB (1:10,000)
Mouse anti-gH	Abcam	110227	WB (1:1,000)
Rabbit anti-H3	Abcam	1791	WB (1:20,000) IF (1:1,000)
Rabbit anti-H3K27me3	Cell Signal Technologies	9733T	WB (1:1,000) CUT&Tag (1:100) IF (1:800)
Rabbit anti-H3K9me3	Abcam	8898	WB (1:1,000)
Rabbit anti-H4	Abcam	10158	WB (1:1,000)
Mouse anti-ICP0	Santa Cruz Biotechnology	53070	WB (1:1,000)
Mouse anti-ICP8	Abcam	20194	IF (1:500)
Rabbit anti-macroH2A1	Abcam	37264	WB (1:1,000) CUT&Tag (1:100)
Rabbit anti-macroH2A1.1	Cell Signaling Technology	12455S	WB (1:1,000)
Mouse anti-macroH2A1.2	Cell Signaling Technology	4827S	WB (1:1,000)
Rabbit anti-macroH2A2	Active Motif	39874	WB (1:1,000)
Rabbit anti-FLAG	Sigma Aldrich	F7425	IF (1:1,000)
HRP-conjugated anti-VP16	Santa Cruz Biotechnology	7546	WB (1:1,000)
Peroxidase-AffiniPure Goat Anti-Mouse	Jackson Immunoresearch Laboratories	115-035-003	WB (1:5,000)
Peroxidase-AffiniPure Goat Anti-Rabbit	Jackson Immunoresearch Laboratories	111-035-045	WB (1:5,000)

Goat anti-mouse Alexa™ Fluor 488	ThermoFisher	A-11001	IF (1:300)
Goat anti-rabbit Alexa™ Fluor 568	ThermoFisher	A-11011	IF (1:300)
Rabbit anti-mouse IgG	Abcam	46540	CUT&Tag (1:100)
Guinea pig anti-rabbit IgG	Antibodies Online	AB1N101961	CUT&Tag (1:100)

Chapter 3. HSV-1 requires heterochromatin channels supported by macroH2A1 and H3K27me3 for efficient nuclear egress.

3.1 Introduction.

Herpes simplex virus 1 (HSV-1) replicates its genome in the host cell nucleus, where it contends with host chromatin to create a nuclear environment favorable for viral infection. The virus utilizes host histones to regulate viral gene expression during both lytic and latent infection (Cliffe et al., 2009a, 2009b, 2015; Cliffe & Knipe, 2008; Lee et al., 2016; Liang, Quenelle, et al., 2013; Raja et al., 2016); the virus also re-organizes host chromatin and the nuclear lamina to impact nuclear architecture (Monier et al., 2000; Reynolds et al., 2004; Silva et al., 2008; Turan et al., 2019). Lytic viral replication occurs in subnuclear regions termed viral replication compartments, which exclude host factors detrimental to viral replication (Roizman et al., 2013). The host genome is also excluded from viral replication compartments and becomes compacted at the periphery of the nucleus (Monier et al., 2000). This redistribution and compaction cause an increase in transcriptionally silenced and condensed heterochromatin at the nuclear periphery (Aho et al., 2021; Myllys et al., 2016).

While small molecules and individual proteins can diffuse freely throughout the nucleus, movement of macromolecular complexes >100 nm are restrained to interchromatin spaces (Bosse et al., 2014, 2015). HSV-1 capsids, which are 125 nm in diameter, are assembled and packaged with viral genomes in replication compartments; they then must traverse the barriers posed by the peripheral heterochromatin and lamina meshwork in order to egress from the nucleus. Electron microscopy and soft x-ray tomography of infected cells have demonstrated that capsids can access the nuclear envelope through regions of less dense chromatin termed heterochromatin channels (Aho et al., 2017, 2019, 2021; Myllys et al., 2016). However, the

mechanism by which these channels form and whether they are necessary for viral egress is unclear.

Heterochromatin density and subnuclear localization is affected by the presence and ratio of specific histone modifications. In uninfected cells, histone modifications such as trimethylation of histone H3 lysine 27 (H3K27me3) and the histone variant macroH2A1 delineate heterochromatin regions that are largely localized at the nuclear periphery. Furthermore, macroH2A1 also demarcates regions of host chromatin that associate with the nuclear lamina, termed lamina-associated domains (LADs), suggesting that macroH2A1 connects peripheral heterochromatin to the nuclear envelope to support nuclear integrity (Douet et al., 2017; Fu et al., 2015). Importantly, loss of macroH2A1 and macroH2A2 results in a significant decrease in heterochromatin in the nuclear periphery observed by electron microscopy (Douet et al., 2017).

The aim of my PhD has been to characterize the role of heterochromatin in HSV-1 infection, specifically through investigating macroH2A1 and H3K27me3 localization and impact on HSV-1 fitness.

3.2 Contributions.

Like the vast majority of science, the project presented in this thesis is the result of a team effort. For completeness and clarity of discussion, in this chapter I have included results that were obtained by members of the Avgousti Lab, our collaborator Srinivas Ramachandran, or collaborative experiments. I will clarify my own and others' contributions in each sub-section. These results are submitted for publication in a manuscript for which I am a co-first author (Lewis and Kelnhofer-Millevolte, BioRxiv 2022).

3.3 Expression of macroH2A1 and H3K27me3 increases during lytic HSV-1 infection.

To determine how lytic infection impacts expression of host heterochromatin factors, Daphne Avgousti, Laurel Kelnhofer-Millevolte and I mined a large dataset of proteomics conducted during

lytic HSV-1 infection in primary human foreskin fibroblasts (HFFs) (Kulej et al., 2017). These data reveal global dysregulation of multiple host heterochromatin factors as a consequence of infection, including dramatic upregulation of macroH2A1 and H3K27me3. Specifically, peptides from macroH2A1.2 are increased in abundance late during infection (Figure 3.1A). Several peptides corresponding to H3K27me3 also increase during infection; when combined, the average trend shows upregulation similar to macroH2A1 protein levels (Figure 3.1B).

I confirmed these expression patterns through western blotting in two cell types: retinal pigment epithelial cells (RPEs) (Figure 3.1C) and HFFs (Figure 3.2). I use primary and immortalized versions of these two cell lines throughout this thesis as they both represent common sites of lytic HSV-1 infection (Spear, 2004; TOPP et al., 1997). I observed consistent increase of isoforms macroH2A1.1 and macroH2A1.2 in both cell types, but detection of the increase in total macroH2A1 and H3K27me3 was variable between experimental replicates. Notably, expression of macroH2A2 does not change during infection in either cell line (Fig 3.1C and Figure 3.2). I also evaluated a panel of viral proteins to examine infection progression: ICP0 (immediate early (Cai & Schaffer, 1992)), VP16 (early-late (Naldinho-Souto et al., 2006)), and gH (late-late (Lorentzen et al., 2001)).

Intriguingly, we found that macroH2A1 phosphorylation increases during infection at two currently uncharacterized phosphosites: serines 170 and 173 (Figure 3.1D). Phosphorylation at both of these residues peaks around 6 hours post infection, which corresponds to the time point at which I consistently detect macroH2A1 increase by western blot. Because no antibodies have yet been raised to detect either of these specific phosphorylation marks, I was unable to validate these phosphorylations through western blotting. Only one post translational mark of macroH2A1 has been characterized to date: phosphorylation at S137 can exclude macroH2A1 from the inactive X chromosome (Bernstein et al., 2008). Although I was unable to investigate the causes or consequence of macroH2A1 phosphorylation during HSV-1 infection, it is an interesting avenue for further study.

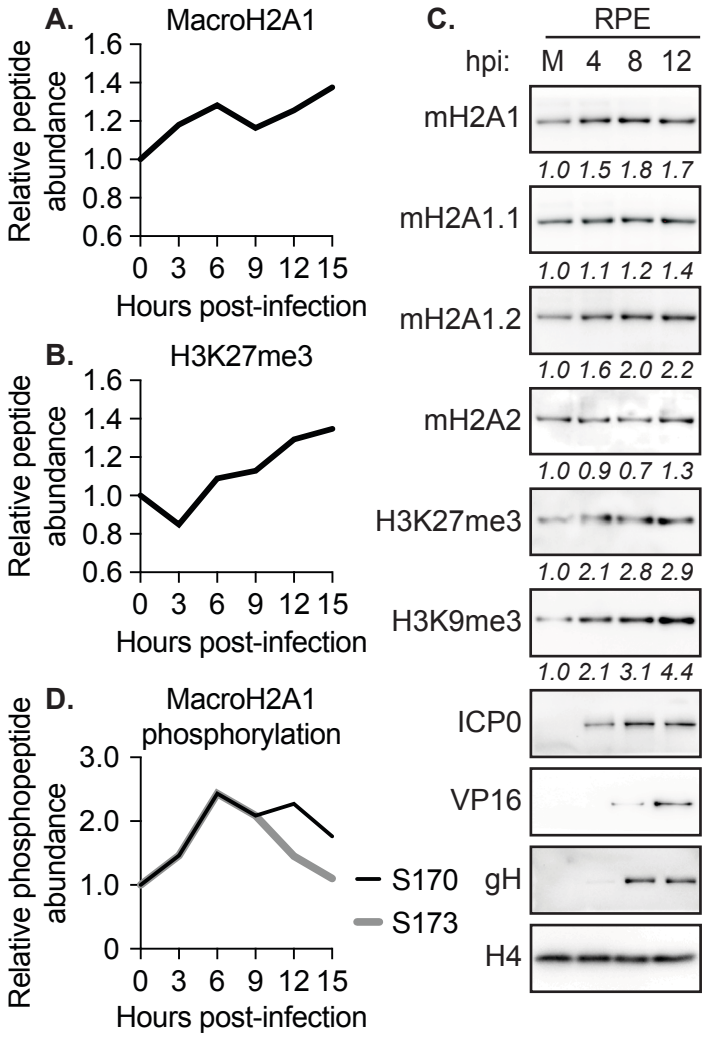

Figure 3.1 Heterochromatin marks macroH2A1 and H3K27me3 increase in abundance during lytic HSV-1 infection.

A. Relative peptide abundance of total macroH2A1 detected by mass spectrometry over the course of HSV-1 infection at MOI 3 in primary HFFs (data mined from Kulej 2017 28179408). Values shown are normalized to mock levels. **B.** Same as *A.* for H3K27me3 peptide levels. **C.** Western blot of total macroH2A1 (mH2A1), mH2A1.1, mH2A1.2, mH2A2, H3K27me3 and H3K9me3 during HSV-1 infection at MOI 3 in hTERT-immortalized RPEs. Time points shown are: mock infected (M), 4, 8, and 12 hours post infection (hpi). Relative quantification below indicated blots shows fold-change of loading control-normalized protein abundance over M. ICP0, VP16, gH are shown as representative HSV-1 proteins. H4 is a loading control. **D.** Relative phosphopeptide abundance of macroH2A1 at two residues detected as in **A.** Levels of phosphorylated peptides are normalized to total protein peptide abundance and to mock values.

To determine whether viral replication is necessary for increase of macroH2A1, I infected HFFs in the presence of viral DNA polymerase inhibitor phosphonoacetic acid (PAA) (Shipkowitz 4356456). (Figure 3.2). I observed markedly decreased levels of viral proteins because of slowed HSV-1 replication (Figure 3.2A). I quantified the intensity of macroH2A1 proteins and corrected for loading through normalization to total histone levels detected by ponceau stain. I then compared protein levels to mock-infected cells and found that expression of macroH2A1 isoforms increase despite reduced HSV-1 replication (Figure 3.2C), albeit at later time points during infection than cells not treated with PAA. This implies that the increase in macroH2A1 during infection may be a host response to viral infection and does not rely on HSV-1 genome replication.

The role of macroH2A1 in response to cell stress has been studied in the context of oncogene overexpression and heat shock (Hongshan Chen et al., 2015; Ouararhni et al., 2006). My results are the first to describe macroH2A1 expression due to viral infection.

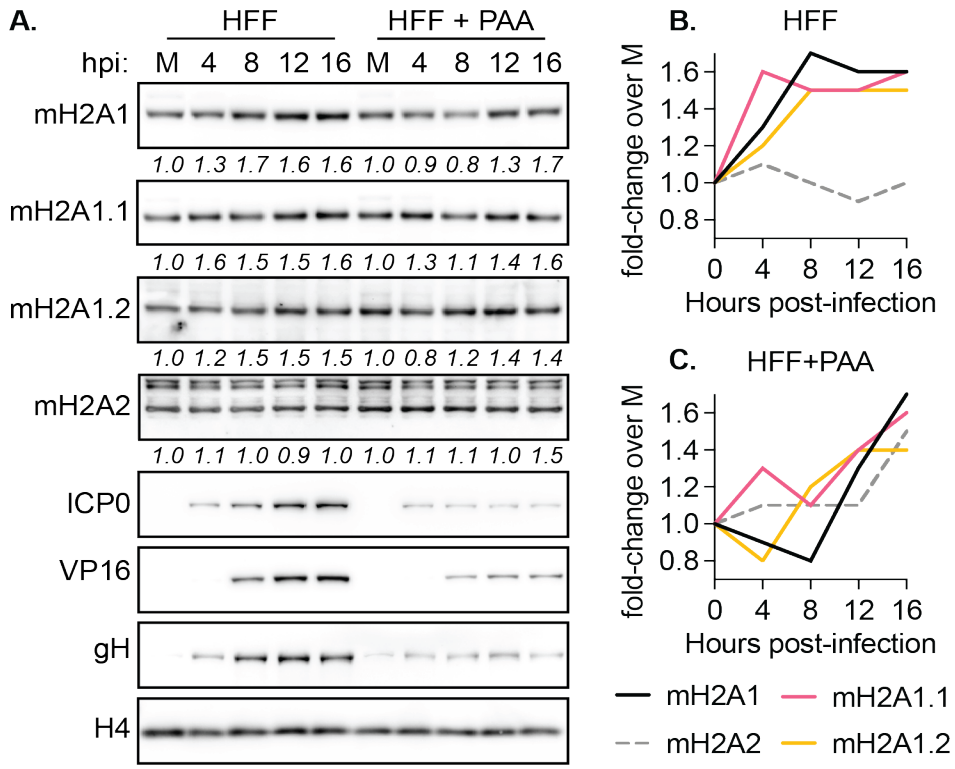

Figure 3.2 MacroH2A1 protein levels increase during HSV-1 infection when viral DNA replication is inhibited. **A.** Western blot of total macroH2A1 (mH2A1), mH2A1.1, mH2A1.2, and mH2A2 during HSV-1 infection at MOI 3 in primary HFFs either untreated (HFF) or treated (HFF + PAA) with HSV-1 polymerase inhibitor PAA. Time points shown are: mock infected (M), 4, 8, 12, and 16 hours post infection (hpi). Relative quantification below indicated blots shows fold-change of loading control-normalized protein abundance over M. ICP0, VP16, gH are shown as representative HSV-1 proteins. H4 is a loading control. **B.** Values from *A.* plotted to show macroH2A1 increase in untreated HFFs. **C.** Values from *A.* plotted to show macroH2A1 increase in HFFs treated with PAA.

3.4 MacroH2A1 and H3K27me3 dynamically bind broad regions on the host genome during infection.

I next asked how macroH2A1 and H3K27me3 genomic profiles changed during HSV-1 infection. I used CUT&Tag (Kaya-Okur et al., 2019) to profile the genomic localization of both marks at 4, 8 and 12 hours post infection and mock-infected cells. To validate the specificity of

the antibody raised against macroH2A1 for CUT&Tag, I profiled macroH2A1 in both WT and macroH2A1 knockout (KO) HFF-T generated through CRISPR/Cas9 mutagenesis (see Chapter 2 for procedure). To evaluate how H3K27me3 localization is disrupted upon macroH2A1 KO, I profiled H3K27me3 in both WT and macroH2A1 KO HFF-T. The H3K27me3 antibody I used was validated for CUT&Tag, so I did not perform a negative control CUT&Tag on H3K27me3-depleted cells. I used IgG as a control for antibody binding and transposase activity in both WT and macroH2A1 KO cells.

With the aid of Srinivas Ramachandran, I aligned my CUT&Tag reads to a custom-built genome encompassing the human genome (hg38), the HSV-1 genome (JN555585.1), and the E. coli genome as a spike-in control. We normalized reads to hg38 or the HSV-1 genome to the spike-in and compared read density across conditions. Due to low reads of our IgG control on the host genome, we combined the reads from all 4 time points (Mock, 4, 8 and 12 hours post infection) into one control “IgG” (Figure 3.3A and B). Both macroH2A1 (Figure 3.3A) and H3K27me3 (Figure 3.3B) have clear enrichment on the host genome compared to IgG in WT cells. However, macroH2A1 enrichment on host genomes is lost in macroH2A1 KO cells as read density at all time points dropped below IgG (Figure 3.3A); H3K27me3 read density on host genomes is not impacted by macroH2A1 KO (Figure 3.3B).

Dr. Ramachandran next compared normalized reads mapped to the HSV-1 genome. Generally, read density on HSV-1 genomes is increased across all conditions compared to the read density on host genomes (Figure 3.3C-D). This dramatic increase in read density may be due to the small size of the HSV-1 genome compared to the human genome, the large number of HSV-1 genomes at late time points during infection and/or to overall increased accessibility of replicating HSV-1 genomes. We observe a similar enrichment of macroH2A1 on viral genomes between WT and macroH2A1 KO cells (Figure 3.3C); this is in contrast to the drastically reduced reads on host genomes upon macroH2A1 KO (Figure 3.3A). Similarly, the read density for H3K27me3 is in the same range as the read density for IgG on viral genomes (Figure 3.3D).

Together, these data indicate that there is a significant background of reads mapping to viral genomes that cannot be accounted for. We therefore focused our analysis on the host genome.

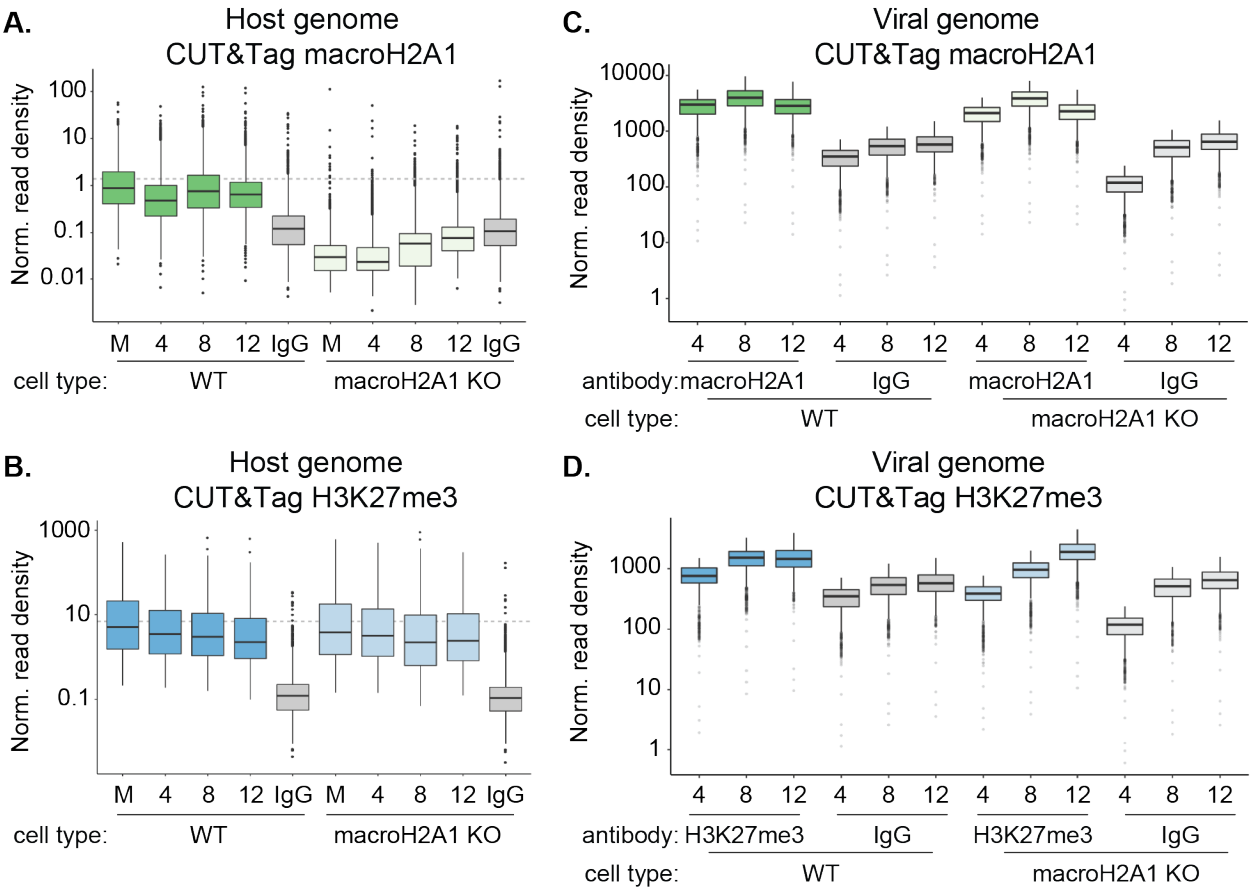

Figure 3.3 Quantification of macroH2A1 and H3K27me3 enrichment on host and viral genomes during HSV-1 infection. A. Spike-in normalized CUT&Tag read density of macroH2A1 on WT and macroH2A1 KO HFF-T host genomes during HSV-1 infection. **B.** Spike-in normalized CUT&Tag read density of H3K27me3 on WT HFF-T and macroH2A1 KO HFF-T host genomes during HSV-1 infection. **C.** Spike-in normalized CUT&Tag read density of macroH2A1 on HSV-1 genomes during infection of WT and macroH2A1 KO HFF-T. **D.** Spike-in normalized CUT&Tag read density of H3K27me3 on HSV-1 genomes during infection of WT and macroH2A1 KO HFF-T.

In agreement with prior reports, we observed that macroH2A1 and H3K27me3 form large domains on the human genome that can span hundreds of kilobases (Hongshan Chen et al., 2014; Gamble et al., 2010; Gaspar-Maia et al., 2013; Sun et al., 2018). These domains are dramatically rearranged during HSV-1 infection; some regions gain macroH2A1 and H3K27me3 (Figure 3.4A) enrichment while others lose enrichment (data not shown). This suggests a large-scale reorganization of heterochromatin in response to HSV-1 infection.

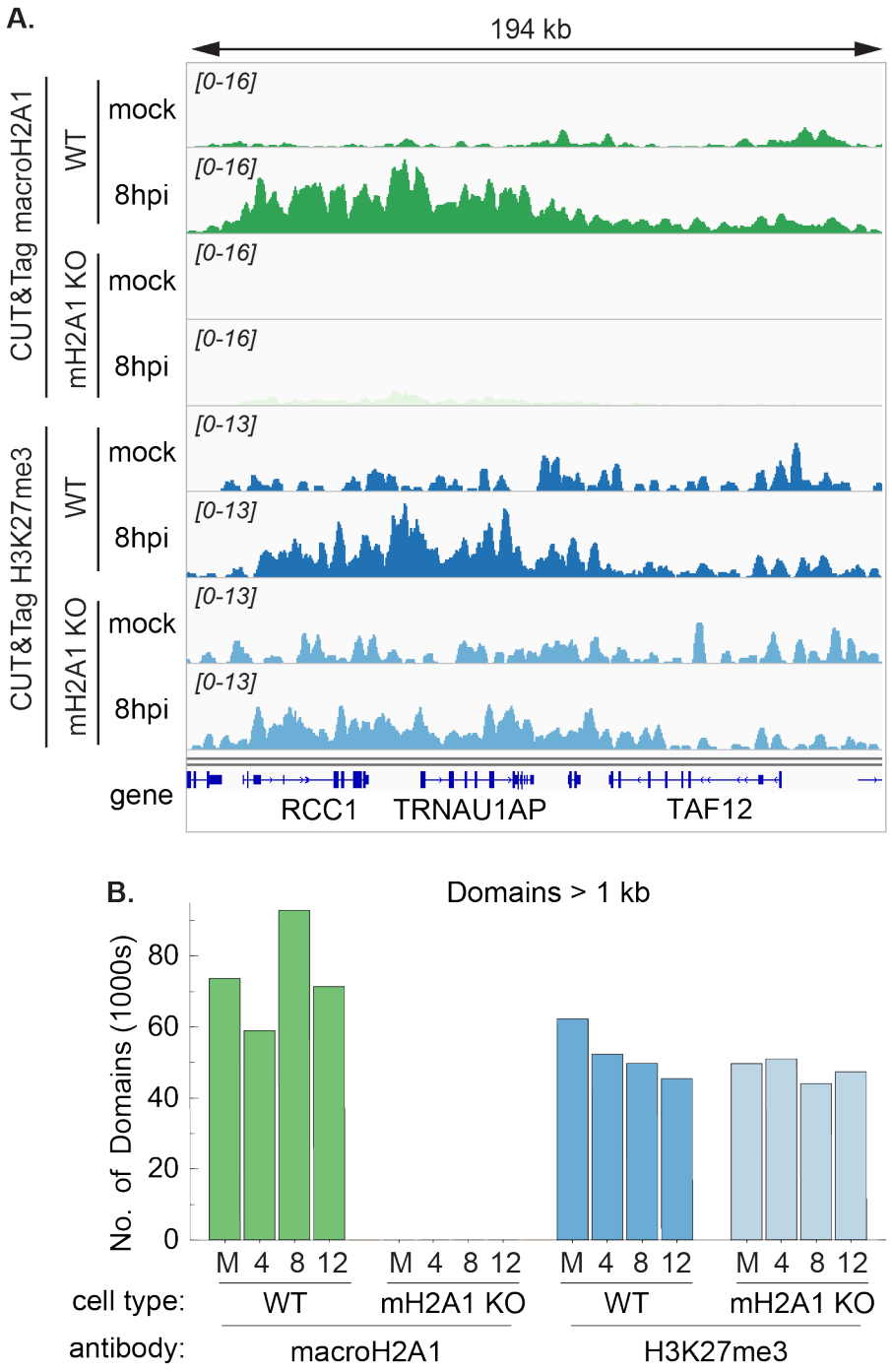

Figure 3.4. MacroH2A1 and H3K27me3 form broad regions on the host genome that change during infection. A. Representative genome browser snapshots of spike-in normalized CUT&Tag enrichment of macroH2A1 and H3K27me3 showing increases at 8 hpi of HSV-1 infection as measured by CUT&Tag in WT or macroH2A1 KO HFF-T as indicated. The region corresponding to chromosome 1, 28,500 kb to 28,660 kb is shown. **B.** Total number of macroH2A1 and H3K27me3 domains over 1 kb as measured by CUT&Tag of WT and macroH2A1 KO HFF-T host genomes during HSV-1 infection.

The large domains formed by macroH2A1 and H3K27me3 are not amenable to peak-based analysis, so we used a tailored domain-based analysis developed by Dr. Ramachandran. Briefly, normalized read density was evaluated in 100 bp windows over the human genome, and domains were called as regions greater than 1,000 bp enriched in macroH2A1 twice over the genome-wide median of macroH2A1 enrichment and four times higher than the IgG control. Using this approach, he identified 70,000 macroH2A1 domains and 50,000 H3K27me3 domains across the genome (Figure 3.4B). In contrast, we observed fewer than 10 macroH2A1 domains in the KO cells, indicating the specificity of the antibodies and algorithms (Figure 3.4B).

To identify patterns of macroH2A1 loss and gain during infection, Dr. Ramachandran then calculated the change in enrichment of macroH2A1 domains at each time point compared to mock-infected domains and stratified into 6 groups using k means clustering (Figure 3.5A). We observed that two clusters gained significantly more macroH2A1 during infection (Clusters 5 and 6), three clusters had a significant decrease in macroH2A1 (Clusters 1-3), and one cluster (Cluster 4) had a minor gain in macroH2A1 (Figure 3.5A left and 3.5C). We then compared the patterns of H3K27me3 enrichment and found that H3K27me3 occupancy overall follows similar patterns to macroH2A1 (Figure 3.5A middle and 3.5C).

We next asked whether H3K27me3 was dependent on macroH2A1. We examined the patterns of H3K27me3 during infection in macroH2A1 KO cells and found that the trends are similar to H3K27me3 patterns in WT cells (Figure 3.5A right and 3.5D). We concluded that H3K27me3 deposition is independent of macroH2A1, which agrees with published results showing that macroH2A1 knockdown in murine fibroblasts does not alter H3K27me3 levels or genome occupancy (Gaspar-Maia et al., 2013). Other results have confirmed that, while the two marks often co-localize, their deposition is independent and leads to functional redundancy for transcriptional repression. Taken together, our results indicate that heterochromatin formation at specific host genomic loci during infection is mediated by at least two redundant mechanisms.

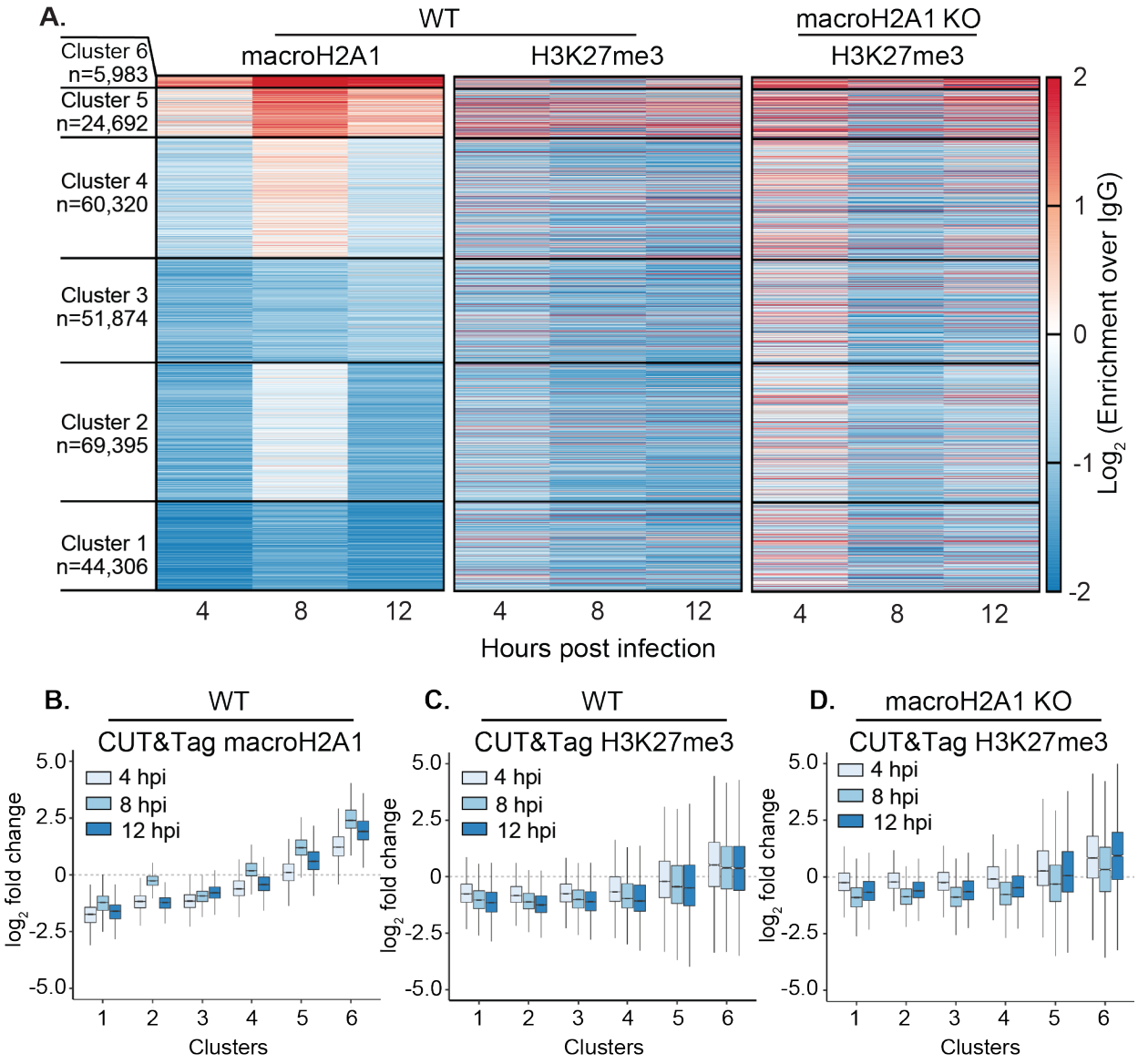

Figure 3.5 Quantification of macroH2A1 and H3K27me3 bound regions on host genomes during HSV-1 infection. A. Changes in log2 enrichment of spike-in normalized CUT&Tag of macroH2A1 and H3K27me3 over IgG compared to mock treatment are shown as a heatmap. Each line in the heatmap represents a domain of macroH2A1 enrichment. **B.** Quantification of heat maps from *A.* showing macroH2A1 enrichment across the clusters. **C.** Quantification of heat maps from *A.* showing H3K27me3 enrichment in clusters defined by macroH2A1 as in *B*. **D.** Quantification of heat maps from *A.* showing H3K27me3 enrichment in clusters defined by macroH2A1 as in *B.*

3.5 Enrichment of macroH2A1 and H3K27me3 corresponds with host transcriptional repression.

To evaluate the transcriptional impact of macroH2A1 deposition during infection, I performed RNA sequencing to measure host and viral gene expression. Dr. Ramachandran calculated the fold-change of host mRNAs at each time point compared to expression in mock infected cells and plotted the trends in gene expression against the previously defined CUT&Tag clusters (Figure 3.6A). We found that macroH2A1 presence anti-correlates with transcription; the clusters that lose macroH2A1 (Clusters 1-3) show a general increase in total RNA levels, where genes within regions that gain macroH2A1 (Clusters 4-6) generally lose expression. Importantly, these overall patterns are unchanged in macroH2A1 KO cells (Figure 3.6B), suggesting macroH2A1 is not driving transcriptional changes and may be deposited after transcription is lost at those loci.

We compared macroH2A1 and H3K27me3 occupancy on host genomes to patterns of new transcription during infection. Dr. Ramachandran plotted the expression of newly transcribed genes from a published dataset of 4sU-labeled RNA during HSV-1 infection in HFFs (Rutkowski et al., 2015) according to their genomic localization in the previously defined clusters (Figure 3.6C). We found that active transcription in mock-infected cells occurs in regions that gain macroH2A1 during infection (Clusters 5-6); new transcription of these genes then decreases during infection, which is consistent with our total mRNA data. Importantly, new transcription decreases over the time course of infection: expression at 7-8 hpi is much lower than at 3-4 hpi which is lower than mock-infected cells (Figure 3.6C). In contrast, genes within Clusters 1-3 are not expressed in mock infected cells but gain expression as a consequence of infection. This is consistent with macroH2A1 and H3K27me3 loss identified by our CUT&Tag analysis. Interestingly, Cluster 4, which showed gain of macroH2A1 only at 8 hpi (Figure 3.5B) and H3K27me3 loss at all time points, showed an intermediate phenotype: new transcription increased whereas total mRNA decreased. This indicates that weak macroH2A1 gain may contribute to general transcriptional repression even if some genes in this region become more

transcribed. Together, these data indicate that macroH2A1 and H3K27me3 occupancy on the host genome correlates with transcriptional repression of regions that were actively transcribed prior to infection, consistent with formation of new heterochromatin during infection.

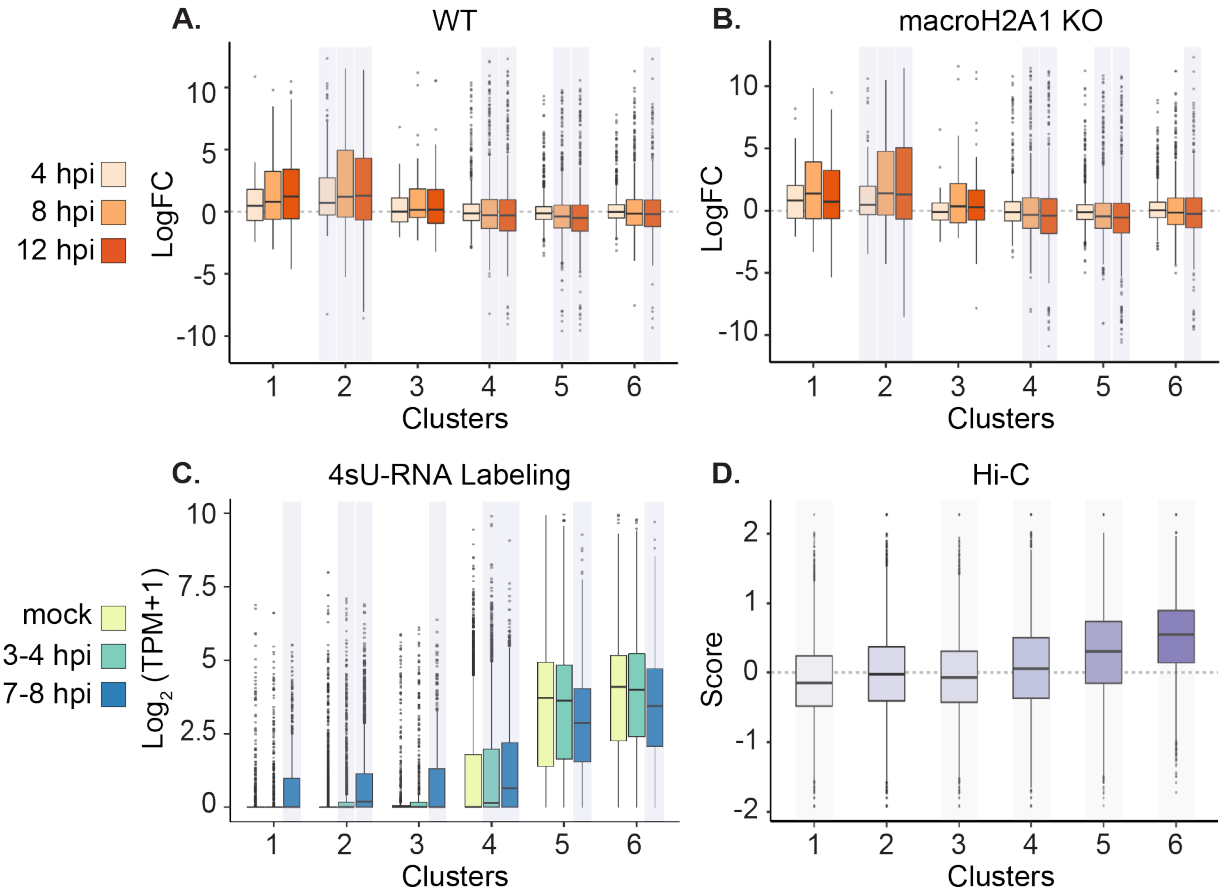

Figure 3.6. MacroH2A1 and H3K27me3 presence on host genomes correlates with decreased transcription. **A.** Box plots of total host RNA from RNA-seq in WT HFF-T for genes within clusters from Figure **3.3**. Kolmogrov-Smirnov test (in R) was performed comparing logCPM values of genes at each time point with logCPM values of genes from mock dataset for each cluster. The p-values were corrected for multiple testing, and the time points and clusters with corrected p-value less than 0.05 are shaded. **B.** Same as *A.* for macroH2A1 KO HFF-T. **C.** 4sU-RNA counts for genes from Hennig overlapping with clusters from Figure **3.3** shown as box plots and shading as indicated in *A.* **D.** Box plots of Hi-C eigenvector scores of regions overlapping with clusters from Figure 2. The Hi-C compartment eigen vector scores were obtained from the 4DN project website. Wilcoxon signed rank test with alternate hypothesis that the true location is not equal to 0 was performed on the distribution of eigen vector scores for each cluster. The p-values were corrected for multiple testing, and the clusters with corrected p-value less than 0.05 are shaded. Bonferroni correction was used for p-value adjustments.

We next asked whether the regions of macroH2A1 and H3K27me3 gain or loss occur in distinct genome compartments. Specifically, we asked which regions are found in the A compartment (associated with open chromatin) or in the B compartment (associated with closed chromatin). Dr. Ramachandran analyzed Hi-C data of fetal lung fibroblast line IMR90 from the 4DN project (Rao et al., 2014) to define the A/B compartments in a cell line that is comparable to our system. He performed an eigenvector analysis of the Hi-C contact matrix to determine which regions fall into the A (positive eigenvalues) or B (negative eigenvalues) compartments and plotted the eigenvalues against the previously defined clusters (Figure 3.6D). We find that all clusters except Cluster 2 are significantly associated with either of the two compartments. Regions in Clusters 1 and 3 have median eigenvalues below zero, indicating that they are far more likely to be found in the inactive B compartment of the genome. Conversely, regions in Clusters 4-6 have median eigenvalues above zero, indicating that they are associated with the active A compartment. Strikingly, the median of the eigenvalues increases moving from Clusters 4 to 6, a pattern that correlates with the increasing gain of macroH2A1 and H3K27me3 at these regions. We concluded that macroH2A1 and H3K27me3 presence correlates with decreased transcription in active compartments during HSV-1 infection. Overall, these data suggest that regions that are the most active and open prior to infection form new heterochromatin during infection due to deposition of macroH2A1 and H3K27me3.

Finally, we asked what classes of genes are found in the regions that macroH2A1 and H3K27me3 bind during the course of infection. Dr. Ramachandran performed a Gene Ontology (GO) analysis of the most significantly enriched GO categories within the 6 clusters (the top 5 of each cluster are plotted in Figure 3.7). We found that certain genes within Clusters 1 and 2 (regions that lose macroH2A1/H3K27me3 during infection and have low RNA expression at baseline that increases during infection) are associated with immune signaling and inflammatory responses such as the response to dsRNA. Increased expression of these genes is consistent with the cellular immune response to viral infection. However, genes within Clusters 4-6 (regions

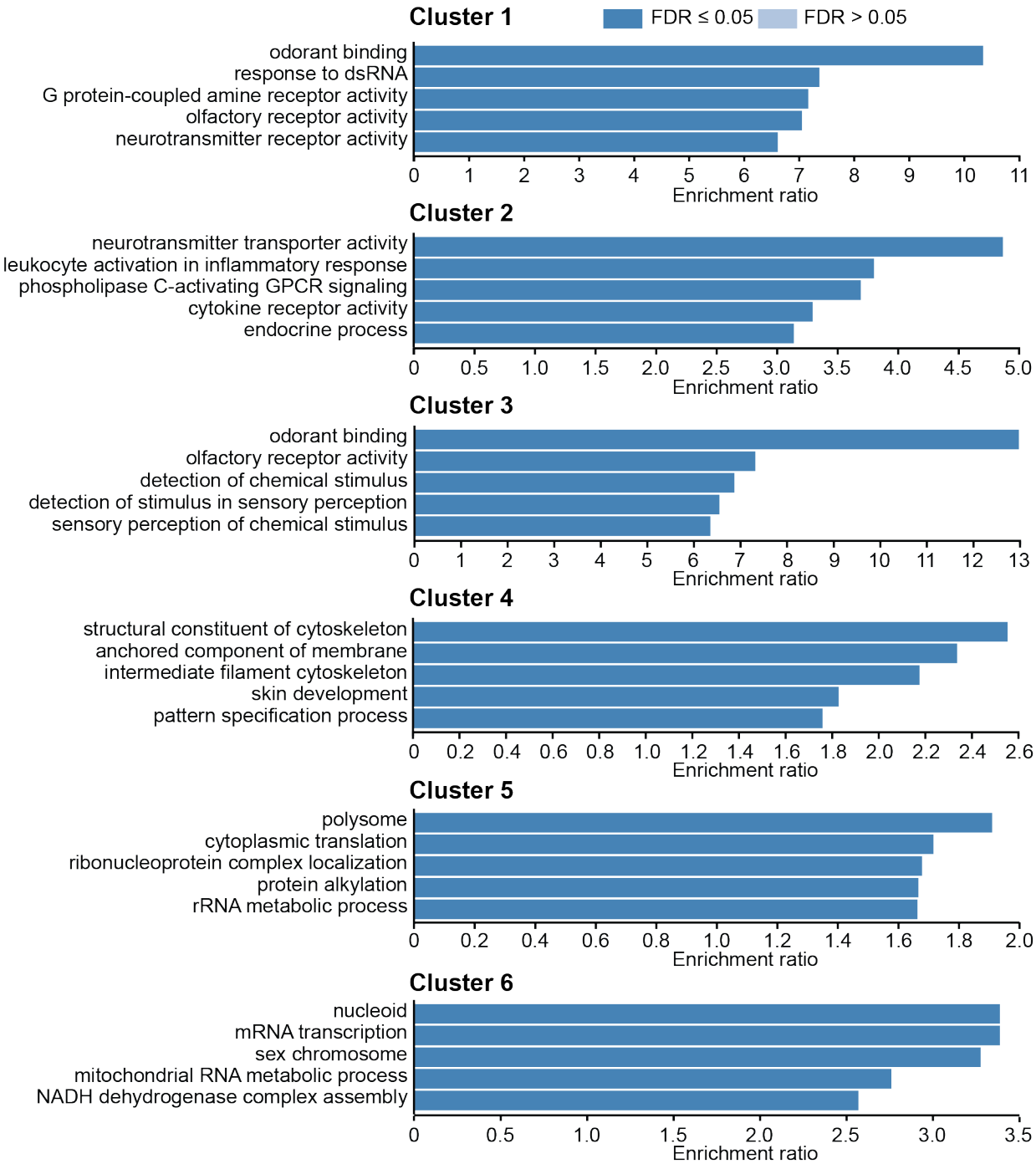

Figure 3.7. Gene ontology enrichment analysis of total host mRNA defined by macroH2A1 clusters.
Gene ontology analysis of mRNA levels between WT HFFs and macroH2A1 KO cells. Cluster 1 (**A.**), Cluster 2 (**B.**), and Cluster 3 (**C.**), Cluster 4 (**D.**), Cluster 5 (**E.**), and Cluster 6 (**F.**) were defined by macroH2A1-enriched domains identified in Figure 1. P-value <0.001 for all shown GO clusters and FDR was <0.05.

with decreasing transcription and increasing macroH2A1/H3K27me3) were found in families of housekeeping genes such as those responsible for maintaining cytoskeleton structure and mRNA/rRNA/cytoplasmic translation. This indicates that increased binding of macroH2A1 and H3K27me3 does not occur specifically at pro- or anti-viral genes. Rather, we concluded that these regions are repressed as part of the cellular stress response to viral infection.

3.6 MacroH2A1 and H3K27me3 are marginalized to the periphery of the nucleus during lytic HSV-1 infection.

I next wanted to visualize the infection-caused macroH2A1 and H3K27me3 reorganization that we detected by CUT&Tag. To do this, I turned to immunofluorescence to delineate subnuclear localization of each mark over an infection time course. I found that the antibodies raised to endogenous macroH2A1 and macroH2A1.1 had strong signal in mock-infected cells but high background in infected cells, possibly due to cross-reaction with viral proteins. The antibody for macroH2A1.2 did not stain brightly and therefore was also unusable for these experiments. I engineered WT HFF-Ts to overexpress cDNA constructs of either macroH2A1.1 and macroH2A1.2 that were FLAG-tagged. Together with Dr. Hannah Arbach, I then stained HFF-Ts at Mock, 4, 8 and 12 post infection with DAPI to mark host DNA and either anti-FLAG or anti-H3K27me3 antibodies. As a control for general host chromatin, we also stained with H2A which is found both in euchromatic and heterochromatic regions.

We first asked whether we could detect either macroH2A1 isoform or H3K27me3 in viral replication compartments. The question of whether these marks associate with viral genomes was not answered with CUT&Tag due to the high background of viral reads. Although I did not expect to find these repressive marks associated with actively transcribing and replicating viral genomes, I wanted to determine whether there is a possibility of association through co-staining for the 4 chromatin marks and ICP8, a viral protein that binds single-stranded viral DNA at replication forks (Roizman et al., 2013).

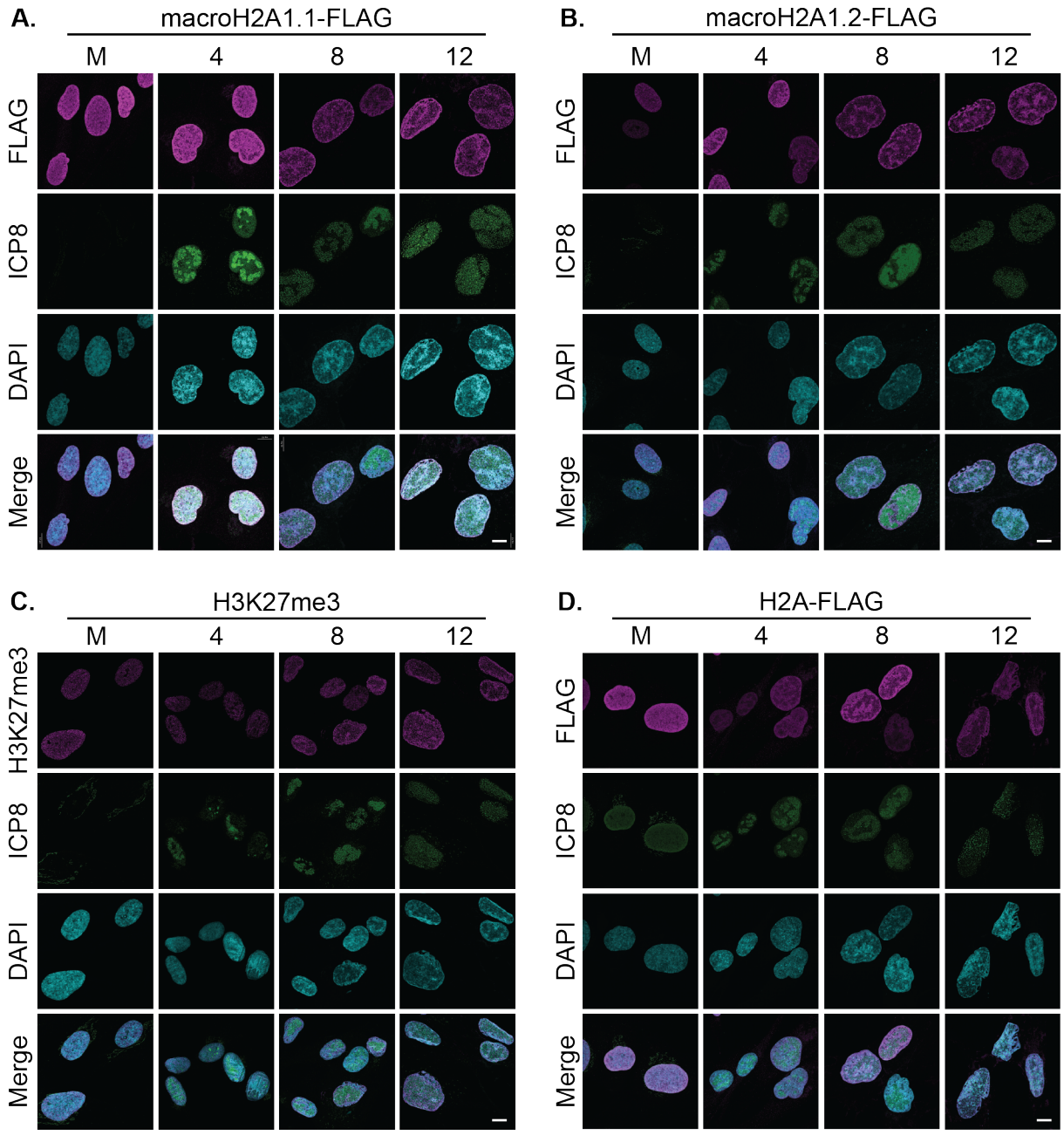

Figure 3.8 MacroH2A1 and H3K27me3 are excluded to the periphery of infected nuclei.

A. Immunofluorescence microscopy of exogenously expressed macroH2A1.1-FLAG (magenta) and HSV-1 ICP8 (green) localization during HSV-1 infection in HFF-Ts. **B.** Immunofluorescence microscopy of exogenously expressed macroH2A1.2-FLAG (magenta) and HSV-1 ICP8 (green) localization during HSV-1 infection in HFF-Ts. **C.** Immunofluorescence microscopy of endogenous H3K27me3 (magenta) and HSV-1 ICP8 (green) localization during HSV-1 infection in HFF-Ts. **D.** Immunofluorescence microscopy of exogenously expressed H2A-FLAG (magenta) and HSV-1 ICP8 (green) localization during HSV-1 infection in HFF-Ts. All scale bars are 10 μm.

In mock-infected cells, both macroH2A1 isoforms and H3K27me3 are diffuse throughout the nucleus with a slight enrichment at the nuclear periphery. Viral replication compartments enlarge over time and eventually merge to occupy most of the nuclear space, which leads to increased enrichment of macroH2A1 isoforms and H3K27me3 at the nuclear periphery (Fig 3.8A-C). This is in contrast to H2A, which remains mostly diffuse in the nucleus throughout infection in both peripheral regions and in viral replication compartments (Figure 3.8D). Notably, neither macroH2A1 isoform nor H3K27me3 co-localizes with ICP8 (Figure 3.8A-C). While we cannot completely rule out that these marks *ever* interact with lytic HSV-1 genomes, we interpreted this result to conclude that these marks are mostly excluded from replication compartments.

3.7 Depletion of macroH2A1 or H3K27me3 results in decreased HSV-1 titers but does not impact viral replication or gene expression.

I next asked how loss of either macroH2A1 or H3K27me3 impacts lytic HSV-1 infection, focusing first on macroH2A1 KO cells. I infected WT and macroH2A1 KO HFF-T and evaluated viral fitness using plaque assays of infectious progeny viruses, quantification of HSV-1 genomes in the supernatant and within the cell, and viral protein production (Figure 3.9). I found that macroH2A1 KO significantly decreased viral titers at 8 and 12 hours post infection (Figure 3.9A). I isolated encapsulated viral DNA in the supernatant (sups) and used ddPCR to quantify this cell-free viral DNA as a measure of total progeny (both infectious and non-infectious) produced by WT and KO cells. I found a 7-fold decrease in viral genomes in the supernatants of KO cells at 12 hpi, although this result did not reach statistical significance (Figure 3.9B). To assay viral replication, I quantified viral genomes within cell pellets using ddPCR. I found no significant difference in viral genome accumulation at any time point (Figure 3.9C).

I used the RNA sequencing dataset generated in section **3.4** to evaluate viral gene expression in WT and macroH2A1 KO lines. Together with Srinivas Ramachandran, I observed no significant difference of expression of any viral gene between the two cell types (Figure 3.9D). Mia Brinkley,

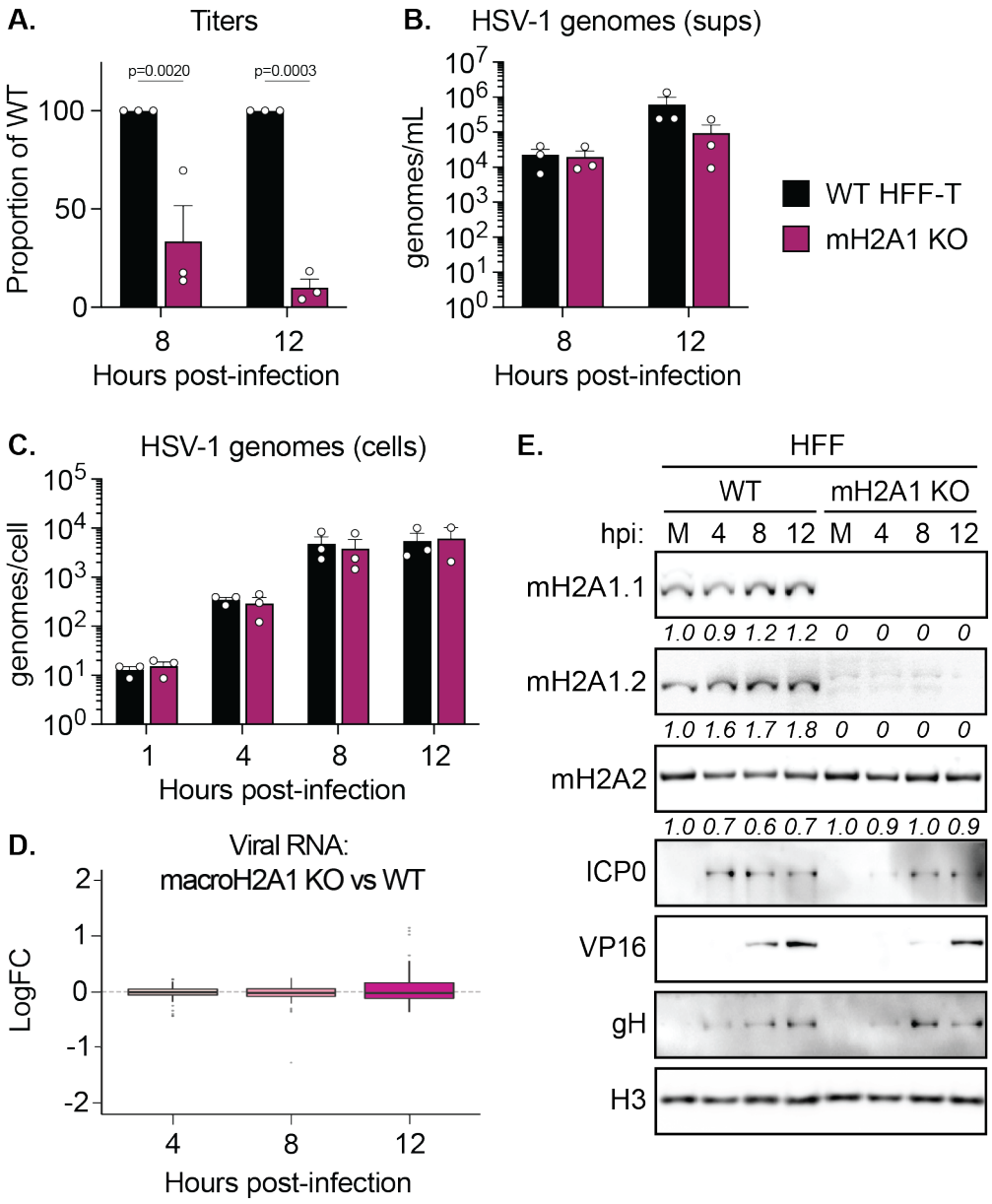

Figure 3.9 MacroH2A1 loss reduces HSV-1 titers but does not impact DNA replication or gene expression. **A.** Infectious progeny produced from HSV-1 infected WT and macroH2A1 KO HFF-T quantified by plaque assay. Viral yield is indicated as the percent yield compared to WT and was calculated through dividing plaque-forming units (pfu) per mL of the treatment group titers by the WT titers at each indicated time point. **B.** Droplet digital PCR (ddPCR) quantification of HSV-1 genomes released from cells and isolated from supernatants (sups). **C.** ddPCR quantification of HSV-1 genomes extracted from infected cells as indicated for each time point. Error bars represent the SEM of three biological replicates. **D.** Log2 fold-change of HSV-1 transcripts at 4, 8 and 12 hpi identified by RNA-seq in macroH2A1 KO compared to WT HFF-T cells. There is no significant difference between the cell types. **E.** Western blot of mH2A1.1 and mH2A1.2 isoforms and mH2A2 during HSV-1 infection at MOI 3 in WT and macroH2A1 KO HFF-Ts. Time points shown are mock infected (M), 4, 8, and 12 hours post infection (hpi). Relative quantification below indicated blots shows fold-change of loading control-normalized protein abundance over M. ICP0, VP16, gH are shown as representative HSV-1 proteins. H3 is shown as a loading control.

Laurel Kelnhofer-Millevolte and I confirmed this result through western blotting the same panel of viral proteins used in Figures 3.1 and 3.2. We observed no consistent change in expression of any gene class upon macroH2A1 KO (Figure 3.9E).

Laurel Kelnhofer-Millevolte and I repeated these results in macroH2A1 KO RPEs and compared viral titers and protein expression to WT RPEs. We again observed a significant decrease in viral progeny produced by macroH2A1 KO cells (Figure 3.10A). MacroH2A1 KO in RPEs again had no impact on viral protein expression (Figure 3.10B). As macroH2A1 loss in two separate cell lines leads to a defect in viral titers but not viral DNA replication or gene expression, we concluded that macroH2A1 is important for HSV-1 egress.

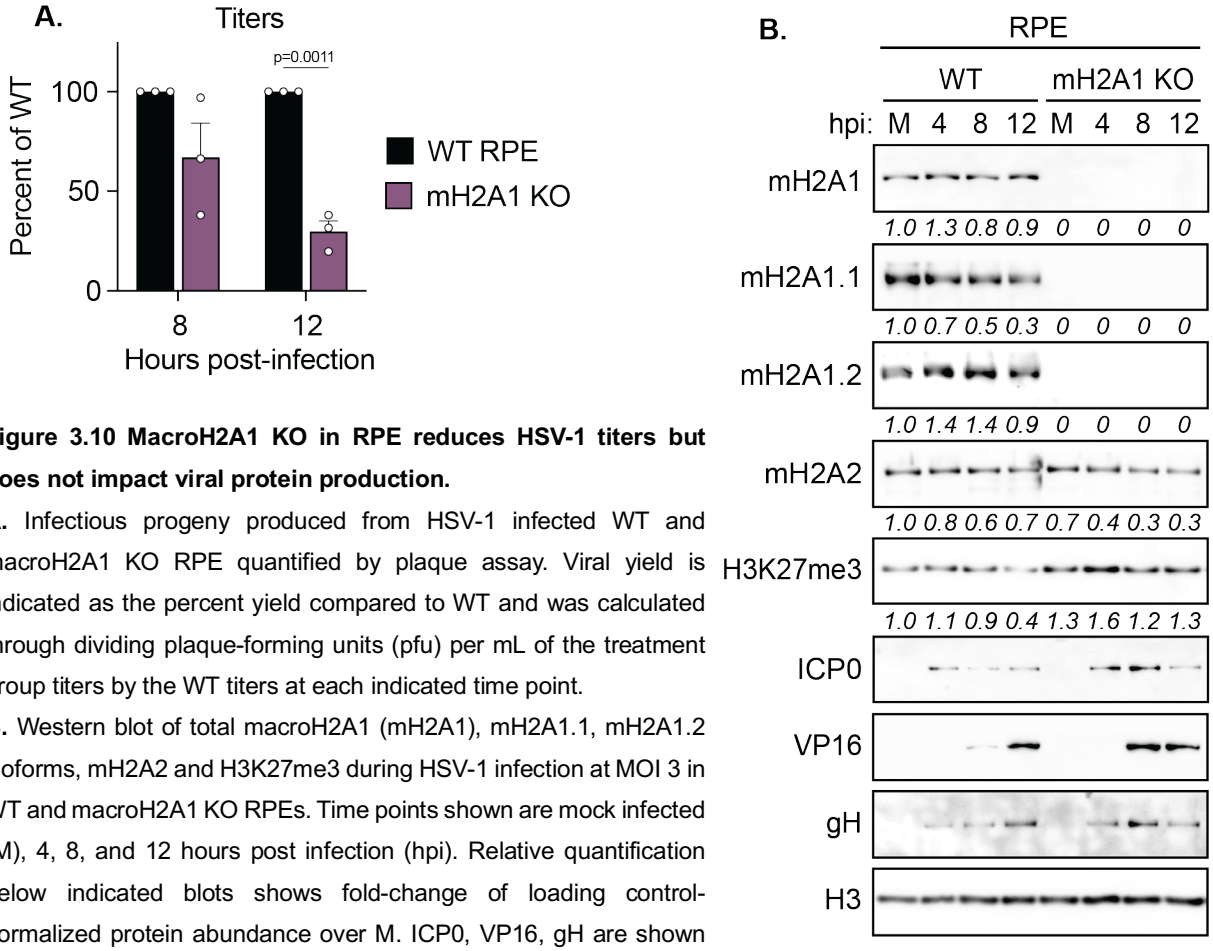

Figure 3.10 MacroH2A1 KO in RPE reduces HSV-1 titers but does not impact viral protein production.

A. Infectious progeny produced from HSV-1 infected WT and macroH2A1 KO RPE quantified by plaque assay. Viral yield is indicated as the percent yield compared to WT and was calculated through dividing plaque-forming units (pfu) per mL of the treatment group titers by the WT titers at each indicated time point.

B. Western blot of total macroH2A1 (mH2A1), mH2A1.1, mH2A1.2 isoforms, mH2A2 and H3K27me3 during HSV-1 infection at MOI 3 in WT and macroH2A1 KO RPEs. Time points shown are mock infected (M), 4, 8, and 12 hours post infection (hpi). Relative quantification below indicated blots shows fold-change of loading control-normalized protein abundance over M. ICP0, VP16, gH are shown as representative HSV-1 proteins. H3 is shown as a loading control.

We next investigated how perturbation of H3K27me3 would impact HSV-1 fitness. We depleted H3K27me3 through chemical inhibition of EZH2 with Tazemetostat (EPZ-6438) for 3 days, and then evaluated viral fitness as above. We treated both WT and macroH2A1 KO cells with inhibitor to examine whether there were any redundancies in this pathway. I found that viral progeny production is significantly impaired upon H3K27me3 depletion by measuring both titers (Figure 3.11A) and HSV-1 genomes in the supernatant (Figure 3.11B), which were both reduced about 4-fold compared to vehicle-treated cells. I observed a mild (~2-fold) decrease in viral genome replication in inhibitor-treated cells, which agrees with published reports (Arbuckle et al., 2017) (Figure 3.11C). I evaluated protein expression through western blotting and found that viral protein production is not impacted upon H3K27me3 depletion (Figure 3.11D). Importantly, these phenotypes were not exacerbated in cells both depleted of H3K27me3 and KO for macroH2A1; this indicates that the two marks function in the same pathway to promote HSV-1 egress.

Together, these data show that heterochromatin perturbation by macroH2A1 knockout or H3K27me3 depletion results in decreased viral progeny but has no impact on viral replication. Therefore, we hypothesized that efficient HSV-1 egress is dependent on heterochromatin formation by macroH2A1 or H3K27me3.

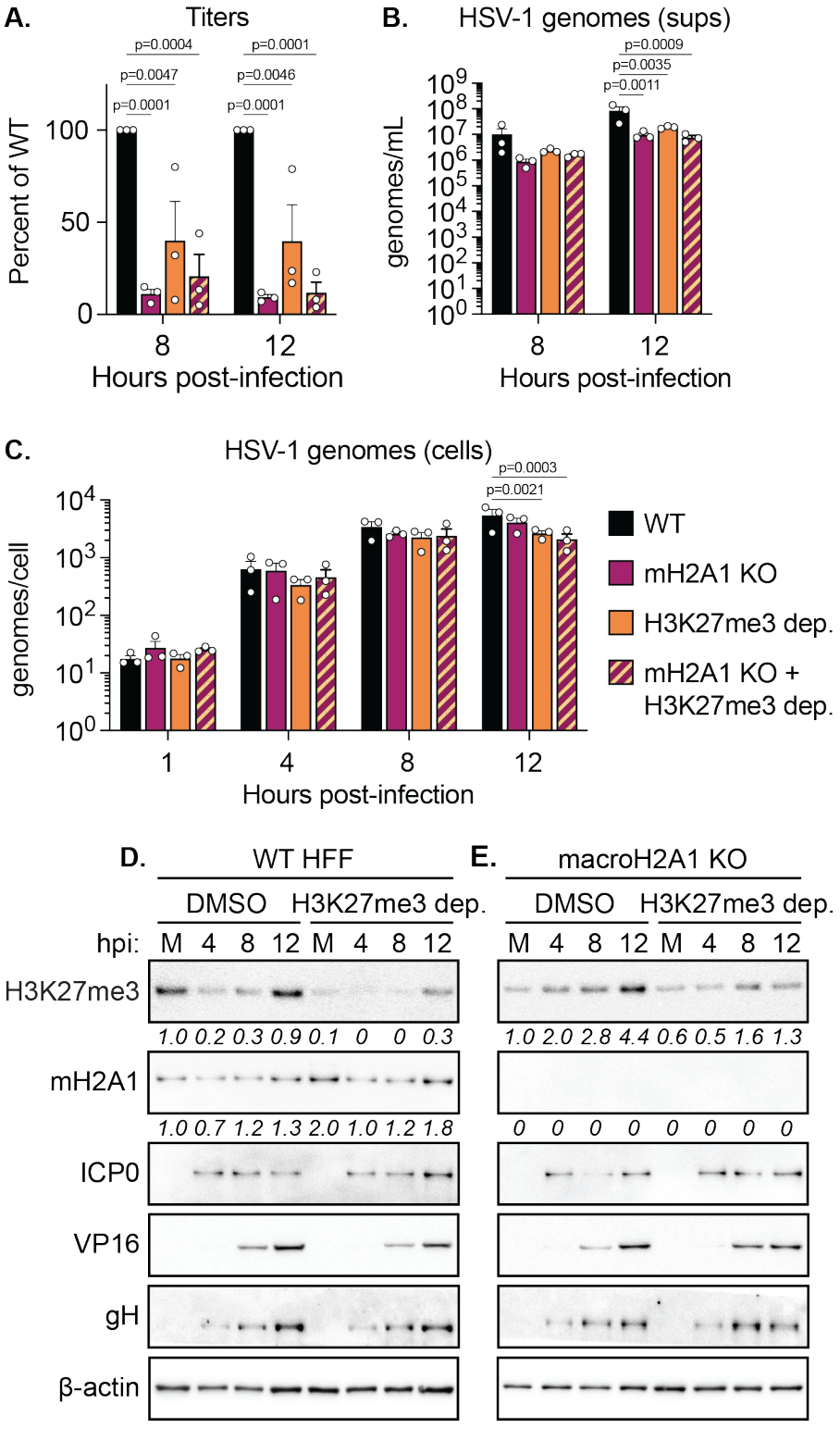

Figure 3.11 H3K27me3 depletion reduces HSV-1 titers and replication.

A. Infectious progeny produced from HSV-1 infected cells treated as indicated and quantified by plaque assay. Cells were treated with EZH2 inhibitor (H3K27me3 depleted) or DMSO for 3 days prior to infection and remained with inhibitor during infection. Viral yield is indicated as the percent yield compared to WT and was calculated through dividing plaque-forming units (pfu) per mL of the treatment group titers by the WT titers of each respective virus at each indicated time point.

B. Droplet digital PCR (ddPCR) quantification of HSV-1 genomes released from cells treated as indicated and isolated from supernatants (sups).

C. ddPCR quantification of HSV-1 genomes extracted from infected cells as indicated for each time point. Error bars represent the SEM of three biological replicates.

(cont. from previous page) **D.** Western blot of H3K27me3 and macroH2A1 during HSV-1 infection at MOI in WT HFF-T. Relative quantification below indicated blots shows fold-change of loading control-normalized protein abundance over M. ICP0, VP16, gH are shown as representative HSV-1 proteins**.** Beta actin is shown as a loading control. **E.** Western blot as in **D.** for macroH2A1 KO cells.

3.8 HSV-1 capsids accumulate in the nucleus of cells depleted for macroH2A1 or H3K27me3.

To make room for viral replication compartments, HSV-1 marginalizes host chromatin to the nuclear periphery (Aho et al., 2017, 2019, 2021; Monier et al., 2000) (Figure 3.8). However, this poses a potential barrier to capsids that must egress from the nucleus in order to further mature and ultimately infect new cells. Previous studies have shown that capsids gain access to the nuclear membrane through channels bracketed by high density chromatin at the nuclear periphery (Myllys et al., 2016). To assay whether heterochromatin channels are formed in our system, I imaged infected nuclei from WT HFF-T cells with transmission electron microscopy (TEM). I observed that HSV-1 capsids near the nuclear envelope were often found in areas of lower density within large regions of heterochromatin (Figure 3.12).

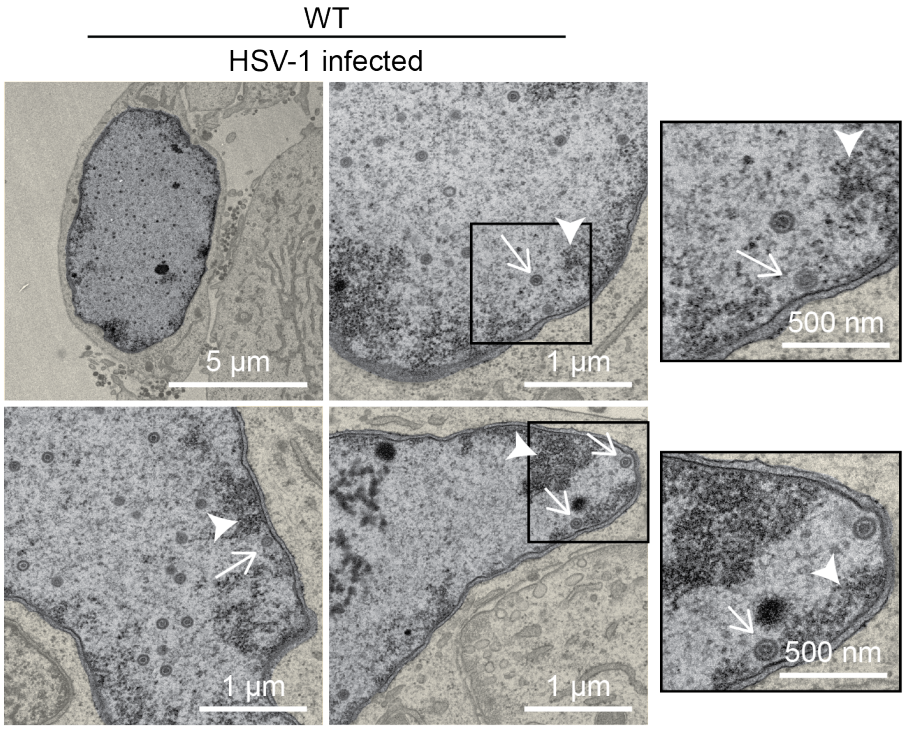

Figure 3.12 HSV-1 capsids traverse channels of less dense chromatin to reach the inner nuclear membrane. Transmission electron microscopy (TEM) images of representative infected nuclei in WT HFF-Ts. Regions outside of the nucleus are colorized yellow. Arrowheads mark high density heterochromatin channels and arrows mark egressing viral capsids. Scale bars as indicated.

We hypothesized that macroH2A1 and H3K27me3 binding at the nuclear periphery is necessary to maintain peripheral heterochromatin. I first assayed heterochromatin content of uninfected nuclei through TEM imaging of uninfected WT, macroH2A1 KO or H3K27me3-depleted cells (Figure 3.13). By eye, it appears as though peripheral heterochromatin decreases upon macroH2A1 KO or H3K27me3 depletion due to a loss of electron density at the nuclear periphery. To quantify this decrease, I used a custom algorithm built by Julien Dubrulle which uses binary thresholding of electron dense regions to measure the width of heterochromatin at the nuclear periphery. Through using this algorithm to analyze 30+ mock-infected cells of each condition, I found that macroH2A1 KO or H3K27me3 depletion results in significant reduction in peripheral heterochromatin (Figure 3.13B-C). This confirms previous reports that macroH2A1 is important for global heterochromatin architecture (Douet et al., 2017) and suggests that H3K27me3 also functions to support heterochromatin structure.

I next asked how depletion of this peripheral heterochromatin through macroH2A1 KO or H3K27me3 depletion impacted capsid formation and accumulation within nuclei. I imaged macroH2A1 KO cells that had been infected with HSV-1 and used an algorithm that identifies the number of HSV-1 capsids built by Dr. Dubrulle to quantify the number of capsids within each nucleus (Figure 3.14). I found a statistically significant increase in the number of capsids per square micron of macroH2A1 KO nuclei (~7 capsids per μm^2, pink bar) compared to WT cells (~5 capsids per μm^2, grey bar) (Figure 3.14 bottom right). In contrast, the number of capsids per square micron was not increased upon H3K27me3 depletion compared to WT (data not shown). However, the numbers of capsids groups found within close proximity to the nuclear membrane was far greater than WT cells (Figure 3.15). In WT cells, we observed ~10% of capsids in groups of 3 or more at the nuclear periphery. In contrast, almost 50% of the capsids we are in groups of 3 or more in H3K27me3 depleted cells (Figure 3.15 bottom right).

I next asked whether there was a difference in the proportion of empty (A), intermediate (B) or full (C) capsids within the nuclei of heterochromatin-depleted cells. An increase in the number

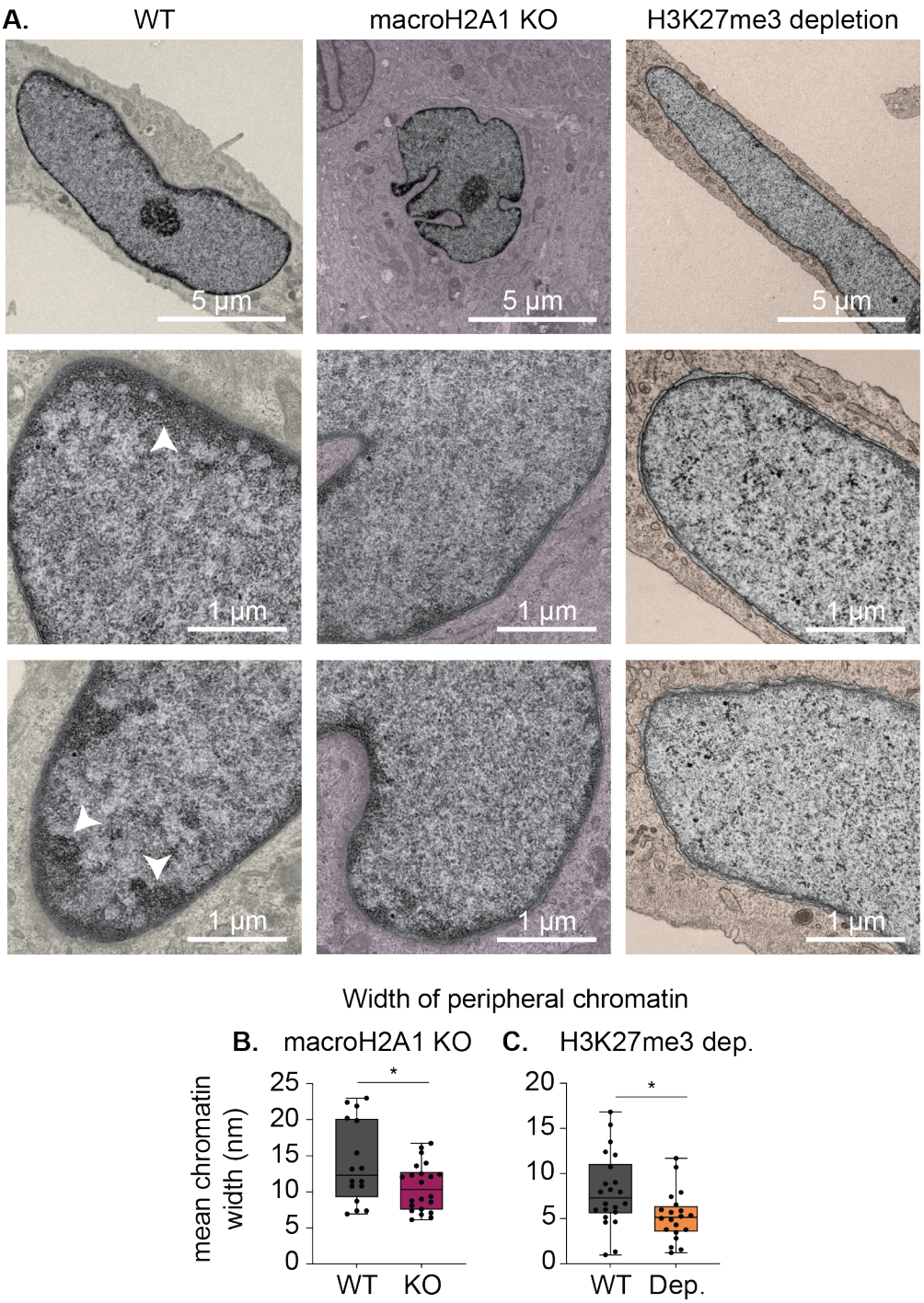

Figure 3.13 MacroH2A1 and H3K27me3 are important for peripheral heterochromatin structure in uninfected cells. A. TEM images of representative of uninfected nuclei in WT (left) macroH2A1 knockout (middle) or H3K27me3 depleted (right) HFF-Ts. Regions outside of the nucleus are colorized yellow, pink or orange, respectively. Dark regions represent high density heterochromatin (arrowhead). Scale bars as indicated. **B.** Quantification of peripheral heterochromatin width in nuclei from **A.** Width was measured in nm from the nuclear periphery via binary thresholding from intensity profiles sampled every 10 pixels. Mean width was plotted for each nucleus. p=0.0275 (n=16 WT, n=22). **C.** Quantification as above in nuclei from **A**. (p= 0.0144, n= 22 WT, n=20).

of empty or intermediate capsids compared to full capsids could indicate a defect in HSV-1 genome packaging which could account for the differences in viral titers. The program developed by Dr. Dubrulle that counts total capsid types also identifies the type of capsid by determining the distribution of pixel greyscale intensities relative to a normal distribution: low intensity indicates A capsids, high intensity at a small radius indicates B capsids, and high intensity throughout the capsid indicates C capsids. I used this program to quantify capsid types and found no significant difference in the proportion of capsid quality between WT and macroH2A1 KO (Figure 3.16B) or H3K27me3 depleted cells (Figure 3.16C). This suggests that HSV-1 capsids form properly but are unable to escape the nucleus upon heterochromatin disruption.

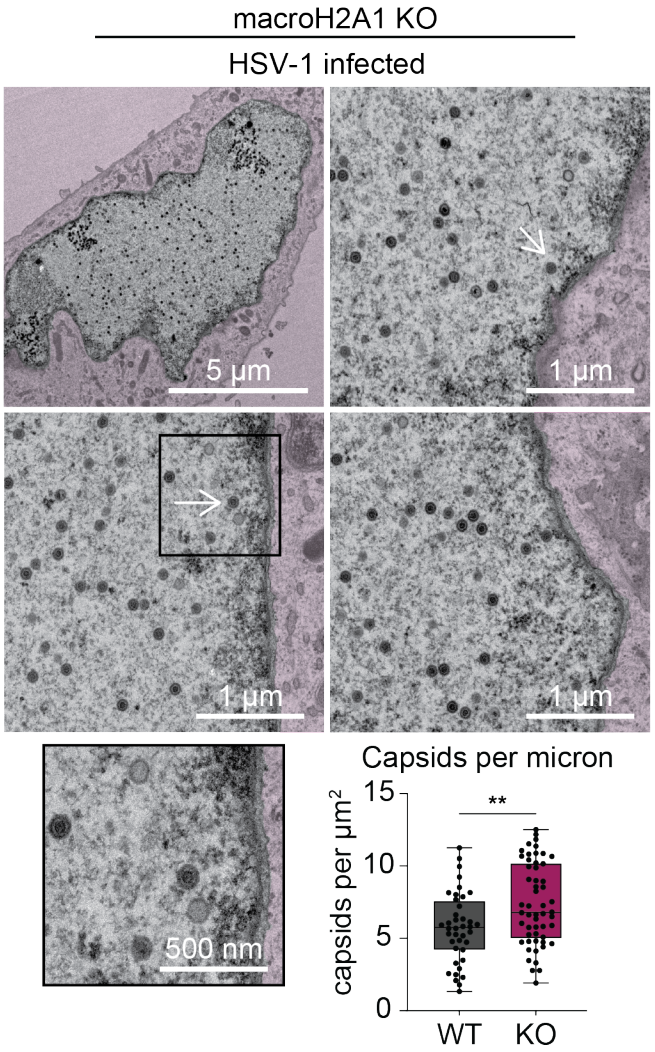

Figure 3.14 HSV-1 capsids accumulate in the nucleus upon macroH2A1 knockout.
TEM images of representative macroH2A1 KO nuclei infected with HSV-1. Inset shows enlarged views of box. Arrows indicate HSV-1 capsids. Scale bars as indicated. (Bottom Right) Quantification of capsids within nuclei compared to Figure 1b. Number of capsids was normalized according to nucleus area in μm^2, p=0.0036 (n=40 WT, n=55 macroH2A1 KO).

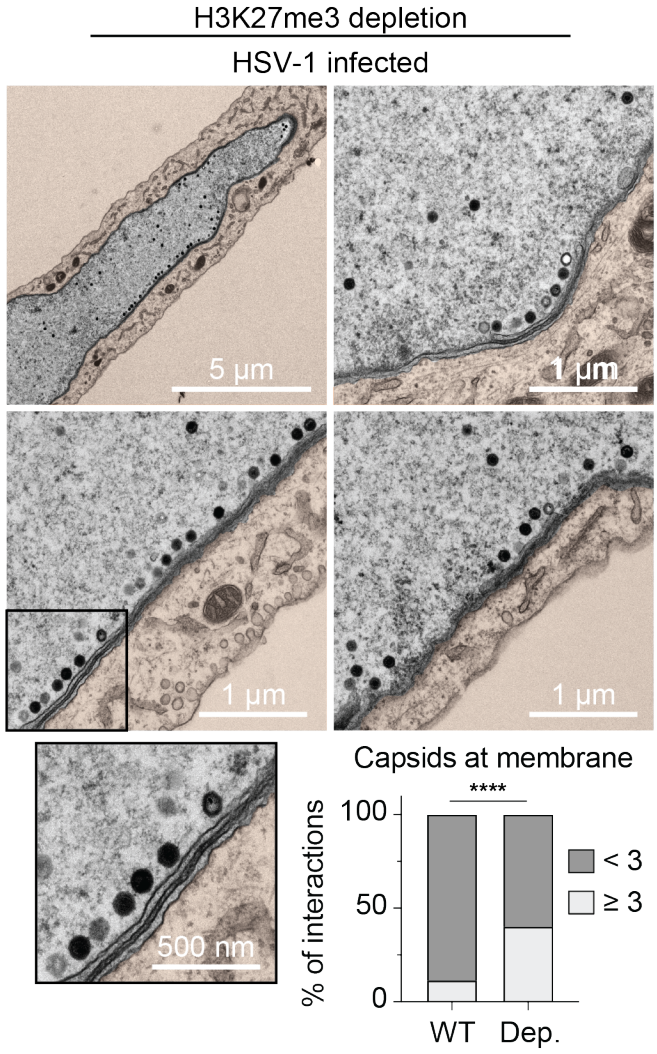

Figure 3.15 HSV-1 capsids accumulate at the nuclear membrane upon H3K27me3 depletion. TEM images of representative H3K27me3 depleted nuclei infected with HSV-1. Inset shows enlarged views of box. Scale bars as indicated. (Bottom Right) Quantification of the number of capsids at the nuclear periphery compared to Figure 1b. p=0.0001 (n=8 cells for DMSO, n=5 cells for H3K27me3 depleted).

HSV-1 produces a large number of defective progeny whose capsids contain HSV-1 genomes but cannot form plaques. These can be detected through measuring the number of genomes per mL isolated from supernatants. When compared to the titers in pfu (the genome to pfu ratio), a rough indication of the quality of HSV-1 progeny can be obtained. I asked whether the genome to pfu ratio was altered upon macroH2A1 KO or H3K27me3 depletion through dividing genomes/mL (Figure 3.11B) by pfu/mL (Figure 3.11A) of each condition at 8 and 12 hours post infection. I found no significant difference in the genome to pfu ratio; in general, there were ~40-60 genomes in the supernatant for every plaque-forming unit (Figure 3.16D). Together with the data that show no

difference in proportion of the capsid types, this result indicates that heterochromatin disruption does not lead to production of defective particles. Rather, I conclude that macroH2A1 and H3K27me3 are important to form heterochromatin at the nuclear periphery that aids efficient HSV-1 nuclear egress.

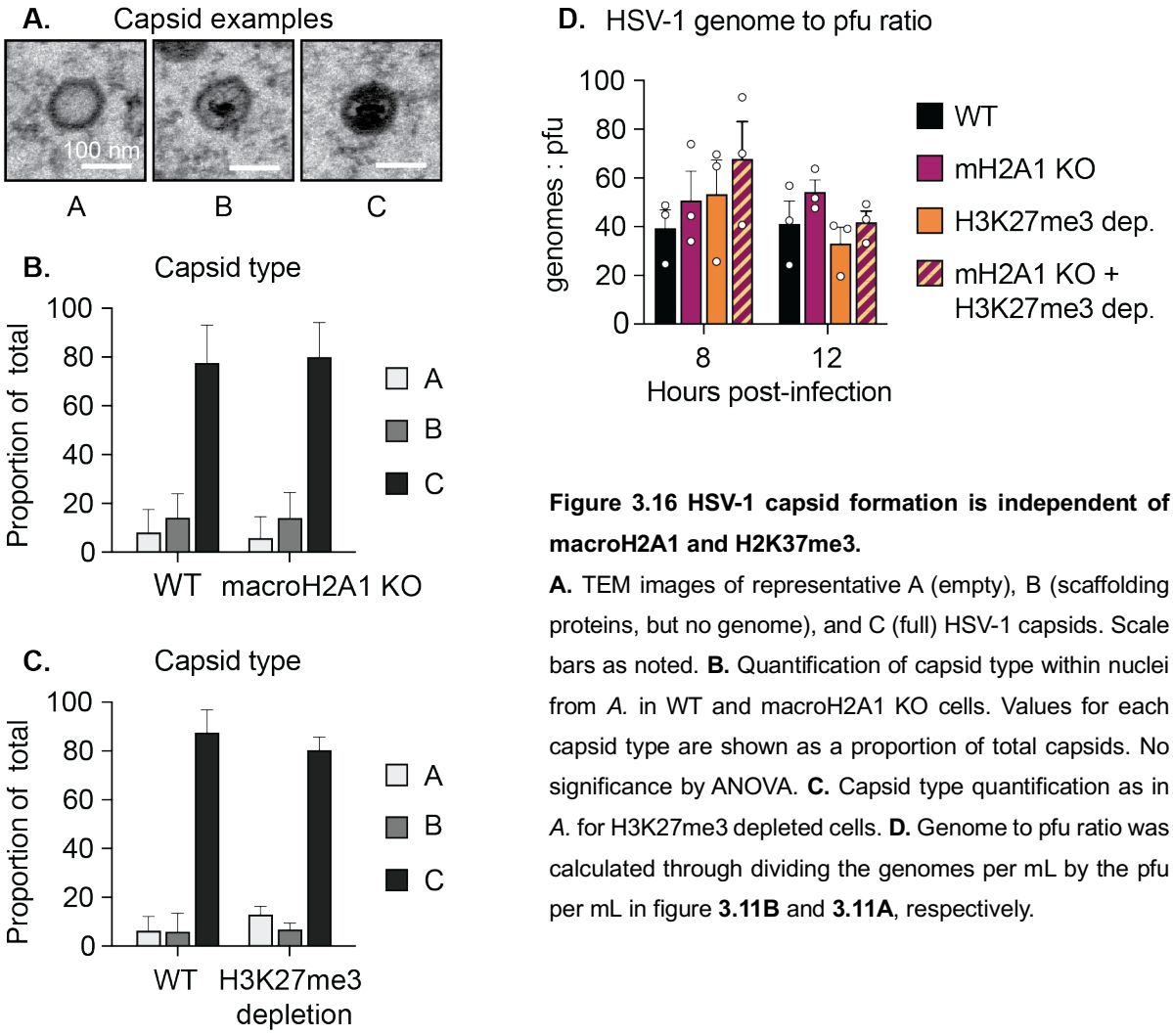

Figure 3.16 HSV-1 capsid formation is independent of macroH2A1 and H2K37me3.

A. TEM images of representative A (empty), B (scaffolding proteins, but no genome), and C (full) HSV-1 capsids. Scale bars as noted. **B.** Quantification of capsid type within nuclei from *A.* in WT and macroH2A1 KO cells. Values for each capsid type are shown as a proportion of total capsids. No significance by ANOVA. **C.** Capsid type quantification as in *A.* for H3K27me3 depleted cells. **D.** Genome to pfu ratio was calculated through dividing the genomes per mL by the pfu per mL in figure **3.11B** and **3.11A**, respectively.

3.9 Reversal of heterochromatin disruption leads to partial rescue of HSV-1 titers.

Since heterochromatin disruption through macroH2A1 KO or H3K27me3 depletion decreases HSV-1 fitness, I asked whether restoration of either mark would rescue HSV-1 titers. To restore macroH2A1 expression, I engineered HA-tagged overexpression constructs of cDNA and

transduced either macroH2A1.1, macroH2A1.2 or both isoforms into macroH2A1 KO cells (Figure 3.17A). Expression of macroH2A1.1 is consistently more robust than macroH2A1.2 as measured by western blotting for HA. I infected these cell lines with HSV-1 and evaluated viral titers through plaque assay of progeny virions. Re-expression of either or both isoforms does not restore HSV-1 progeny production, as titers were not different from macroH2A1 KO cells but were significantly reduced compared to WT cells (Figure 3.17B). I next measured HSV-1 replication through qPCR of viral genomes and found no significant difference in genome accumulation between WT, macroH2A1 KO or any macroH2A1-rexpressing line (Figure 3.17C).

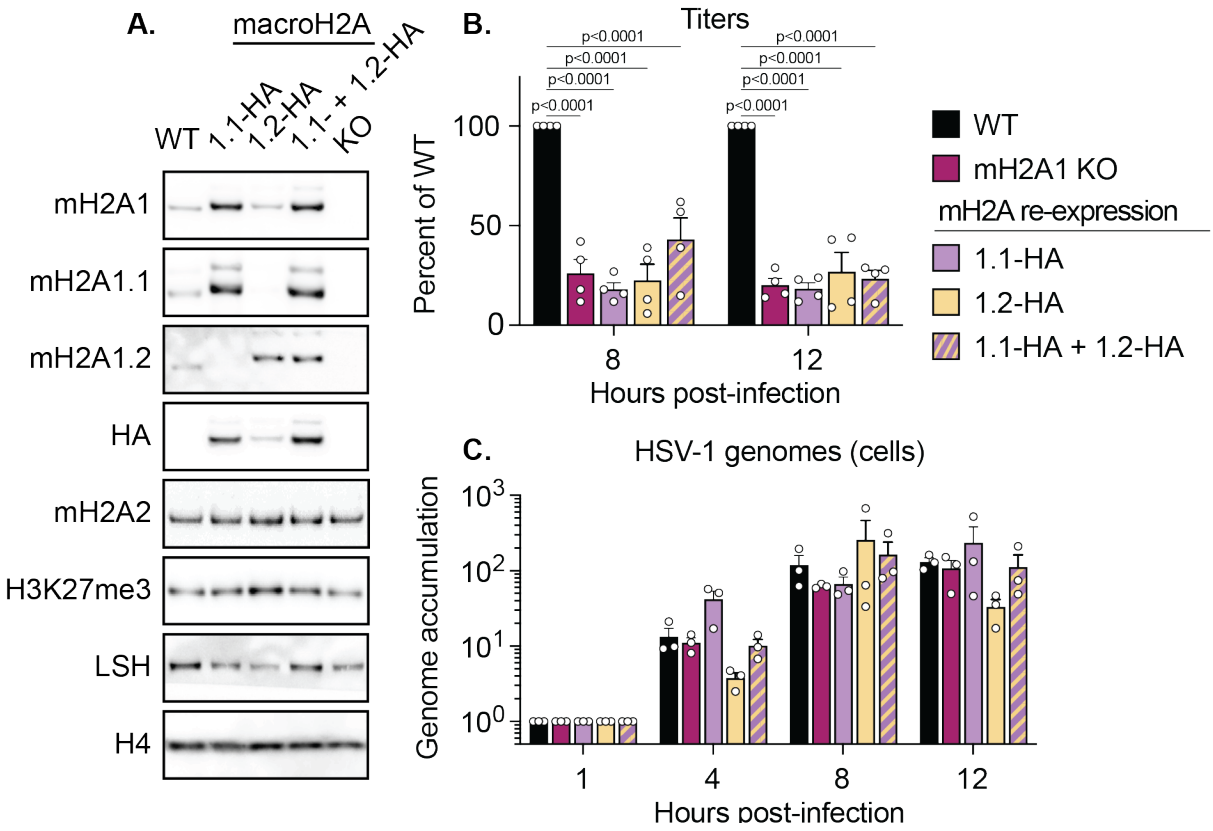

Figure 3.17 MacroH2A1 re-expression does not rescue HSV-1 titers. A. Western blot of total macroH2A1 (mH2A1), mH2A1.1, mH2A1.2, HA, mH2A2, H3K27me3 and LSH in uninfected HFF-T that (right to left) are WT, re-express mH2A1.1-HA, re-express mH2A1.2-HA, re-express both mH2A1.1-HA and mH2A1.2-HA, or are KO for mH2A1. H4 is a loading control. **B.** Infectious progeny produced from HSV-1 infected cell lines from *A*. Viral yield is indicated as the percent yield compared to WT and was calculated through dividing plaque-forming units (pfu) per mL of the treatment group titers by the WT titers of each respective virus at each indicated time point. **C.** qPCR quantification of HSV-1 genomes extracted from infected cells as indicated for each time point. Values are normalized to 1 hpi input sample. Error bars represent the SEM of three biological replicates.

For these experiments, Laurel Kelnhofer-Millevolte and I depleted H3K27me3 depletion through 3 days of chemical inhibition of EZH2 using Tazemetostat. This short time frame circumvents the long process of creating gene knockout cell lines. We therefore asked whether H3K27me3 restoration would rescue HSV-1 titers. We inhibited EZH2 in WT HFF-Ts for 3 days and then cultured without Tazemetostat for several days. After 7 days, H3K27me3 levels were restored to ~70% of their pre-inhibitor treated levels (Figure 3.18A). We infected cells that had been cultured without drug for 7 days and compared their viral progeny formation with H3K27me3 depleted cells (3 days pre-treatment) and WT cells. In contrast to the macroH2A1 rescue experiments, H3K27me3 restoration led to a partial but statistically significant rescue in viral progeny production at both 8 and 12 hours (Figure 3.18B).

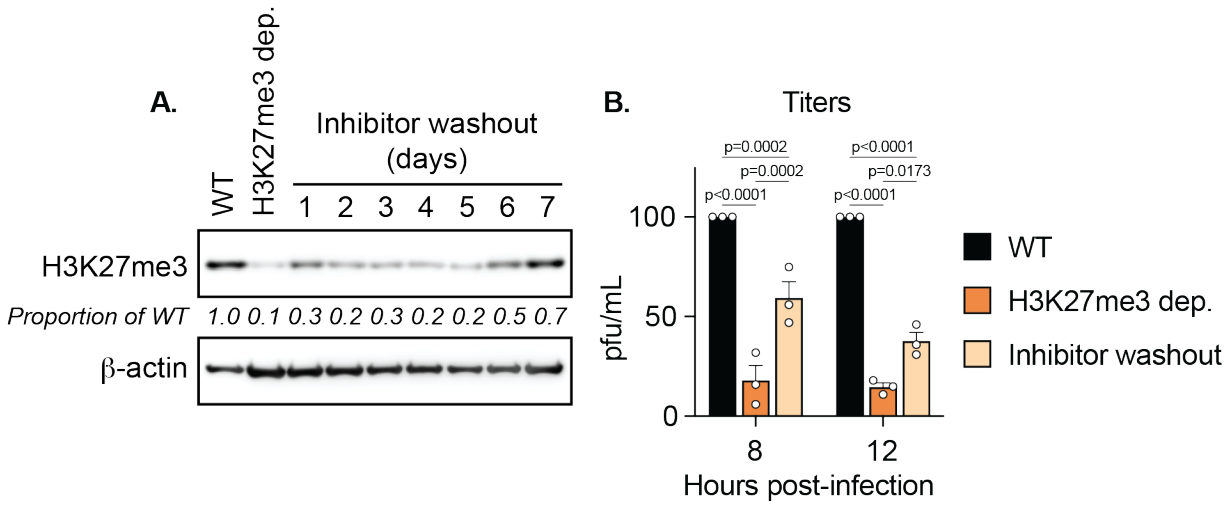

Figure 3.18 H3K27me3 restoration through inhibitor washout leads to a significant but incomplete rescue in HSV-1 titers. A. Western blot of H3K27me3 in uninfected HFF-T. Cells were treated with EZH2 inhibitor (H3K27me3 depleted) or DMSO (WT) for 3 days. Inhibitor was then removed and cells were cultured for an additional 7 days (inhibitor washout). Samples were harvested once per day post washout. H4 is a loading control. **B.** Infectious progeny produced from HSV-1 infected cell lines from *A*. Viral yield is indicated as the percent yield compared to WT and was calculated through dividing plaque-forming units (pfu) per mL of the treatment group titers by the WT titers of each respective virus at each indicated time point.

Loss of heterochromatin and consequential aberrant gene expression can be detrimental to cell fitness, so the cell employs several redundant mechanisms to maintain heterochromatin in a repressive state. This could explain why progeny production is only partially rescued upon

H3K27me3 restoration; not only are H3K27me3 levels not completely back to baseline, but other factors may have occupied regions that lost repression by H3K27me3. In addition, this could explain why the macroH2A1 re-expression cells do not see a rescue in viral progeny. After several months in cell culture without macroH2A1, the cells may have adapted in a way that is not reversible. The time frame between the H3K27me3 restoration (7 days) and macroH2A1 re-expression (months) could explain the difference in how cells adapt to the loss of these marks. Future experiments with macroH2A1 KO and restoration may need to account for potential cellular adaptation to global heterochromatin loss.

3.10 MacroH2A1 overexpression leads to increased HSV-1 titers.

I next asked whether increasing expression of macroH2A1 would enhance HSV-1 egress. I infected HFF-T that overexpressed cDNA constructs of FLAG-tagged macroH2A1.1 or macroH2A1.2 and evaluated viral fitness. I observed that HSV-1 titers were increased by 2-fold upon overexpression of macroH2A1.1 and this result was statistically significant (Figure 3.19A). Titers appeared to increase mildly in macroH2A1.2 overexpressing lines, approximately by 1.5-fold, although this quantification did not reach significance. This may result from generally lower expression of macroH2A1.2 as measured by western blotting for FLAG (Figure 3.19D). Intriguingly, there was no difference in the number of HSV-1 genomes detected within the supernatant of either macroH2A1.1- or macroH2A1.2-overexpressing lines (Figure 3.19B). This suggests that that either macroH2A1.1 overexpression does not lead to new heterochromatin domains or HSV-1 has maximized its egress through existing heterochromatin channels. As expected, neither viral replication nor protein production was impacted by macroH2A1.1 or 1.2 overexpression (Figure 3.19C-D). Together with the knockout data, these results suggest that heterochromatin is necessary for efficient viral egress and that increasing heterochromatin further may not lead to much fitness advantage for the virus.

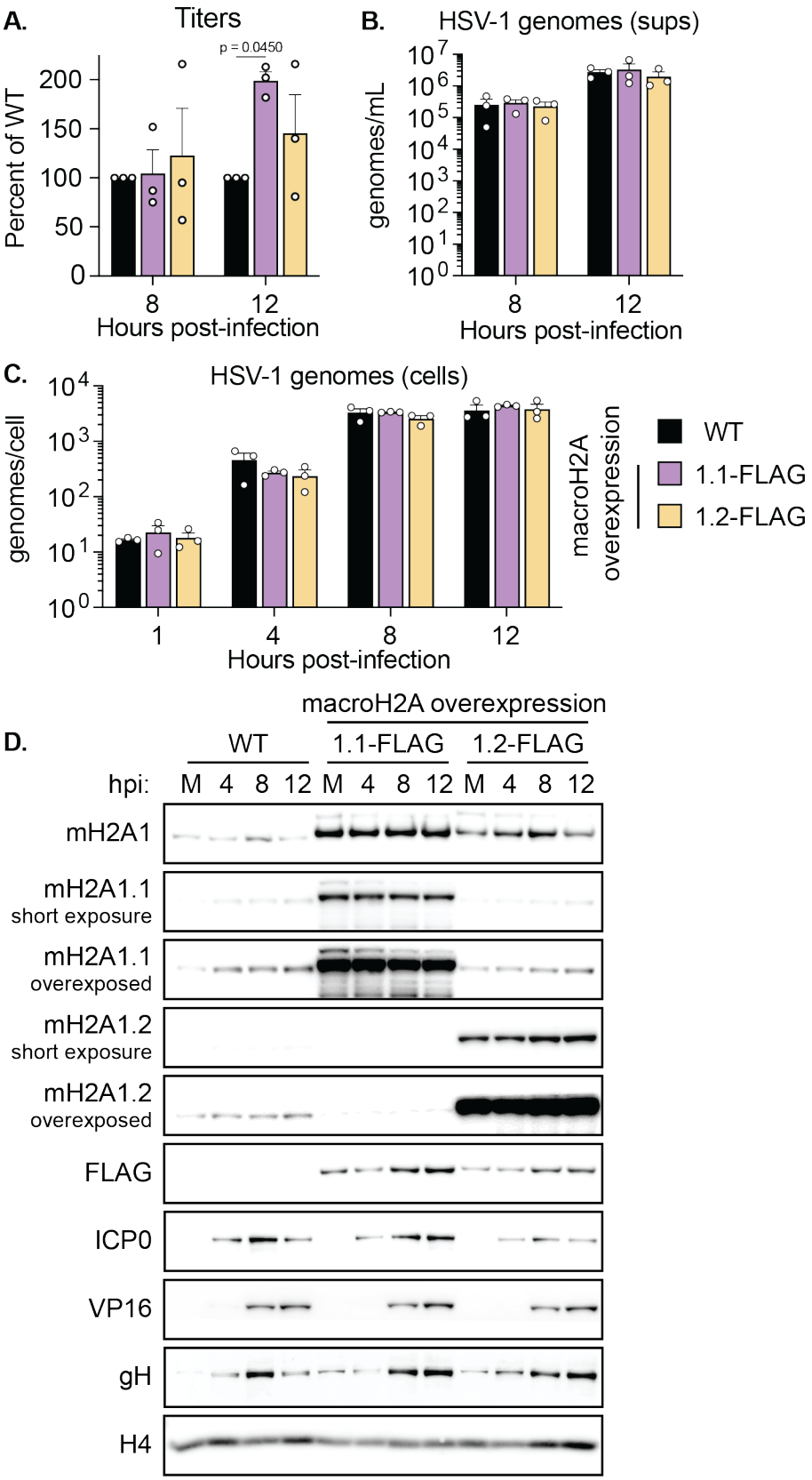

Figure 3.19 MacroH2A1.1 overexpression promotes HSV-1 progeny production.

(Cont. from previous) **A.** Infectious progeny produced from HSV-1 infected HFF-T that overexpress either mH2A1.1-FLAG or mH2A1.2-FLAG. Viral yield is indicated as the percent yield compared to WT and was calculated through dividing plaque-forming units (pfu) per mL of the treatment group titers by the WT titers of each respective virus at each indicated time point. **B.** Droplet digital PCR (ddPCR) quantification of HSV-1 genomes released from cells from *A.* isolated from supernatants (sups). Error bars represent the SEM of three biological replicates. **C.** ddPCR quantification of HSV-1 genomes extracted from infected cells as indicated for each time point. Error bars represent the SEM of three biological replicates. **D.** Western blot of total macroH2A1 (mH2A1), mH2A1.1, mH2A1.2, and FLAG during HSV-1 infection at MOI 3 in cell lines from *A*. Time points shown are: mock infected (M), 4, 8, and 12 hours post infection (hpi). ICP0, VP16, gH are shown as representative HSV-1 proteins. H4 is a loading control.

3.11 Egress of clinical HSV-1 strains is impacted by macroH2A1 KO but not H3K27me3 depletion.

To evaluate the clinical significance of heterochromatin impact on HSV-1 egress, I asked whether the phenotypes I observed with lab-adapted strain 17*syn*+ recapitulate during infection with clinical isolates of HSV-1. I obtained stocks of two clinical isolates from the lab of Keith Jerome that were collected in 1994 and 1995 from daily oral swabs. Patients with HSV-1 detectable by qPCR in only a few swabs were classified as “low shedders” (isolate 6676) and patients with high percentage of days of positive swabs were classified as “high shedders” (isolate 7258).

Together with Laurel Kelnhofer-Millevolte and Mia Brinkley, I first focused on the impact of macroH2A1 KO on low- and high-shedding clinical isolates. We infected WT and macroH2A1 KO HFF-T with either isolate and measured viral fitness through quantification of viral titers, encapsulated genomes in the supernatant, viral replication, and protein production (Figure 3.20). Both isolates have a significant 3-4 fold reduction in titers at 12 hpi in macroH2A1 KO cells (Figure 3.20A). There is slight decrease in supernatant genomes at 12 hpi (3-fold and 1.7-fold in low- and high- shedding isolates, respectively); however, these differences did not reach statistical significance (Figure 3.20B). Although there is a significant 1.6-fold decrease in HSV-1 genomes in cell pellets at 12 hpi with the low-shedding isolate (Figure 3.20C), this does not fully explain the >4-fold decrease in titers at the same time point. Given the higher 3-fold (albeit not significant)

decrease in HSV-1 genomes within supernatants of this isolate, I concluded that macroH2A1 KO likely reduces egress of the low-shedding isolate. Further, macroH2A1 KO has no impact on replication of the high-shedding isolate. Finally, macroH2A1 KO has no impact on protein production of any of the 3 HSV-1 gene classes of either clinical isolate (Figure 3.20D). Taken together, these data suggest that macroH2A1 is important for efficient egress of clinical HSV-1. Intriguingly, this effect is more subtle than we observed in the lab-adapted HSV-1 strain. The lab-adapted HSV-1 strain, 17*syn*+, has been passaged through cell culture for years; in contrast, the clinical HSV-1 strains were passaged only 3 times before this experiment. Perhaps the clinical HSV-1 strains are less sensitive to macroH2A1 loss because of mutations they encode in their nuclear egress components.

Finally, we asked whether H3K27me3 depletion also impacts fitness of clinical HSV-1 isolates. We inhibited EZH2 with Tazemetostat for 3 days to reduce levels of H3K27me3 as described previously; we then infected with the low- and high-shedding clinical isolates and measured viral fitness. In contrast to macroH2A1 KO, H3K27me3 depletion does not significantly alter HSV-1 titers. At 8 hpi, titers for the low shedding isolate appear slightly lower but at 12 hpi titers for the high-shedding isolate are higher (Figure 3.21A); however, the spread of the replicates lead me to conclude that titers are not impacted by H3K27me3 reduction. I confirmed that H3K27me3 was depleted in these experiments through western blotting (Figure 3.21B). I also evaluated production of viral protein ICP0 and found no difference in DMSO- or Tazemetostat-treated lines (3.22B). I concluded that H3K27me3 depletion does not impact egress of clinical HSV-1 isolates. Again, this differs from the lab-adapted strain 17*syn*+ and points to specific mutations within the clinical isolates that allow their egress despite loss of host heterochromatin.

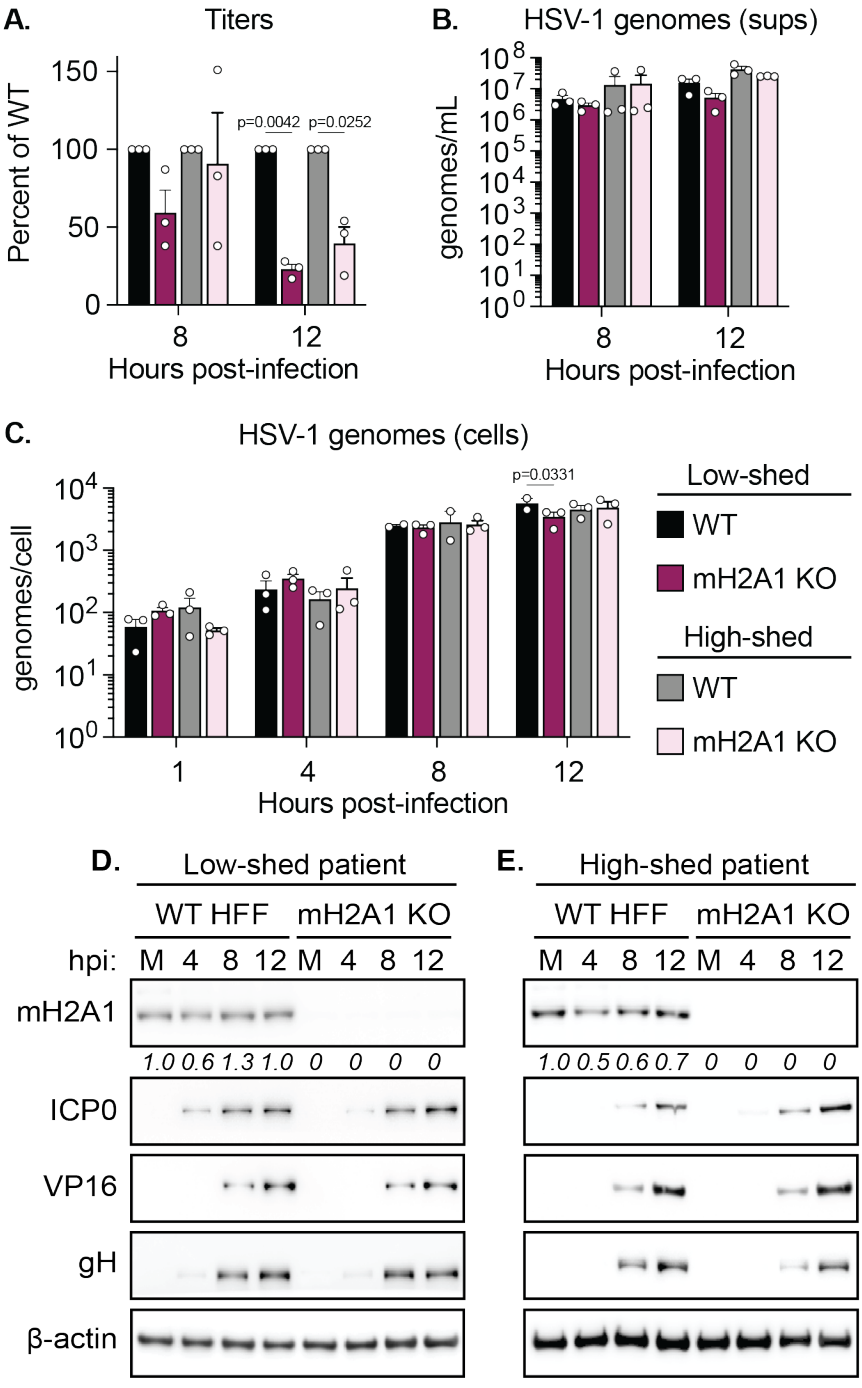

Figure 3.20 MacroH2A1 KO impacts egress of clinical HSV-1 strains. A. Infectious progeny of cells infected as

(Cont from previous) indicated with clinical HSV-1 isolates quantified by plaque assay. Viral yield is indicated as the percent yield compared to WT. **B.** Droplet digital (ddPCR) quantification of HSV-1 genomes released from cells infected with low- or high-shedding clinical isolates that were isolated from supernatants (sups). Error bars represent the SEM of three biological replicates. **C.** ddPCR quantification of HSV-1 genomes extracted from cells infected with low- or high-shedding clinical isolates as indicated for each time point. Error bars represent the SEM of three biological replicates. **D.** Western blot of total macroH2A1 during infections with a low-shedding clinical HSV-1 isolate in WT or macroH2A1 KO HFF-Ts. Time points shown are: mock infected (M), 4, 8, and 12 hours post infection (hpi). Relative quantification below indicated blots shows fold-change of loading control-normalized protein abundance over M. ICP0, VP16, gH are shown as representative HSV-1 proteins. Beta actin is shown as a loading control. **E.** Western blot as in *D.* for HFF-Ts infected with a high-shedding clinical HSV-1 isolate.

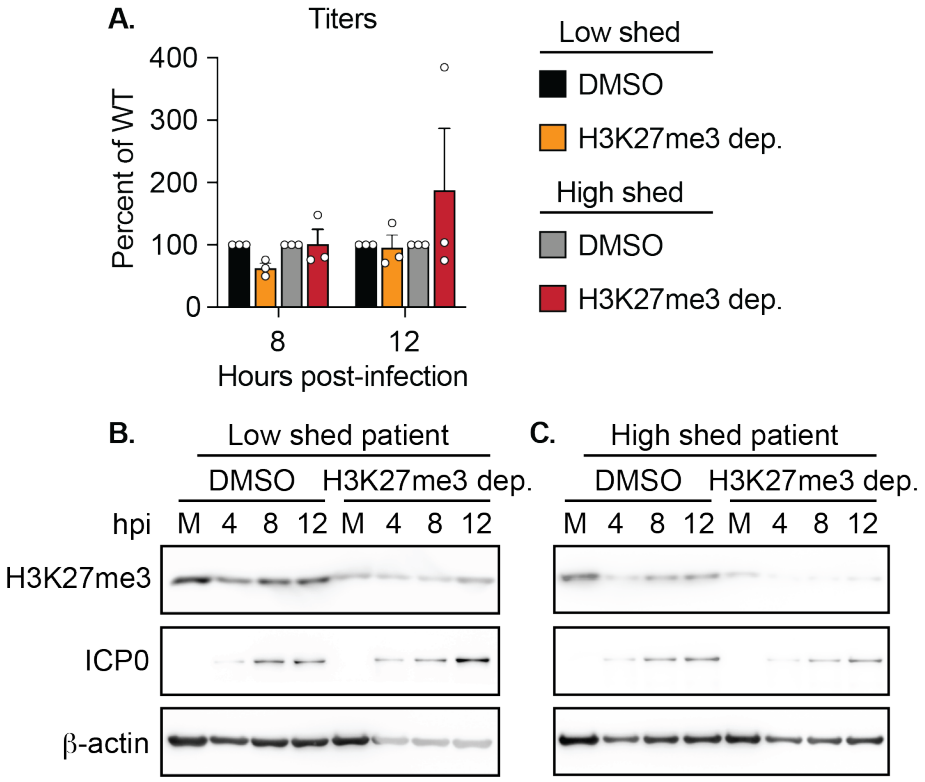

Figure 3.21 H3K27me3 depletion does not impact progeny formation of clinical HSV-1 strains.

A. Infectious progeny of cells treated with EZH2 inhibitor (H3K27me3 depletion) and infected as indicated with clinical HSV-1 isolates quantified by plaque assay. Cells were treated with EZH2 inhibitor (H3K27me3 depleted) or treated with DMSO for 3 days prior to infection and remained with inhibitor over the course of infection. Viral yield is indicated as the percent yield compared to WT. **B.** Western blot of total macroH2A1 during infection with a low-shedding clinical HSV-1 isolate in WT or H3K27me3 depleted HFF-T cells. Time points shown are: mock infected (M), 4, 8, and 12 hours post infection (hpi). ICP0 is shown as representative HSV-1 proteins. Beta actin is shown as a loading control. **C.** Western blot as in *B.* for HFF-Ts infected with a high-shedding clinical HSV-1 isolate.

Chapter 4. Discussion and conclusions.

4.1 HSV-1 exploits new heterochromatin formed during infection for efficient egress.

4.1.a HSV-1 lytic infection causes increased abundance of heterochromatin marks.

While the host cell nucleus provides HSV-1 with resources for replication, the virus must compete with pre-existing host chromatin for space to produce progeny. This is a complicated undertaking, as the nucleus is a crowded molecular environment with defined chromatin territories and hubs of transcriptional or repressive activity (Cremer & Cremer, 2010; Quinodoz et al., 2018). Lytic HSV-1 infection significantly increases volume of the nucleus late during infection to accommodate large viral replication compartments, which marginalize compacted host chromatin to the nuclear periphery (Aho et al., 2017, 2019, 2021; Monier et al., 2000; Myllys et al., 2016; Simpson-Holley et al., 2004). Although this virally induced chromatin marginalization has been described in several studies, my thesis work is the first to find that perturbation of factors that mediate host heterochromatin reorganization has little effect on viral expression, but rather impairs HSV-1 egress.

We find that several markers of heterochromatin increase in abundance as a consequence of lytic HSV-1 infection (Figure 3.1A and B). This includes facultative heterochromatin marker H3K27me3 (Figure 3.1B and D), constitutive heterochromatin marker H3K9me3 (Figure 3.1D), and macroH2A1 (Figure 3.1A and D), which has been found to be enriched in regions of facultative and constitutive heterochromatin (Buschbeck et al., 2009; Douet et al., 2017; Gamble & Kraus, 2010; Hussey et al., 2014). MacroH2A1 in particular is overexpressed during infection of regular diploid HFF and RPE cell lines (Figure 3.1 and 3.2), as well as cancer cell lines HeLa and U2OS (data not shown). The increase in these heterochromatin marks may facilitate the increased compaction of peripheral host chromatin late during infection.

Intriguingly, inhibition of viral replication with PAA does not prevent macroH2A1 protein levels from increasing, albeit the increase may be potentially slower (Figure 3.2). This suggests that the increase in macroH2A1, which may cause host chromatin compaction, is not due to an increase in viral replication compartment size. Instead, I hypothesize that macroH2A1 overexpression may be part of a cellular stress response to infection. One such possible pathway to macroH2A1 overexpression is the DNA damage response, which HSV-1 infection activates even when replication is inhibited by PAA (Lilley et al., 2005). Both isoforms of macroH2A1 are involved in DNA damage repair (Jeongkyu Kim et al., 2018, 2019; Kozlowski et al., 2018; Sebastian et al., 2020; Timinszky et al., 2009), and both isoforms increase during HSV-1 infection. It is conceivable that DNA damage triggered by incoming viral genomes leads to upregulation of macroH2A1.

4.1.b HSV-1 infection induces new heterochromatin formation in active compartments.

In addition to an increase in macroH2A1 and H3K27me3 abundance during infection, my dissertation work identified large-scale concurrent genomic and physical reorganization of both marks in response to viral infection. Using CUT&Tag in collaboration with Dr. Srinivas Ramachandran, we find that thousands of large regions of macroH2A1 and H3K27me3 enrichment are rearranged across the genome during infection (Figure 3.4 and 3.5). Dr. Hannah Arbach, Laurel Kelnhofer-Millevolte and I also observed physical marginalization of macroH2A1 and H3K27me3 to the nuclear periphery of infected cells using immunofluorescence (Figure 3.8). Importantly, we observed exclusion of macroH2A1 and H3K27me3 from viral replication compartments (Figure 3.8). While we were not able to use our CUT&Tag to discern whether macroH2A1 and H3K27me3 localize to viral genomes due to high background (Figure 3.3B and D), our findings are consistent with a reported exclusion of other heterochromatin marks such as H1 or H3K9me3 from viral replication compartments (Cabral et al., 2018; Cliffe & Knipe, 2008; Lee et al., 2016; Simpson-Holley et al., 2004).

MacroH2A1 is enriched in broad regions over autosomal genes, where it is frequently co-localized with H3K27me3 (Hongshan Chen et al., 2014; Gamble et al., 2010; Gaspar-Maia et al., 2013; Sun et al., 2018). When these two marks are co-enriched, they are thought to function in transcriptional repression (Buschbeck et al., 2009). We observed many regions of the genome have strikingly similar patterns of gain or loss of macroH2A1 and H3K27me3 (Figure 3.4 A and 3.5A). Additionally, we found that genes in regions that lose these marks have overall higher gene expression induction during infection (Figure 3.6A and 3.B). The regions with the highest increase in macroH2A1 and/or H3K27me3 are those with highest transcriptional activity prior to viral infection (Figure 3.6C), which is consistent with a lack of these marks at actively transcribed genes (Gamble et al., 2010; Sun et al., 2018). During infection, deposition of macroH2A1 and/or H3K27me3 correlates with decrease in new transcription at these loci as measured by 4SU RNA sequencing (Figure 3.6C). Furthermore, macroH2A1 and H3K27me3 gain occurs in active A compartments and loss occurs in inactive B compartments (Figure 3.6D). These data show that macroH2A1 and H3K27me3 form *new* regions of heterochromatin in response to HSV-1 infection.

To explore the transcriptional impact of macroH2A1 during infection, I performed RNA sequencing in both WT and macroH2A1 KO cells. Together with Dr. Ramachandran, we found that macroH2A1 loss does not greatly alter the transcriptional profile of infected cells (compare Figure 3.6 A to B). This could be due to redundant transcriptional regulation through H3K27me3 (Figure 3.5A). MacroH2A redundancy with H3K27me3 or other markers of transcriptional silencing has also been reported in other contexts (Hongshan Chen et al., 2014; Gaspar-Maia et al., 2013; Hernández-Muñoz et al., 2005).

Given that we observe formation of new heterochromatin during infection, I was curious whether macroH2A1 KO would impact chromatin nanostructure. MacroH2As were recently shown to maintain heterochromatin structure in a hepatocellular carcinoma cell line, as double knockout of both macroH2A1 and macroH2A2 leads to widespread loss of heterochromatin visible by TEM (Douet et al., 2017). Part of this phenotype may be due to a loss of lamina-chromatin contacts

facilitated by macroH2A (Douet et al., 2017; Fu et al., 2015). My work shows that loss of macroH2A1 alone is sufficient to see heterochromatin reduction and nuclear distortion in regular diploid HFFs (Figure 3.14). H3K27me3 has also been reported to be enriched at the border of lamina associated domains; EZH2 knockdown in fibroblasts also leads to loss of DNA-lamina contacts (Harr et al., 2015). We added to these reports by demonstrating that H3K27me3 reduction leads to a dramatic loss of peripheral heterochromatin (Figure 3.14).

4.1.c Loss of macroH2A1 or H3K27me3 leads to viral egress defects.

MacroH2A1 knockout, H3K27me3 depletion, or loss of both factors leads to significantly decreased viral titers compared to WT cells (Figure 3.9A, 3.10A, 3.11A). However, viral mRNA production is not impacted by macroH2A1 KO (Figure 3.9D), nor can we detect viral protein production defects in either macroH2A1 KO or H3K27me3 depleted cells (Figure 3.9E, 3.10B, 3.11D, 3.11E). I quantified viral genomes within cell pellets to determine whether depletion of either mark negatively impacts viral replication. Strikingly, there is no significant replication defect in macroH2A1 KO cells despite a consistent ~10-fold reduction in progeny across experiments.

A previous report depleted H3K27me3 with different EZH2 inhibitors and observed decreased viral gene expression, progeny production and viral spread. The authors attributed these defects to enhanced immune signaling upon H3K27me3 depletion (Arbuckle et al., 2017). In our experiments, we observe a slight ~2-fold decrease in viral replication in cells depleted of H3K27me3 (regardless of whether macroH2A1 is also present). It is possible that this replication defect is due to decreased viral gene expression reported by Arbuckle et. al, which we may not have detected with western blotting of a limited panel of viral proteins. A recent publication also used Tazemetostat to deplete H3K27me3 in monocytes and saw no impact on HSV-1 gene expression (Chuan et al., 2020). Future work in this direction should include RNA sequencing to investigate the full host and viral transcriptome in H3K27me3 depleted cells.

Because the overall defect in progeny production is not explained by an equivalent impairment of viral replication in macroH2A1 KO or H3K27me3 depleted cells, I decided to quantify virions released by the cell. To do this, I developed a protocol to isolate and quantify encapsulated HSV-1 genomes from supernatants. I removed cells through filtering supernatants and treated with DNase to degrade all DNA not protected by viral capsids. I then used proteinase K to extract viral genomes from capsids and quantified using ddPCR. I anticipated two potential outcomes of this experiment: 1) If the amount of encapsulated viral DNA produced by macroH2A1 KO or H3K27me3 depleted cells is similar to that produced by WT cells, the defect in titers may be due to defective virion production; or 2) fewer encapsulated HSV-1 genomes produced by heterochromatin-depleted cells indicates a viral egress defect. This second scenario is what we observe: there is a consistent decrease in HSV-1 genomes within the supernatant of macroH2A1 KO and/or H3K27me3 depleted cells. I therefore concluded that viral egress is aided by host heterochromatin.

To explore this idea further, I turned to transmission electron microscopy to visualize infected nuclei of macroH2A1 KO or H3K27me3 depleted cells. I first asked whether the proportion of full, intermediate, and empty capsids is altered by removal of either mark (Figure 3.16). If the number of capsids within the nucleus is similar between heterochromatin-depleted cells and WT cells but the ratio of capsid types was different, I could conclude that heterochromatin is important for packaging viral genomes. I do not observe this result: capsid proportions are similar across all samples (Figure 3.16B and C). Instead, I find that a significantly increased number of capsids are concentrated in the nucleus of macroH2A1 KO cells (Figure 3.14). H3K27me3 depletion, in contrast, leads to an increased proportion of HSV-1 capsids accumulating the nuclear periphery (Figure 3.15).

Although many viral proteins including UL31, UL34, ICP34.5 and UL26 are important for mediating viral egress (Gao et al., 2017; Reynolds et al., 2001; Roller et al., 2000; Yu Wang et al., 2014), less is known about host proteins that promote capsid exit from the nucleus. Most of the

host proteins that have been found to be important for HSV-1 egress, such as PKC, p32 and emerin, have been suggested to play a role specifically in lamina disruption (Leach et al., 2007; Morris et al., 2007; Richard Park & Baines, 2006; Yu Wang et al., 2014). My EM phenotypes upon macroH2A1 KO and H3K27me3 depletion are similar to those observed when primary envelopment of viral capsids at the inner nuclear membrane is inhibited, which implies that the defect in nuclear egress I observe is downstream of capsid formation and upstream of PEV formation or de-envelopment. This further suggests that viral egress defects in macroH2A1 KO and H3K27me3 depleted cells are directly due to loss of heterochromatin structure.

4.1.d Model of HSV-1 nuclear egress through marginalized host chromatin channels.

HSV-1 egress is thought to rely on capsids breaching the peripheral heterochromatin and subsequent targeted dispersal of the lamina network (Bjerke & Roller, 2006; Simpson-Holley et al., 2004). Disruption of peripheral heterochromatin through lamin protein knockdown or centrosome destabilization (via knockdown of centrosome regulator TRIM43) has been shown to alter viral titers (Full et al., 2019; Silva et al., 2008, 2012); however, the mechanisms by which these occur differ from my results. In these three studies, the authors described that gene expression and chromatin states on viral genomes are altered as a consequence of lamina perturbation. Knockdown of Lamins A and C leads to reduced occupancy of VP16/Oct-1/HCV-1 at viral gene promoters early during infection and increased immunofluorescence staining of heterochromatin markers H1, H3K9me3, H4K20me3 and HP1 in viral replication compartments ((Silva et al., 2008, 2012). Conversely, TRIM43 knockdown destabilizes the nuclear lamina and leads to increased co-localization of viral genomes with euchromatin mark H3K4me3 and increased expression of some viral transcripts (Full et al., 2019).

In contrast to these studies, my RNA sequencing dataset does not indicate alterations in viral transcription nor do I detect differences in viral replication upon macroH2A1 knockout. Although H3K27me3 depletion results in a slight decrease in viral replication, which is consistent with

previous reports (Arbuckle et al., 2017), I observe defects in viral titers and viral genomes in the supernatant not fully explained by reduced viral replication. I do not observe differences in viral protein production upon loss of macroH2A1 and/or H3K27me3. Overall, my data suggest that disrupting heterochromatin structure can impact HSV-1 egress without disrupting viral replication.

I propose a model by which increased heterochromatin formation is exploited by HSV-1 for viral egress. It is counterintuitive to imagine compacted host chromatin at the nuclear periphery as a positive factor for viral egress; however, HSV-1 capsids have been reported to access the nuclear periphery by diffusing through channels of low-density chromatin. Regions of high-density chromatin bracket these channels and restrict capsid movement (Aho et al., 2017, 2019, 2021; Myllys et al., 2016). Our data indicate that macroH2A1 and H3K27me3 may be required to form dense heterochromatin during infection. Additionally, lack of either mark may interrupt channel formation, which leads to increased retention of HSV-1 capsids within the nucleus (Figure 4.1).

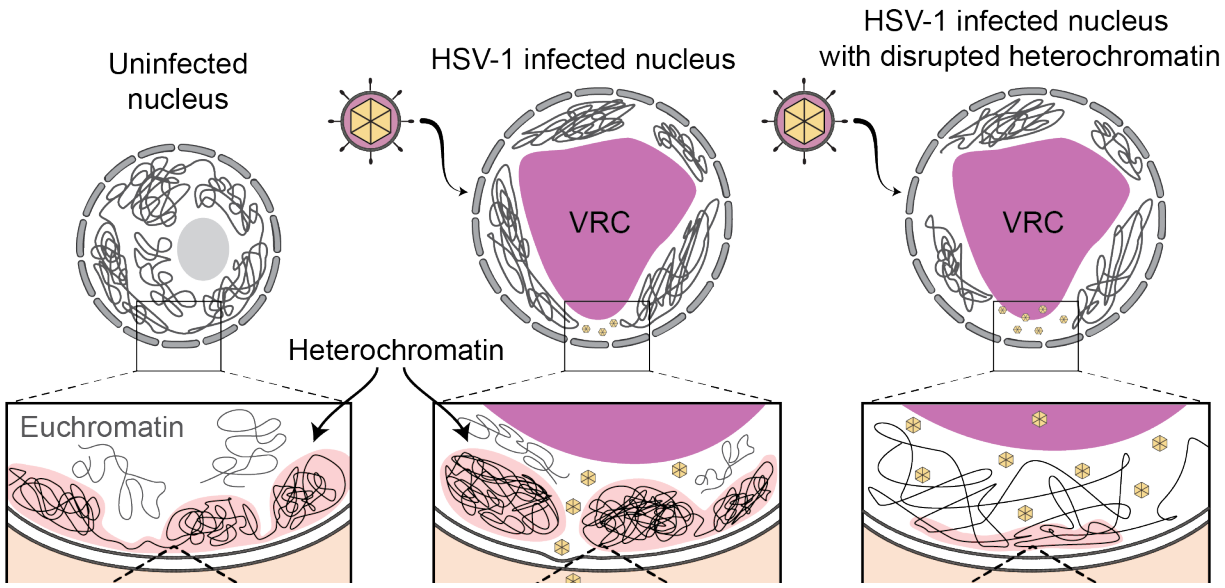

Figure 4.1 Model for heterochromatin support of HSV-1 egress.

In uninfected cells (left), heterochromatin is enriched in the nuclear periphery. Upon infection with HSV-1 (middle), there is an increase in heterochromatin at specific regions in the nuclear periphery that form heterochromatin channels. The regions of low chromatin density within these channels allow capsids to traverse from the viral replication centers (VRCs) to the inner nuclear membrane where they bud into the perinuclear space and subsequently fuse with the outer nuclear membrane into the cytoplasm. In infected cells missing heterochromatin markers macroH2A1 or H3K27me3 (right), heterochromatin channels cannot form properly which results in increased capsids trapped in the nuclear compartment.

4.2 Outstanding questions and future directions.

4.2.1 Do macroH2A1 isoforms or H3K27me3 have different roles in HSV-1 egress?

My data suggest that macroH2A1 and H3K27me3 form peripheral heterochromatin domains during infection to support HSV-1 egress. MacroH2A1 KO and H3K27me3 depletion leads to reduced peripheral heterochromatin width in uninfected cells (Figure 3.13), reduced viral titers (Figures 3.9A, 3.10A and 3.11A) and reduced encapsulated genomes within the supernatant (Figures 3.9B and 3.11B). Importantly, depletion of both markers does not further exacerbate these defects, suggesting that formation of heterochromatin during infection may be redundantly mediated by several factors (Figure 3.11). This is consistent with previous reports suggesting functional redundancy between macroH2A1 and H3K27me3 in transcriptional repression and redundancy of macroH2A1 with other silencing factors (Douet et al., 2017; Gaspar-Maia et al., 2013; Hernández-Muñoz et al., 2005).

However, I do observe differences in specific egress phenotypes upon macroH2A1 and H3K27me3 depletion. H3K27me3 depletion leads to accumulation of capsids along the nuclear periphery (Figure 3.15) but not an overall increased abundance of capsids within the nucleus. Additionally, although macroH2A1 KO significantly decreases egress of two clinical HSV-1 strains (Figure 3.21), H3K27me3 depletion does not alter clinical viral titers (Figure 3.22). These results suggest that H3K27me3 may dispensable for efficient egress of clinical HSV-1 while macroH2A1 remains important, albeit to a lower degree than for egress of the lab-adapted 17*syn*+ strain. To my knowledge, the clinical HSV-1 strains I used in this study have not been sequenced. I anticipate that sequencing these strains would reveal mutations in genes involved in viral egress that may allow the viruses to compensate for host heterochromatin disruption.

There are a few reasons that macroH2A1 and H3K27me3 depletion can cause different egress phenotypes both in lab-adapted and clinical HSV-1 strains. First, the mechanisms by which each mark promotes chromatin compaction are different. The linker domain of macroH2A1 can directly promote chromatin compaction both *in vitro* and in cells (Chakravarthy et al., 2012;

Kozlowski & Ladurner, 2015). In contrast, reader proteins such as PRC1 are responsible for chromatin compaction at regions decorated with H3K27me3 (Guo et al., 2021). This network of co-factors that reads H3K27me3 and promotes chromatin condensation may not be fully activated in cells infected with clinical HSV-1 strains.

Alternatively, the levels to which I can deplete these marks differs between knockout and drug treatment. EZH2 inhibition consistently leads to an incomplete depletion of H3K27me3. Perhaps the ~10% remaining H3K27me3 is sufficient to allow efficient egress of clinical HSV-1 strains. For lab adapted HSV-1, the phenotype of capsids lining the nuclear periphery may also be mediated by this remaining H3K27me3. In contrast, the macroH2A1 KO cell line has a complete loss of both macroH2A1.1 and macroH2A1.2 isoforms. This complete knockout results in a significant reduction of both lab-adapted and clinical HSV-1 progeny as well as increased accumulations of capsids within the nucleus of 17*syn*+ infected cells. Future TEM of clinical HSV-1 infections in H3K27me3 depleted and macroH2A1 KO cells will be important to illuminate the differences in nuclear egress in these conditions.

To evaluate the roles of macroH2A1.1 and macroH2A1.2 in HSV-1 egress, I overexpressed each isoform in WT fibroblasts. I found that macroH2A1.1 overexpression, but not macroH2A1.2, increases HSV-1 titers (Figure 3.19A). Overexpression of either isoform does not impact encapsulated DNA within the supernatant (Figure 3.19B), viral replication (Figure 3.19C) or viral protein production (Figure 3.19D). I concluded from this experiment that macroH2A1.1 promotes viral progeny production slightly, but that egress of lab-adapted HSV-1 may be already optimized in cell culture. Although overexpression of macroH2A1.2 does not significantly increase viral titers, this may be because macroH2A1.2 is not overexpressed as highly as macroH2A1.1 using this particular expression system. To resolve this inconsistency, future experiments could use colony selection of these lines to obtain populations of cells that express macroH2A1.1 and macroH2A1.2 equally. A caveat to this potential approach is that macroH2A1.1 overexpression can induce senescence in primary cells (Hongshan Chen et al., 2015). Although I do not observe

significant growth defects in hTERT-immortalized HFFs that overexpress macroH2A1.1, prolonged overexpression during colony selection may lead to arrest or death of these cells.

An additional complication to the macroH2A1 overexpression experiments is that ectopic macroH2A1 can post-translationally downregulate endogenous macroH2A1 in a macrodomain-dependent process that is not fully characterized (Hongshan Chen et al., 2014; Ruiz et al., 2019). For the most consistent expression of proteins across replicates, I infected with HSV-1 very soon after lentiviral transduction and selection for isoform overexpression (~3 days). Even in this short time frame, I observe loss of endogenous macroH2A1.2 in macroH2A1.1-overexpressing cells and vice-versa (Figure 3.19D, overexposed western blots). Thus, my infections were conducted in cells with both isoforms of macroH2A1 present but at altered ratios. The consequence of performing infections in these conditions is that I was not able to tease out the impact of each isoform independently. Culturing these cells longer will likely lead to the complete replacement of endogenous isoforms with the single isoform overexpressed. Identifying the different roles of each isoform in infection is a worthwhile avenue for future study.

4.2.b What is the role of macroH2A1 in infection-induced PARP-1 signaling?

MacroH2A1.1 is the only isoform of the three human macroH2A proteins that can bind ADPr and PAR chains (Kozlowski et al., 2018; Kustatscher et al., 2005; Timinszky et al., 2009). In doing so, it links chromatin organization and DNA damage to global cellular metabolism through its interactions with polymerase PARP-1. Upon sensing DNA damage, PARP-1 is activated to remove the ADPr moiety is from NAD+, leaving nicotinamide as a side product. PARP-1 then adds ADPr to various substrates, either as a mono-ADPr or as linear or branched PAR chains. Importantly, PAR is removed by eraser enzyme PARG. The macrodomain of macroH2A1.1 binds PAR chains, performing three main functions depending on its local concentration: 1) it binds auto-PARylated PARP-1, recruiting it to chromatin to perform gene regulatory functions, 2) its binding to PARP-1 inhibits further PARylation of nearby substrates, and 3) its binding to existing

PAR chains prevents PAR degradation by PARG (Hurtado-Bagès, Knobloch, et al., 2020; Hurtado-Bagès, Marjanovic, et al., 2020). In this way, macroH2A1.1 both promotes PARP-1 activity while preventing overactivation that can lead to NAD+ depletion and cell death (Ruiz et al., 2019).

Intriguingly, HSV-1 infection induces PARP-1 overactivation. Chemical inhibition of PARP-1 or interruption of PAR recycling through siRNA degradation of PARG leads to decreased titers in cell culture and reduced viral spread in mouse models (Grady et al., 2012; Fei Wang et al., 2022). *In vivo*, PARP-1 activation specifically downregulates antiviral signaling through PARylation of inflammatory effector proteins (Fei Wang et al., 2022). PARP-1 inhibition or knockout in mice leads to decreased inflammation and increased survival of disseminated HSV-1 infection. These results indicate that PARP-1 overactivation is beneficial to viral progeny production and spread, although neither study differentiated between viral genome replication and progeny egress in their respective systems.

Given the extensive interactions between macroH2A1.1 and PARP-1 in gene regulation and DNA damage, it is possible that macroH2A1.1 is the key isoform required for heterochromatin formation during infection (Hongshan Chen et al., 2014; Timinszky et al., 2009). This may explain the significant increase in viral titers that I observe when I overexpress macroH2A1.1 (Figure 3.19A). One experiment to explore this question is CUT&Tag of macroH2A1.1 and PARP-1 during infection: if both these proteins show consistent co-localization to the broad domains identified in our total macroH2A1 CUT&Tag dataset (Figure 3.4A and 3.5A), PARP-1 and macroH2A1.1 may act together to form large heterochromatic regions during infection. However, it is equally possible that macroH2A1.2 may have an additional impact on heterochromatin formation, as it is also recruited to sites of PARP-1 activation where it mediates chromatin compaction (Khurana et al., 2014; Kozlowski et al., 2018). Although we observe no increase in macroH2A2 during infection nor compensation of macroH2A2 upon knockout of macroH2A1.1 and macroH2A1.2, it is

additionally possible that macroH2A2 functions in these processes as well. Future experiments should explore the independent contribution of each macroH2A protein on HSV-1 infection.

Intriguingly, one study has found that UL31 of HSV-2 contains a PAR-binding motif in its N-terminal domain. Exogenously expressed HSV-2 UL31 localizes to sites of laser-induced DNA damage in a manner dependent on PARP-1 activity and enhanced by PARG inhibition. When co-expressed with viral kinase US3, however, the ability to localize to sites of DNA damage is reduced for both UL31 and an exogenously expressed macroH2A1.1 macrodomain used as a control (Sherry et al., 2017). In addition to its role in the nuclear egress complex, HSV-1 UL31 has been found to be present on replicated viral genomes, and orthologs in murine cytomegalovirus and EBV have been implicated in viral genome packaging (Dembowski & DeLuca, 2015; Granato et al., 2008; Popa et al., 2010). HSV-1 and HSV-2 UL31 are 90% identical at the amino acid sequence, and the specific residues predicted to bind PAR (RRASRKSLP) are conserved between the two orthologs. It is tempting to speculate that macroH2A1.1 may interact directly with UL31 to connect host heterochromatin to the HSV-1 nuclear egress complex.

4.2.c How does host heterochromatin formation impact other nuclear-replicating viruses?

So far in my thesis work, I have only investigated the impact of host heterochromatin on HSV-1 nuclear egress. I found that lab-adapted HSV-1 strain *17syn+* efficient egress is sensitive to depletion of macroH2A1 and H3K27me3, and that egress of two clinical HSV-1 strains is also impacted by macroH2A1 KO. However, other viruses that replicate in the host cell nuclei, including the eight other human herpesviruses, must also contend with host chromatin to create space for progeny production and to exit the nucleus.

To test whether other herpesviruses are impacted by macroH2A1, I infected WT and macroH2A1 KO cells with HCMV strain *Towne* at MOI 1. I performed plaque assays to quantify viral progeny production and ddPCR to quantify HCMV genomes both in cells and within encapsulated virions in the supernatant (Figure 4.2). I observe a striking >10-fold loss in HCMV

progeny produced by cells lacking macroH2A1 (Figure 4.2A). However, there is no decrease in encapsulated HCMV genomes produced by macroH2A1 KO cells (Figure 4.2B) nor impact of macroH2A1 KO on HCMV replication (Figure 4.2C). The lack of difference of viral genomes within the supernatant compared to a significant decrease in infectious viral progeny indicates that macroH2A1 KO causes HCMV to produce a high number of defective virions. This is in contrast to the impact of macroH2A1 KO on HSV-1, which does not impact particle formation (Figure 3.16) but instead impairs efficient HSV-1 egress.

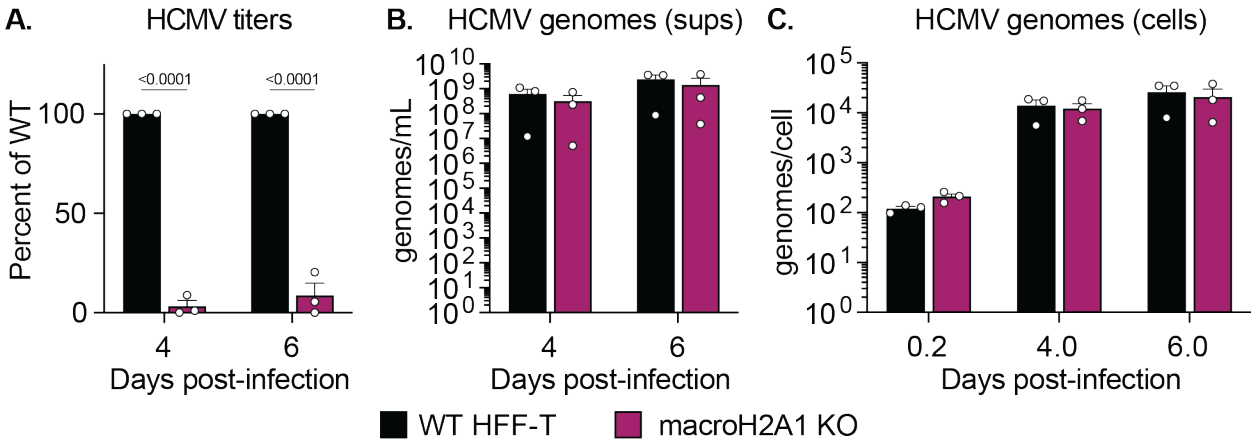

Figure 4.2 MacroH2A1 loss reduces HCMV titers but does not impact DNA replication.
A. Infectious progeny produced from HCMV infected WT and macroH2A1 KO HFF-T quantified by plaque assay. Viral yield is indicated as the percent yield compared to WT and was calculated through dividing plaque-forming units (pfu) per mL of the treatment group titers by the WT titers at each indicated time point. **B.** Droplet digital (ddPCR) quantification of HCMV genomes released from cells isolated from supernatants (sups). **C.** ddPCR quantification of HCMV genomes extracted from infected cells as indicated for each time point. Error bars represent the SEM of three biological replicates.

Although HSV-1 is studied as a prototype for herpesvirus nuclear egress, it is becoming more apparent that there are fundamental differences in how nuclear remodeling and egress occur in different herpesvirus families. For instance, HCMV infections causes the nucleus to distort into a signature “kidney bean” shape that wraps around a structure known as the viral cytoplasmic assembly compartment. HCMV capsids (which are already assembled with genomes within) bud

through the inner nuclear membrane into the assembly compartment to acquire their mature envelope and viral glycoproteins (Alwine, 2012).

Formation of these structures involves nuclear polarization and distribution of euchromatin and heterochromatin in different regions of the nucleus. Strikingly, heterochromatin marked by H3K9me3 is polarized *towards* the assembly compartment where euchromatin marked by H3K4me3 is polarized away from the assembly compartment (Procter et al., 2020). The authors of this study propose that H3K9me3 polarization towards the assembly compartment is a mechanism by which HCMV sequesters repressive heterochromatin away from viral replication compartments, which are located at the opposite pole from assembly compartments. They suggest that this is a strategy to prevent chromatinization of HCMV genomes which could impair viral replication. While this is similar to the explanation for why HSV-1 marginalizes host heterochromatin to the nuclear periphery, it is curious that HCMV replication compartments do not lead directly into assembly compartments. Instead, a potential barrier of dense heterochromatin forms between replication and assembly compartments, which is reminiscent of the dense peripheral heterochromatin we observe during HSV-1 infection.

My preliminary results show decreased infectious HCMV progeny upon macroH2A1 KO, possibly indicating a defect in HCMV genome packaging or maturation. This may suggest a functional role in heterochromatin polarized towards the assembly compartment in viral assembly or maturation, far beyond mere sequestration of repressive marks. This is an exciting avenue for future research into herpesvirus manipulation of host heterochromatin.

Beyond herpesviruses, many other nuclear-replicating viruses have different strategies for exiting the nucleus (Mettenleiter, 2016). HIV shuttles spliced and unspliced viral transcripts through a nuclear export signal in the Rev protein (Fischer et al., 1995). Hepadnaviruses similarly export pre-genomic RNAs into the cytoplasm, which are then reverse-transcribed into DNA while being encapsulated. Heterochromatin architecture and three-dimensional genome organization may influence activity of membrane-less bodies that are hubs for splicing and export, termed

nuclear speckles. Nuclear speckles are disrupted and recruited to the periphery of replication compartments in many viral infections (Faber et al., 2022). While increased heterochromatin compaction during infection could increase physical space for nuclear speckles to expand, I could also envision the increased space decreasing concentrations of splicing or export factors, which could negatively impact viral RNA export.

Orthomyxovirus packages its RNA genome with proteins into ribonucleic particles (RNPs), which are thought to be exported through nuclear pores and encapsulated in the cytoplasm. TEM during orthomyovirus infection shows enlargement of nuclear pore complexes to allow RNP export (Mühlbauer et al., 2015). Although I am not aware of evidence for viral RNP transport using an envelopment/de-envelopment process, large RNP granules in *Drosophila melanogaster* can use this route to bypass nuclear pores (Speese et al., 2012). If certain RNPs are too large to traverse the nuclear pore, it is possible that chromatin channels could promote efficient nuclear export similar to how they may promote HSV-1 egress.

Baculovirus, which is a family of large invertebrate-specific DNA viruses, packages its ~80-180 kb genomes into rod-shaped capsids within nuclei. Because of the size of the baculovirus capsid (200-450 nm long and 30-100 nm in diameter), this family of viruses also egresses using an envelopment and de-envelopment process similar to herpesviruses (Mettenleiter, 2016). Baculovirus infection in silkworm cell culture was also recently described to marginalize host chromatin to the nuclear periphery. However, in contrast to host chromatin compaction caused by HSV-1, ATAC-seq profiling of accessible chromatin during baculovirus infection revealed global chromatin *decondensation* and H3K27me3 downregulation as a consequence of infection (Kong et al., 2020). It is possible that silkworm cells susceptible to baculovirus infection typically have compressed genomes that need to be de-compressed to allow for viral replication and/or transit of the large rod-shaped capsids. It is also possible that some regions must de-compress while others stay compacted until the end of infection. Looking at the TEM images in this publication, I

observed large regions of electron density marginalized at the nuclear periphery that may be similar to the heterochromatin channels I see during HSV-1 egress.

Non-enveloped viruses such as adenovirus, polyomavirus and potentially papillomavirus are thought to rupture the nuclear membrane during cell lysis, bypassing a need for complicated egress and maturation pathways. Parvovirus also lyses the nuclear envelope during late stages of infection, but may egress through nuclear pore complexes or through transiting the ER or Golgi apparatus prior to cell lysis (Mettenleiter, 2016). It is possible formation of new heterochromatin during infection with nuclear-lysing viruses could prove beneficial to viruses post-lysis, as capsid entanglement with DNA strands may inhibit viral spread. An example of the antimicrobial properties of cell-free DNA are neutrophil extracellular traps (NETs). Neutrophils which have sensed a pathogen can induce widespread DNA decondensation, which results in DNA release from the cell still associated with histones (Brinkmann et al., 2004). Although originally considered a defense mechanism to ensnare large pathogens like bacteria, NETs have been shown to trap and neutralize HIV capsids (Saitoh et al., 2012). This suggests that decondensed but still chromatinized extracellular DNA has antiviral properties, and that it may benefit viruses to induce global chromatin condensation during infection.

4.3 Conclusions and perspectives.

In summary, I have shown through my dissertation work that infection with HSV-1 dramatically increases protein levels of heterochromatin marks macroH2A1 and H3K27me3. Infection leads to simultaneous genomic and physical reordering of macroH2A1 and H3K27me3 in broad regions that correlate with transcriptional repression. Loss of these markers results in reduced heterochromatin width at the nuclear periphery and impaired HSV-1 capsid egress from the nucleus. These data align with models developed by other groups suggesting that dense chromatin is a barrier to HSV-1 capsid access to the nuclear membrane, which the virus exploits by egressing through channels of low density heterochromatin. Future studies in our lab will focus

on whether other herpesviruses or even other large DNA viruses cause similar disruption of global host heterochromatin structure, and whether these interactions impact viral fitness. Ultimately, this work may lead to insights on how to pharmacologically target viral egress to prevent spread and dissemination of disease.

References

Ace, C. I., McKee, T. A., Ryan, J. M., Cameron, J. M., & Preston, C. M. (1989). Construction and characterization of a herpes simplex virus type 1 mutant unable to transinduce immediate-early gene expression. *Journal of Virology*, *63*(5), 2260–2269. https://doi.org/10.1128/jvi.63.5.2260-2269.1989

Agelopoulos, Marios, & Thanos, Dimitris. (2006). Epigenetic determination of a cell-specific gene expression program by ATF-2 and the histone variant macroH2A. *The EMBO Journal*, *25*(20), 4843–4853. https://doi.org/10.1038/sj.emboj.7601364

Aho, Vesa, Mäntylä, Elina, Ekman, Axel, Hakanen, Satu, Mattola, Salla, Chen, Jian-Hua, Weinhardt, Venera, Ruokolainen, Visa, Sodeik, Beate, Larabell, Carolyn, & Vihinen-Ranta, Maija. (2019). Quantitative Microscopy Reveals Stepwise Alteration of Chromatin Structure during Herpesvirus Infection. *Viruses*, *11*(10), 935. https://doi.org/10.3390/v11100935

Aho, Vesa, Myllys, Markko, Ruokolainen, Visa, Hakanen, Satu, Mäntylä, Elina, Virtanen, Jori, Hukkanen, Veijo, Kühn, Thomas, Timonen, Jussi, Mattila, Keijo, Larabell, Carolyn A., & Vihinen-Ranta, Maija. (2017). Chromatin organization regulates viral egress dynamics. *Scientific Reports*, *7*(1), 3692. https://doi.org/10.1038/s41598-017-03630-y

Aho, Vesa, Salminen, Sami, Mattola, Salla, Gupta, Alka, Flomm, Felix, Sodeik, Beate, Bosse, Jens B., & Vihinen-Ranta, Maija. (2021). Infection-induced chromatin modifications facilitate translocation of herpes simplex virus capsids to the inner nuclear membrane. *PLoS Pathogens*, *17*(12), e1010132. https://doi.org/10.1371/journal.ppat.1010132

Akhtar, Lisa N., & Kimberlin, David W. (2021). The Changing Landscape of Neonatal Herpes Simplex Virus Disease. *Journal of the Pediatric Infectious Diseases Society*, *11*(4), 121–123. https://doi.org/10.1093/jpids/piab118

Allfrey, V. G., Faulkner, R., & Mirsky, A. E. (1964). ACETYLATION AND METHYLATION OF HISTONES AND THEIR POSSIBLE ROLE IN THE REGULATION OF RNA SYNTHESIS*. *Proceedings of the National Academy of Sciences*, *51*(5), 786–794. https://doi.org/10.1073/pnas.51.5.786

Alwine, James C. (2012). The Human Cytomegalovirus Assembly Compartment: A Masterpiece of Viral Manipulation of Cellular Processes That Facilitates Assembly and Egress. *PLoS Pathogens*, *8*(9), e1002878. https://doi.org/10.1371/journal.ppat.1002878

Angelov, Dimitar, Molla, Annie, Perche, Pierre-Yves, Hans, Fabienne, Côté, Jacques, Khochbin, Saadi, Bouvet, Philippe, & Dimitrov, Stefan. (2003). The Histone Variant MacroH2A Interferes with Transcription Factor Binding and SWI/SNF Nucleosome Remodeling. *Molecular Cell*, *11*(4), 1033–1041. https://doi.org/10.1016/s1097-2765(03)00100-x

Arbuckle, Jesse H., Gardina, Paul J., Gordon, David N., Hickman, Heather D., Yewdell, Jonathan W., Pierson, Theodore C., Myers, Timothy G., & Kristie, Thomas M. (2017).

Inhibitors of the Histone Methyltransferases EZH2/1 Induce a Potent Antiviral State and Suppress Infection by Diverse Viral Pathogens. *MBio*, *8*(4), e01141-17. https://doi.org/10.1128/mbio.01141-17

Arents, G., Burlingame, R. W., Wang, B. C., Love, W. E., & Moudrianakis, E. N. (1991). The nucleosomal core histone octamer at 3.1 A resolution: a tripartite protein assembly and a left-handed superhelix. *Proceedings of the National Academy of Sciences*, *88*(22), 10148–10152. https://doi.org/10.1073/pnas.88.22.10148

Arents, G., & Moudrianakis, E. N. (1995). The histone fold: a ubiquitous architectural motif utilized in DNA compaction and protein dimerization. *Proceedings of the National Academy of Sciences*, *92*(24), 11170–11174. https://doi.org/10.1073/pnas.92.24.11170

Atherton, T. J., & Kerbyson, D. J. (1999). Size invariant circle detection. *Image and Vision Computing*, *17*(11), 795–803. https://doi.org/10.1016/s0262-8856(98)00160-7

Aubert, Martine, Boyle, Nicole M., Stone, Daniel, Stensland, Laurence, Huang, Meei-Li, Magaret, Amalia S., Galetto, Roman, Rawlings, David J., Scharenberg, Andrew M., & Jerome, Keith R. (2014). In vitro Inactivation of Latent HSV by Targeted Mutagenesis Using an HSV-specific Homing Endonuclease. *Molecular Therapy - Nucleic Acids*, *3*, e146. https://doi.org/10.1038/mtna.2013.75

Avgousti, Daphne C., & Weitzman, Matthew D. (2015). Stress Flips a Chromatin Switch to Wake Up Latent Virus. *Cell Host & Microbe*, *18*(6), 639–641. https://doi.org/10.1016/j.chom.2015.11.011

Ayoub, Houssein H., Chemaitelly, Hiam, & Abu-Raddad, Laith J. (2019). Characterizing the transitioning epidemiology of herpes simplex virus type 1 in the USA: model-based predictions. *BMC Medicine*, *17*(1), 57. https://doi.org/10.1186/s12916-019-1285-x

Barrero, María J., Sese, Borja, Martí, Mercè, & Belmonte, Juan Carlos Izpisua. (2013). Macro Histone Variants Are Critical for the Differentiation of Human Pluripotent Cells*. *Journal of Biological Chemistry*, *288*(22), 16110–16116. https://doi.org/10.1074/jbc.m113.466144

Bernstein, Emily, Muratore-Schroeder, Tara L., Diaz, Robert L., Chow, Jennifer C., Changolkar, Lakshmi N., Shabanowitz, Jeffrey, Heard, Edith, Pehrson, John R., Hunt, Donald F., & Allis, C. David. (2008). A phosphorylated subpopulation of the histone variant macroH2A1 is excluded from the inactive X chromosome and enriched during mitosis. *Proceedings of the National Academy of Sciences*, *105*(5), 1533–1538. https://doi.org/10.1073/pnas.0711632105

Bjerke, Susan L., & Roller, Richard J. (2006). Roles for herpes simplex virus type 1 UL34 and US3 proteins in disrupting the nuclear lamina during herpes simplex virus type 1 egress. *Virology*, *347*(2), 261–276. https://doi.org/10.1016/j.virol.2005.11.053

Boissière, Sylvie La, Hughes, Thomas, & O'Hare, Peter. (1999). HCF-dependent nuclear import of VP16. *The EMBO Journal*, *18*(2), 480–489. https://doi.org/10.1093/emboj/18.2.480

Bosse, Jens B., Hogue, Ian B., Feric, Marina, Thiberge, Stephan Y., Sodeik, Beate, Brangwynne, Clifford P., & Enquist, Lynn W. (2015). Remodeling nuclear architecture allows

efficient transport of herpesvirus capsids by diffusion. *Proceedings of the National Academy of Sciences*, *112*(42), E5725–E5733. https://doi.org/10.1073/pnas.1513876112

Bosse, Jens B., Virding, Stina, Thiberge, Stephan Y., Scherer, Julian, Wodrich, Harald, Ruzsics, Zsolt, Koszinowski, Ulrich H., & Enquist, Lynn W. (2014). Nuclear Herpesvirus Capsid Motility Is Not Dependent on F-Actin. *MBio*, *5*(5), e01909-14. https://doi.org/10.1128/mbio.01909-14

Bowerman, Samuel, Hickok, Robert J., & Wereszczynski, Jeff. (2019). Unique Dynamics in Asymmetric macroH2A–H2A Hybrid Nucleosomes Result in Increased Complex Stability. *The Journal of Physical Chemistry B*, *123*(2), 419–427. https://doi.org/10.1021/acs.jpcb.8b10668

Bowerman, Samuel, & Wereszczynski, Jeff. (2016). Effects of MacroH2A and H2A.Z on Nucleosome Dynamics as Elucidated by Molecular Dynamics Simulations. *Biophysical Journal*, *110*(2), 327–337. https://doi.org/10.1016/j.bpj.2015.12.015

Boyle, Shelagh, Gilchrist, Susan, Bridger, Joanna M., Mahy, Nicola L., Ellis, Juliet A., & Bickmore, Wendy A. (2001). The spatial organization of human chromosomes within the nuclei of normal and emerin-mutant cells. *Human Molecular Genetics*, *10*(3), 211–220. https://doi.org/10.1093/hmg/10.3.211

Brandariz-Nuñez, Alberto, Liu, Ting, Du, Te, & Evilevitch, Alex. (2019). Pressure-driven release of viral genome into a host nucleus is a mechanism leading to herpes infection. *ELife*, *8*, e47212. https://doi.org/10.7554/elife.47212

Brinkmann, Volker, Reichard, Ulrike, Goosmann, Christian, Fauler, Beatrix, Uhlemann, Yvonne, Weiss, David S., Weinrauch, Yvette, & Zychlinsky, Arturo. (2004). Neutrophil Extracellular Traps Kill Bacteria. *Science*, *303*(5663), 1532–1535. https://doi.org/10.1126/science.1092385

Brown, S. Moira, Ritchie, D. A., & Subak-Sharpe, J. H. (1973). Genetic Studies with Herpes Simplex Virus Type 1. The Isolation of Temperature-sensitive Mutants, their Arrangement into Complementation Groups and Recombination Analysis Leading to a Linkage Map. *Journal of General Virology*, *18*(3), 329–346. https://doi.org/10.1099/0022-1317-18-3-329

Bruni, C., & Porter, K. R. (1965). The Fine Structure of the Parenchymal Cell of the Normal Rat Liver: I. General Observations. *The American Journal of Pathology*, *46*(5), 691–755.

Buschbeck, Marcus, & Hake, Sandra B. (2017). Variants of core histones and their roles in cell fate decisions, development and cancer. *Nature Reviews Molecular Cell Biology*, *18*(5), 299–314. https://doi.org/10.1038/nrm.2016.166

Buschbeck, Marcus, Uribesalgo, Iris, Wibowo, Indra, Rué, Pau, Martin, David, Gutierrez, Arantxa, Morey, Lluís, Guigó, Roderic, López-Schier, Hernán, & Croce, Luciano Di. (2009). The histone variant macroH2A is an epigenetic regulator of key developmental genes. *Nature Structural & Molecular Biology*, *16*(10), 1074–1079. https://doi.org/10.1038/nsmb.1665

Cabral, Joseph M., Oh, Hyung Suk, & Knipe, David M. (2018). ATRX promotes maintenance of herpes simplex virus heterochromatin during chromatin stress. *ELife*, *7*, e40228. https://doi.org/10.7554/elife.40228

Cai, W., & Schaffer, P. A. (1992). Herpes simplex virus type 1 ICP0 regulates expression of immediate-early, early, and late genes in productively infected cells. *Journal of Virology*, *66*(5), 2904–2915. https://doi.org/10.1128/jvi.66.5.2904-2915.1992

Carrozza, M. J., & DeLuca, N. A. (1996). Interaction of the viral activator protein ICP4 with TFIID through TAF250. *Molecular and Cellular Biology*, *16*(6), 3085–3093. https://doi.org/10.1128/mcb.16.6.3085

Chadwick, Brian P., Valley, Cory M., & Willard, Huntington F. (2001). Histone variant macroH2A contains two distinct macrochromatin domains capable of directing macroH2A to the inactive X chromosome. *Nucleic Acids Research*, *29*(13), 2699–2705. https://doi.org/10.1093/nar/29.13.2699

Chakravarthy, Srinivas, Gundimella, Sampath Kumar Y., Caron, Cecile, Perche, Pierre-Yves, Pehrson, John R., Khochbin, Saadi, & Luger, Karolin. (2005). Structural Characterization of the Histone Variant macroH2A. *Molecular and Cellular Biology*, *25*(17), 7616–7624. https://doi.org/10.1128/mcb.25.17.7616-7624.2005

Chakravarthy, Srinivas, & Luger, Karolin. (2006). The Histone Variant Macro-H2A Preferentially Forms “Hybrid Nucleosomes”* ♦. *Journal of Biological Chemistry*, *281*(35), 25522–25531. https://doi.org/10.1074/jbc.m602258200

Chakravarthy, Srinivas, Patel, Ashok, & Bowman, Gregory D. (2012). The basic linker of macroH2A stabilizes DNA at the entry/exit site of the nucleosome. *Nucleic Acids Research*, *40*(17), 8285–8295. https://doi.org/10.1093/nar/gks645

Chang, Evelyn Y., Ferreira, Helder, Somers, Joanna, Nusinow, Dmitri A., Owen-Hughes, Tom, & Narlikar, Geeta J. (2008). MacroH2A Allows ATP-Dependent Chromatin Remodeling by SWI/SNF and ACF Complexes but Specifically Reduces Recruitment of SWI/SNF †. *Biochemistry*, *47*(51), 13726–13732. https://doi.org/10.1021/bi8016944

Chang, Y. E., Sant, C. Van, Krug, P. W., Sears, A. E., & Roizman, B. (1997). The null mutant of the U(L)31 gene of herpes simplex virus 1: construction and phenotype in infected cells. *Journal of Virology*, *71*(11), 8307–8315. https://doi.org/10.1128/jvi.71.11.8307-8315.1997

Changolkar, Lakshmi N., & Pehrson, John R. (2002). Reconstitution of Nucleosomes with Histone MacroH2A1.2 †. *Biochemistry*, *41*(1), 179–184. https://doi.org/10.1021/bi0157417

Changolkar, Lakshmi N., & Pehrson, John R. (2006). macroH2A1 Histone Variants Are Depleted on Active Genes but Concentrated on the Inactive X Chromosome†. *Molecular and Cellular Biology*, *26*(12), 4410–4420. https://doi.org/10.1128/mcb.02258-05

Changolkar, Lakshmi N., Singh, Geetika, Cui, Kairong, Berletch, Joel B., Zhao, Keji, Disteche, Christine M., & Pehrson, John R. (2010). Genome-Wide Distribution of MacroH2A1 Histone Variants in Mouse Liver Chromatin. *Molecular and Cellular Biology*, *30*(23), 5473–5483. https://doi.org/10.1128/mcb.00518-10

Changolkar, Lakshmi N., Singh, Geetika, & Pehrson, John R. (2008). macroH2A1-Dependent Silencing of Endogenous Murine Leukemia Viruses ▿ †. *Molecular and Cellular Biology*, *28*(6), 2059–2065. https://doi.org/10.1128/mcb.01362-07

Chen, Hongshan, Ruiz, Penelope D., McKimpson, Wendy M., Novikov, Leonid, Kitsis, Richard N., & Gamble, Matthew J. (2015). MacroH2A1 and ATM Play Opposing Roles in Paracrine Senescence and the Senescence-Associated Secretory Phenotype. *Molecular Cell*, *59*(5), 719–731. https://doi.org/10.1016/j.molcel.2015.07.011

Chen, Hongshan, Ruiz, Penelope D., Novikov, Leonid, Casill, Alyssa D., Park, Jong Woo, & Gamble, Matthew J. (2014). MacroH2A1.1 and PARP-1 cooperate to regulate transcription by promoting CBP-mediated H2B acetylation. *Nature Structural & Molecular Biology*, *21*(11), 981–989. https://doi.org/10.1038/nsmb.2903

Chen, I. Hsiung Brandon, Sciabica, Kathryn S., & Sandri-Goldin, Rozanne M. (2002). ICP27 Interacts with the RNA Export Factor Aly/REF To Direct Herpes Simplex Virus Type 1 Intronless mRNAs to the TAP Export Pathway. *Journal of Virology*, *76*(24), 12877–12889. https://doi.org/10.1128/jvi.76.24.12877-12889.2002

Chen, S. H., Kramer, M. F., Schaffer, P. A., & Coen, D. M. (1997). A viral function represses accumulation of transcripts from productive-cycle genes in mouse ganglia latently infected with herpes simplex virus. *Journal of Virology*, *71*(8), 5878–5884. https://doi.org/10.1128/jvi.71.8.5878-5884.1997

Child, Stephanie J., Greninger, Alexander L., & Geballe, Adam P. (2021). Rapid adaptation to human protein kinase R by a unique genomic rearrangement in rhesus cytomegalovirus. *PLoS Pathogens*, *17*(1), e1009088. https://doi.org/10.1371/journal.ppat.1009088

Chuan, Gao, Chen, Lin, Tang, Shan-Bo, Long, Qiao-Yun, He, Jia-Li, Zhang, Na-An, Shu, Hong-Bing, Chen, Zhen-Xia, Wu, Min, & Li, Lian-Yun. (2020). The epigenetic landscapes of histone modifications on HSV-1 genome in human THP-1 cells. *Antiviral Research*, *176*, 104730. https://doi.org/10.1016/j.antiviral.2020.104730

Cliffe, Anna R., Arbuckle, Jesse H., Vogel, Jodi L., Geden, Matthew J., Rothbart, Scott B., Cusack, Corey L., Strahl, Brian D., Kristie, Thomas M., & Deshmukh, Mohanish. (2015). Neuronal Stress Pathway Mediating a Histone Methyl/Phospho Switch Is Required for Herpes Simplex Virus Reactivation. *Cell Host & Microbe*, *18*(6), 649–658. https://doi.org/10.1016/j.chom.2015.11.007

Cliffe, Anna R., Coen, Donald M., & Knipe, David M. (2013). Kinetics of Facultative Heterochromatin and Polycomb Group Protein Association with the Herpes Simplex Viral Genome during Establishment of Latent Infection. *MBio*, *4*(1), e00590-12. https://doi.org/10.1128/mbio.00590-12

Cliffe, Anna R., Garber, David A., & Knipe, David M. (2009a). Transcription of the Herpes Simplex Virus Latency-Associated Transcript Promotes the Formation of Facultative Heterochromatin on Lytic Promoters. *Journal of Virology*, *83*(16), 8182–8190. https://doi.org/10.1128/jvi.00712-09

Cliffe, Anna R., Garber, David A., & Knipe, David M. (2009b). Transcription of the Herpes Simplex Virus Latency-Associated Transcript Promotes the Formation of Facultative Heterochromatin on Lytic Promoters ▿ . *Journal of Virology*, *83*(16), 8182–8190. https://doi.org/10.1128/jvi.00712-09

Cliffe, Anna R., & Knipe, David M. (2008). Herpes Simplex Virus ICP0 Promotes both Histone Removal and Acetylation on Viral DNA during Lytic Infection ▿ . *Journal of Virology*, *82*(24), 12030–12038. https://doi.org/10.1128/jvi.01575-08

Cliffe, Anna R., & Wilson, Angus C. (2017). Restarting Lytic Gene Transcription at the Onset of Herpes Simplex Virus Reactivation. *Journal of Virology*, *91*(2), e01419-16. https://doi.org/10.1128/jvi.01419-16

Costanzi, Carl, & Pehrson, John R. (1998). Histone macroH2A1 is concentrated in the inactive X chromosome of female mammals. *Nature*, *393*(6685), 599–601. https://doi.org/10.1038/31275

Costanzi, Carl, & Pehrson, John R. (2001). MACROH2A2, a New Member of the MACROH2A Core Histone Family. *Journal of Biological Chemistry*, *276*(24), 21776–21784. https://doi.org/10.1074/jbc.m010919200

Cremer, Thomas, & Cremer, Marion. (2010). Chromosome Territories. *Cold Spring Harbor Perspectives in Biology*, *2*(3), a003889. https://doi.org/10.1101/cshperspect.a003889

Creppe, Catherine, Janich, Peggy, Cantariño, Neus, Noguera, Marc, Valero, Vanesa, Musulén, Eva, Douet, Julien, Posavec, Melanija, Martín-Caballero, Juan, Sumoy, Lauro, Croce, Luciano Di, Benitah, Salvador A., & Buschbeck, Marcus. (2012). MacroH2A1 Regulates the Balance between Self-Renewal and Differentiation Commitment in Embryonic and Adult Stem Cells. *Molecular and Cellular Biology*, *32*(8), 1442–1452. https://doi.org/10.1128/mcb.06323-11

Croft, Jenny A., Bridger, Joanna M., Boyle, Shelagh, Perry, Paul, Teague, Peter, & Bickmore, Wendy A. (1999). Differences in the Localization and Morphology of Chromosomes in the Human Nucleus. *The Journal of Cell Biology*, *145*(6), 1119–1131. https://doi.org/10.1083/jcb.145.6.1119

Dai-Ju, Jenny Q., Li, Ling, Johnson, Lisa A., & Sandri-Goldin, Rozanne M. (2006). ICP27 Interacts with the C-Terminal Domain of RNA Polymerase II and Facilitates Its Recruitment to Herpes Simplex Virus 1 Transcription Sites, Where It Undergoes Proteasomal Degradation during Infection. *Journal of Virology*, *80*(7), 3567–3581. https://doi.org/10.1128/jvi.80.7.3567-3581.2006

Dalrymple, M. A., McGeoch, D. J., Davison, A. J., & Preston, CM. (1985). DNA sequence of the herpes simplex virus type 1 gene whose product is responsible for transcriptional activation of immediate early promoters. *Nucleic Acids Research*, *13*(21), 7865–7879. https://doi.org/10.1093/nar/13.21.7865

Dardenne, Etienne, Pierredon, Sandra, Driouch, Keltouma, Gratadou, Lise, Lacroix-Triki, Magali, Espinoza, Micaela Polay, Zonta, Eleonora, Germann, Sophie, Mortada, Hussein,

Villemin, Jean-Philippe, Dutertre, Martin, Lidereau, Rosette, Vagner, Stéphan, & Auboeuf, Didier. (2012). Splicing switch of an epigenetic regulator by RNA helicases promotes tumor-cell invasiveness. *Nature Structural & Molecular Biology*, *19*(11), 1139–1146. https://doi.org/10.1038/nsmb.2390

Davison, Andrew J. (2007). *Human Herpesviruses*. 10–26. https://doi.org/10.1017/cbo9780511545313.003

Davison, Andrew J., Eberle, Richard, Ehlers, Bernhard, Hayward, Gary S., McGeoch, Duncan J., Minson, Anthony C., Pellett, Philip E., Roizman, Bernard, Studdert, Michael J., & Thiry, Etienne. (2009). The order Herpesvirales. *Archives of Virology*, *154*(1), 171–177. https://doi.org/10.1007/s00705-008-0278-4

Dembowski, Jill A., & DeLuca, Neal A. (2015). Selective Recruitment of Nuclear Factors to Productively Replicating Herpes Simplex Virus Genomes. *PLoS Pathogens*, *11*(5), e1004939. https://doi.org/10.1371/journal.ppat.1004939

Dembowski, Jill A., & DeLuca, Neal A. (2018). Temporal Viral Genome-Protein Interactions Define Distinct Stages of Productive Herpesviral Infection. *MBio*, *9*(4), e01182-18. https://doi.org/10.1128/mbio.01182-18

Deshmane, S. L., & Fraser, N. W. (1989). During latency, herpes simplex virus type 1 DNA is associated with nucleosomes in a chromatin structure. *Journal of Virology*, *63*(2), 943–947. https://doi.org/10.1128/jvi.63.2.943-947.1989

Dolan, Aidan, Jamieson, Fiona E., Cunningham, Charles, Barnett, Barbara C., & McGeoch, Duncan J. (1998). The Genome Sequence of Herpes Simplex Virus Type 2. *Journal of Virology*, *72*(3), 2010–2021. https://doi.org/10.1128/jvi.72.3.2010-2021.1998

Douet, Julien, Corujo, David, Malinverni, Roberto, Renauld, Justine, Sansoni, Viola, Marjanović, Melanija Posavec, Cantari'o, Neus, Valero, Vanesa, Mongelard, Fabien, Bouvet, Philippe, Imhof, Axel, Thiry, Marc, & Buschbeck, Marcus. (2017). MacroH2A histone variants maintain nuclear organization and heterochromatin architecture. *J Cell Sci*, *130*(9), jcs.199216. https://doi.org/10.1242/jcs.199216

Douglas, Mark W., Diefenbach, Russell J., Homa, Fred L., Miranda-Saksena, Monica, Rixon, Frazer J., Vittone, Valerio, Byth, Karen, & Cunningham, Anthony L. (2004). Herpes Simplex Virus Type 1 Capsid Protein VP26 Interacts with Dynein Light Chains RP3 and Tctex1 and Plays a Role in Retrograde Cellular Transport*. *Journal of Biological Chemistry*, *279*(27), 28522–28530. https://doi.org/10.1074/jbc.m311671200

Doyen, Cécile-Marie, An, Woojin, Angelov, Dimitar, Bondarenko, Vladimir, Mietton, Flore, Studitsky, Vassily M., Hamiche, Ali, Roeder, Robert G., Bouvet, Philippe, & Dimitrov, Stefan. (2006). Mechanism of Polymerase II Transcription Repression by the Histone Variant macroH2A. *Molecular and Cellular Biology*, *26*(3), 1156–1164. https://doi.org/10.1128/mcb.26.3.1156-1164.2006

Dremel, Sarah E., & DeLuca, Neal A. (2019). Herpes simplex viral nucleoprotein creates a competitive transcriptional environment facilitating robust viral transcription and host shut off. *ELife*, *8*, e51109. https://doi.org/10.7554/elife.51109

Entrevan, Marianne, Schuettengruber, Bernd, & Cavalli, Giacomo. (2016). Regulation of Genome Architecture and Function by Polycomb Proteins. *Trends in Cell Biology*, *26*(7), 511–525. https://doi.org/10.1016/j.tcb.2016.04.009

Ertel, Monica K., Cammarata, Amy L., Hron, Rebecca J., & Neumann, Donna M. (2012). CTCF Occupation of the Herpes Simplex Virus 1 Genome Is Disrupted at Early Times Postreactivation in a Transcription-Dependent Manner. *Journal of Virology*, *86*(23), 12741–12759. https://doi.org/10.1128/jvi.01655-12

Everett, Roger D., Rechter, Sabine, Papior, Peer, Tavalai, Nina, Stamminger, Thomas, & Orr, Anne. (2006). PML contributes to a cellular mechanism of repression of herpes simplex virus type 1 infection that is inactivated by ICP0. *Journal of Virology*, *80*(16), 7995–8005. https://doi.org/10.1128/jvi.00734-06

Faber, Gabriel P., Nadav-Eliyahu, Shani, & Shav-Tal, Yaron. (2022). Nuclear speckles – a driving force in gene expression. *Journal of Cell Science*, *135*(13). https://doi.org/10.1242/jcs.259594

Feierbach, Becket, Piccinotti, Silvia, Bisher, Margaret, Denk, Winfried, & Enquist, Lynn W. (2006). Alpha-Herpesvirus Infection Induces the Formation of Nuclear Actin Filaments. *PLoS Pathogens*, *2*(8), e85. https://doi.org/10.1371/journal.ppat.0020085

Fernandes, Neil D., Arya, Kapil, & Ward, Rebecca. (2022). *Congenital Herpes Simplex*. StatPearls Publishing.

Fischer, Utz, Huber, Jochen, Boelens, Wilbert C., Mattajt, Lain W., & Lührmann, Reinhard. (1995). The HIV-1 Rev Activation Domain is a nuclear export signal that accesses an export pathway used by specific cellular RNAs. *Cell*, *82*(3), 475–483. https://doi.org/10.1016/0092-8674(95)90436-0

Fischle, Wolfgang, Tseng, Boo Shan, Dormann, Holger L., Ueberheide, Beatrix M., Garcia, Benjamin A., Shabanowitz, Jeffrey, Hunt, Donald F., Funabiki, Hironori, & Allis, C. David. (2005). Regulation of HP1–chromatin binding by histone H3 methylation and phosphorylation. *Nature*, *438*(7071), 1116–1122. https://doi.org/10.1038/nature04219

Forest, Thomas, Barnard, Sandra, & Baines, Joel D. (2005). Active intranuclear movement of herpesvirus capsids. *Nature Cell Biology*, *7*(4), 429–431. https://doi.org/10.1038/ncb1243

Fu, Yuhua, Lv, Pin, Yan, Guoquan, Fan, Hui, Cheng, Lu, Zhang, Feng, Dang, Yongjun, Wu, Hao, & Wen, Bo. (2015). MacroH2A1 associates with nuclear lamina and maintains chromatin architecture in mouse liver cells. *Scientific Reports*, *5*(1), 17186. https://doi.org/10.1038/srep17186

Full, Florian, Gent, Michiel van, Sparrer, Konstantin M. J., Chiang, Cindy, Zurenski, Matthew A., Scherer, Myriam, Brockmeyer, Norbert H., Heinzerling, Lucie, Stürzl, Michael, Korn, Klaus, Stamminger, Thomas, Ensser, Armin, & Gack, Michaela U. (2019). Centrosomal protein TRIM43 restricts herpesvirus infection by regulating nuclear lamina integrity. *Nature Microbiology*, *4*(1), 164–176. https://doi.org/10.1038/s41564-018-0285-5

Fyodorov, Dmitry V., Zhou, Bing-Rui, Skoultchi, Arthur I., & Bai, Yawen. (2018). Emerging roles of linker histones in regulating chromatin structure and function. *Nature Reviews Molecular Cell Biology*, *19*(3), 192–206. https://doi.org/10.1038/nrm.2017.94

Gamble, Matthew J., Frizzell, Kristine M., Yang, Christine, Krishnakumar, Raga, & Kraus, W. Lee. (2010). The histone variant macroH2A1 marks repressed autosomal chromatin, but protects a subset of its target genes from silencing. *Genes & Development*, *24*(1), 21–32. https://doi.org/10.1101/gad.1876110

Gamble, Matthew J., & Kraus, W. Lee. (2010). Multiple facets of the unique histone variant macroH2A: From genomics to cell biology. *Cell Cycle*, *9*(13), 2568–2574. https://doi.org/10.4161/cc.9.13.12144

Gao, Jie, Hay, Thomas J. M., & Banfield, Bruce W. (2017). The Product of the Herpes Simplex Virus 2 UL16 Gene Is Critical for the Egress of Capsids from the Nuclei of Infected Cells. *Journal of Virology*, *91*(10). https://doi.org/10.1128/jvi.00350-17

Garber, D A, Schaffer, P. A., & Knipe, D. M. (1997). A LAT-associated function reduces productive-cycle gene expression during acute infection of murine sensory neurons with herpes simplex virus type 1. *Journal of Virology*, *71*(8), 5885–5893. https://doi.org/10.1128/jvi.71.8.5885-5893.1997

Garber, David A., Beverley, Stephen M., & Coen, Donald M. (1993). Demonstration of Circularization of Herpes Simplex Virus DNA Following infection Using Pulsed Field Gel Electrophoresis. *Virology*, *197*(1), 459–462. https://doi.org/10.1006/viro.1993.1612

Gaspar-Maia, Alexandre, Qadeer, Zulekha A., Hasson, Dan, Ratnakumar, Kajan, Leu, N. Adrian, Leroy, Gary, Liu, Shichong, Costanzi, Carl, Valle-Garcia, David, Schaniel, Christoph, Lemischka, Ihor, Garcia, Benjamin, Pehrson, John R., & Bernstein, Emily. (2013). MacroH2A histone variants act as a barrier upon reprogramming towards pluripotency. *Nature Communications*, *4*(1), 1565. https://doi.org/10.1038/ncomms2582

Gatherer, Derek, Depledge, Daniel P., Hartley, Carol A., Szpara, Moriah L., Vaz, Paola K., Benkő, Mária, Brandt, Curtis R., Bryant, Neil A., Dastjerdi, Akbar, Doszpoly, Andor, Gompels, Ursula A., Inoue, Naoki, Jarosinski, Keith W., Kaul, Rajeev, Lacoste, Vincent, Norberg, Peter, Origgi, Francesco C., Orton, Richard J., Pellett, Philip E., … Davison, Andrew J. (2021). ICTV Virus Taxonomy Profile: Herpesviridae 2021. *The Journal of General Virology*, *102*(10), 001673. https://doi.org/10.1099/jgv.0.001673

Geraghty, Robert J., Krummenacher, Claude, Cohen, Gary H., Eisenberg, Roselyn J., & Spear, Patricia G. (1998). Entry of Alphaherpesviruses Mediated by Poliovirus Receptor-Related Protein 1 and Poliovirus Receptor. *Science*, *280*(5369), 1618–1620. https://doi.org/10.1126/science.280.5369.1618

Gibeault, Rebecca L., Conn, Kristen L., Bildersheim, Michael D., & Schang, Luis M. (2016). An Essential Viral Transcription Activator Modulates Chromatin Dynamics. *PLOS Pathogens*, *12*(8), e1005842. https://doi.org/10.1371/journal.ppat.1005842

Gibson, Wade, & Roizman, Bernard. (1971). Compartmentalization of Spermine and Spermidine in the Herpes Simplex Virion. *Proceedings of the National Academy of Sciences*, *68*(11), 2818–2821. https://doi.org/10.1073/pnas.68.11.2818

Gibson, Wade, & Roizman, Bernard. (1972). Proteins Specified by Herpes Simplex Virus VIII. Characterization and Composition of Multiple Capsid Forms of Subtypes 1 and 2. *Journal of Virology*, *10*(5), 1044–1052. https://doi.org/10.1128/jvi.10.5.1044-1052.1972

Godowski, P. J., & Knipe, D. M. (1986). Transcriptional control of herpesvirus gene expression: gene functions required for positive and negative regulation. *Proceedings of the National Academy of Sciences*, *83*(2), 256–260. https://doi.org/10.1073/pnas.83.2.256

Görisch, Sabine M., Wachsmuth, Malte, Ittrich, Carina, Bacher, Christian P., Rippe, Karsten, & Lichter, Peter. (2004). Nuclear body movement is determined by chromatin accessibility and dynamics. *Proceedings of the National Academy of Sciences*, *101*(36), 13221–13226. https://doi.org/10.1073/pnas.0402958101

Grady, Sarah L., Hwang, Jesse, Vastag, Livia, Rabinowitz, Joshua D., & Shenk, Thomas. (2012). Herpes Simplex Virus 1 Infection Activates Poly(ADP-Ribose) Polymerase and Triggers the Degradation of Poly(ADP-Ribose) Glycohydrolase. *Journal of Virology*, *86*(15), 8259–8268. https://doi.org/10.1128/jvi.00495-12

Granato, Marisa, Feederle, Regina, Farina, Antonella, Gonnella, Roberta, Santarelli, Roberta, Hub, Birgit, Faggioni, Alberto, & Delecluse, Henri-Jacques. (2008). Deletion of Epstein-Barr Virus BFLF2 Leads to Impaired Viral DNA Packaging and Primary Egress as Well as to the Production of Defective Viral Particles. *Journal of Virology*, *82*(8), 4042–4051. https://doi.org/10.1128/jvi.02436-07

Greally, John M. (2018). A user's guide to the ambiguous word "epigenetics." *Nature Reviews Molecular Cell Biology*, *19*(4), 207–208. https://doi.org/10.1038/nrm.2017.135

Guberovic, Iva, Hurtado-Bagès, Sarah, Rivera-Casas, Ciro, Knobloch, Gunnar, Malinverni, Roberto, Valero, Vanesa, Leger, Michelle M., García, Jesús, Basquin, Jerome, Cedrón, Marta Gómez de, Frigolé-Vivas, Marta, Cheema, Manjinder S., Pérez, Ainhoa, Ausió, Juan, Molina, Ana Ramírez de, Salvatella, Xavier, Ruiz-Trillo, Iñaki, Eirin-Lopez, Jose M., Ladurner, Andreas G., & Buschbeck, Marcus. (2021). Evolution of a histone variant involved in compartmental regulation of NAD metabolism. *Nature Structural & Molecular Biology*, *28*(12), 1009–1019. https://doi.org/10.1038/s41594-021-00692-5

Guo, Yiran, Zhao, Shuai, & Wang, Gang Greg. (2021). Polycomb Gene Silencing Mechanisms: PRC2 Chromatin Targeting, H3K27me3 "Readout", and Phase Separation-Based Compaction. *Trends in Genetics*, *37*(6), 547–565. https://doi.org/10.1016/j.tig.2020.12.006

Halford, William P., & Schaffer, Priscilla A. (2001). ICP0 Is Required for Efficient Reactivation of Herpes Simplex Virus Type 1 from Neuronal Latency. *Journal of Virology*, *75*(7), 3240–3249. https://doi.org/10.1128/jvi.75.7.3240-3249.2001

Harr, Jennifer C., Luperchio, Teresa Romeo, Wong, Xianrong, Cohen, Erez, Wheelan, Sarah J., & Reddy, Karen L. (2015). Directed targeting of chromatin to the nuclear lamina is mediated

by chromatin state and A-type lamins. *Journal of Cell Biology*, *208*(1), 33–52. https://doi.org/10.1083/jcb.201405110

Hatch, Emily M., Kulukian, Anita, Holland, Andrew J., Cleveland, Don W., & Stearns, Tim. (2010). Cep152 interacts with Plk4 and is required for centriole duplication. *Journal of Cell Biology*, *191*(4), 721–729. https://doi.org/10.1083/jcb.201006049

Haws, Spencer A., Simandi, Zoltan, Barnett, R. Jordan, & Phillips-Cremins, Jennifer E. (2022). 3D genome, on repeat: Higher-order folding principles of the heterochromatinized repetitive genome. *Cell*, *185*(15), 2690–2707. https://doi.org/10.1016/j.cell.2022.06.052

Heming, Jason D., Conway, James F., & Homa, Fred L. (2017). Cell Biology of Herpes Viruses. *Advances in Anatomy, Embryology, and Cell Biology*, *223*, 119–142. https://doi.org/10.1007/978-3-319-53168-7_6

Hernández-Muñoz, Inmaculada, Lund, Anders H., Stoop, Petra van der, Boutsma, Erwin, Muijrers, Inhua, Verhoeven, Els, Nusinow, Dmitri A., Panning, Barbara, Marahrens, York, & Lohuizen, Maarten van. (2005). Stable X chromosome inactivation involves the PRC1 Polycomb complex and requires histone MACROH2A1 and the CULLIN3/SPOP ubiquitin E3 ligase. *Proceedings of the National Academy of Sciences*, *102*(21), 7635–7640. https://doi.org/10.1073/pnas.0408918102

Hetzer, Martin W. (2010). The Nuclear Envelope. *Cold Spring Harbor Perspectives in Biology*, *2*(3), a000539. https://doi.org/10.1101/cshperspect.a000539

Hill, James M., Quenelle, Debra C., Cardin, Rhonda D., Vogel, Jodi L., Clement, Christian, Bravo, Fernando J., Foster, Timothy P., Bosch-Marce, Marta, Raja, Priya, Lee, Jennifer S., Bernstein, David I., Krause, Philip R., Knipe, David M., & Kristie, Thomas M. (2014). Inhibition of LSD1 reduces herpesvirus infection, shedding, and recurrence by promoting epigenetic suppression of viral genomes. *Science Translational Medicine*, *6*(265), 265ra169-265ra169. https://doi.org/10.1126/scitranslmed.3010643

Holliday, Robin. (1987). The Inheritance of Epigenetic Defects. *Science*, *238*(4824), 163–170. https://doi.org/10.1126/science.3310230

Hu, MiYao, Depledge, Daniel P., Cortes, Esteban Flores, Breuer, Judith, & Schang, Luis M. (2019). Chromatin dynamics and the transcriptional competence of HSV-1 genomes during lytic infections. *PLOS Pathogens*, *15*(11), e1008076. https://doi.org/10.1371/journal.ppat.1008076

Hurtado-Bagès, Sarah, Knobloch, Gunnar, Ladurner, Andreas G., & Buschbeck, Marcus. (2020). The taming of PARP1 and its impact on NAD+ metabolism. *Molecular Metabolism*, 100950. https://doi.org/10.1016/j.molmet.2020.01.014

Hurtado-Bagès, Sarah, Marjanovic, Melanija Posavec, Valero, Vanesa, Malinverni, Roberto, Corujo, David, Bouvet, Philippe, Lavigne, Anne-Claire, Bystricky, Kerstin, & Buschbeck, Marcus. (2020). The Histone Variant MacroH2A1 Regulates Key Genes for Myogenic Cell Fusion in a Splice-Isoform Dependent Manner. *Cells*, *9*(5), 1109. https://doi.org/10.3390/cells9051109

Hussey, Kristine M., Chen, Hongshan, Yang, Christine, Park, Eugene, Hah, Nasun, Erdjument-Bromage, Hediye, Tempst, Paul, Gamble, Matthew J., & Kraus, W. Lee. (2014). The Histone Variant MacroH2A1 Regulates Target Gene Expression in Part by Recruiting the Transcriptional Coregulator PELP1. *Molecular and Cellular Biology*, *34*(13), 2437–2449. https://doi.org/10.1128/mcb.01315-13

James, Charlotte, Harfouche, Manale, Welton, Nicky J., Turner, Katherine ME, Abu-Raddad, Laith J., Gottlieb, Sami L., & Looker, Katharine J. (2020). Herpes simplex virus: global infection prevalence and incidence estimates, 2016. *Bulletin of the World Health Organization*, *98*(5), 315–329. https://doi.org/10.2471/blt.19.237149

Jenuwein, Thomas, & Allis, C. David. (2001). Translating the Histone Code. *Science*, *293*(5532), 1074–1080. https://doi.org/10.1126/science.1063127

Kapoor, Avnish, Goldberg, Matthew S., Cumberland, Lara K., Ratnakumar, Kajan, Segura, Miguel F., Emanuel, Patrick O., Menendez, Silvia, Vardabasso, Chiara, LeRoy, Gary, Vidal, Claudia I., Polsky, David, Osman, Iman, Garcia, Benjamin A., Hernando, Eva, & Bernstein, Emily. (2010). The histone variant macroH2A suppresses melanoma progression through regulation of CDK8. *Nature*, *468*(7327), 1105–1109. https://doi.org/10.1038/nature09590

Kaya-Okur, Hatice S., Wu, Steven J., Codomo, Christine A., Pledger, Erica S., Bryson, Terri D., Henikoff, Jorja G., Ahmad, Kami, & Henikoff, Steven. (2019). CUT&Tag for efficient epigenomic profiling of small samples and single cells. *Nature Communications*, *10*(1), 1930. https://doi.org/10.1038/s41467-019-09982-5

Kent, J. R., Zeng, P. Y., Atanasiu, D., Gardner, J., Fraser, N. W., & Berger, S. L. (2004). During Lytic Infection Herpes Simplex Virus Type 1 Is Associated with Histones Bearing Modifications That Correlate with Active Transcription. *Journal of Virology*, *78*(18), 10178–10186. https://doi.org/10.1128/jvi.78.18.10178-10186.2004

Khurana, Simran, Kruhlak, Michael J., Kim, Jeongkyu, Tran, Andy D., Liu, Jinping, Nyswaner, Katherine, Shi, Lei, Jailwala, Parthav, Sung, Myong-Hee, Hakim, Ofir, & Oberdoerffer, Philipp. (2014). A Macrohistone Variant Links Dynamic Chromatin Compaction to BRCA1-Dependent Genome Maintenance. *Cell Reports*, *8*(4), 1049–1062. https://doi.org/10.1016/j.celrep.2014.07.024

Kim, Jeongkyu, Sturgill, David, Sebastian, Robin, Khurana, Simran, Tran, Andy D., Edwards, Garrett B., Kruswick, Alex, Burkett, Sandra, Hosogane, Eri K., Hannon, William W., Weyemi, Urbain, Bonner, William M., Luger, Karolin, & Oberdoerffer, Philipp. (2018). Replication Stress Shapes a Protective Chromatin Environment across Fragile Genomic Regions. *Molecular Cell*, *69*(1), 36-47.e7. https://doi.org/10.1016/j.molcel.2017.11.021

Kim, Jeongkyu, Sun, Chongkui, Tran, Andy D., Chin, Pei-Ju, Ruiz, Penelope D., Wang, Kun, Gibbons, Richard J., Gamble, Matthew J., Liu, Yie, & Oberdoerffer, Philipp. (2019). The macroH2A1.2 histone variant links ATRX loss to alternative telomere lengthening. *Nature Structural & Molecular Biology*, *26*(3), 213–219. https://doi.org/10.1038/s41594-019-0192-3

Kim, Ju Youn, Mandarino, Angelo, Chao, Moses V., Mohr, Ian, & Wilson, Angus C. (2012). Transient Reversal of Episome Silencing Precedes VP16-Dependent Transcription during

Reactivation of Latent HSV-1 in Neurons. *PLoS Pathogens*, *8*(2), e1002540. https://doi.org/10.1371/journal.ppat.1002540

Kind, Jop, Pagie, Ludo, Ortabozkoyun, Havva, Boyle, Shelagh, de Vries, Sandra S., Janssen, Hans, Amendola, Mario, Nolen, Leisha D., Bickmore, Wendy A., & van Steensel, Bas. (2013). Single-Cell Dynamics of Genome-Nuclear Lamina Interactions. *Cell*, *153*(1), 178–192. https://doi.org/10.1016/j.cell.2013.02.028

Knipe, David M., & Cliffe, Anna. (2008). Chromatin control of herpes simplex virus lytic and latent infection. *Nature Reviews Microbiology*, *6*(3), 211–221. https://doi.org/10.1038/nrmicro1794

Kolb, Gaelle, & Kristie, Thomas M. (2008). Association of the Cellular Coactivator HCF-1 with the Golgi Apparatus in Sensory Neurons. *Journal of Virology*, *82*(19), 9555–9563. https://doi.org/10.1128/jvi.01174-08

Kong, Xiangshuo, Wei, Guisheng, Chen, Nan, Zhao, Shudi, Shen, Yunwang, Zhang, Jianjia, Li, Yang, Zeng, Xiaoqun, & Wu, Xiaofeng. (2020). Dynamic chromatin accessibility profiling reveals changes in host genome organization in response to baculovirus infection. *PLoS Pathogens*, *16*(6), e1008633. https://doi.org/10.1371/journal.ppat.1008633

Kozlowski, Marek, Corujo, David, Hothorn, Michael, Guberovic, Iva, Mandemaker, Imke K., Blessing, Charlotte, Sporn, Judith, Gutierrez-Triana, Arturo, Smith, Rebecca, Portmann, Thomas, Treier, Mathias, Scheffzek, Klaus, Huet, Sebastien, Timinszky, Gyula, Buschbeck, Marcus, & Ladurner, Andreas G. (2018). MacroH2A histone variants limit chromatin plasticity through two distinct mechanisms. *EMBO Reports*, *19*(10). https://doi.org/10.15252/embr.201744445

Kozlowski, Marek, & Ladurner, Andreas G. (2015). ATM, MacroH2A.1, and SASP: The Checks and Balances of Cellular Senescence. *Molecular Cell*, *59*(5), 713–715. https://doi.org/10.1016/j.molcel.2015.08.010

Kristie, Thomas M. (2007). *Human Herpesviruses*. 112–127. https://doi.org/10.1017/cbo9780511545313.009

Kubat, Nicole J., Tran, Robert K., McAnany, Peterjon, & Bloom, David C. (2004). Specific Histone Tail Modification and Not DNA Methylation Is a Determinant of Herpes Simplex Virus Type 1 Latent Gene Expression. *Journal of Virology*, *78*(3), 1139–1149. https://doi.org/10.1128/jvi.78.3.1139-1149.2004

Kulej, Katarzyna, Avgousti, Daphne C., Sidoli, Simone, Herrmann, Christin, Fera, Ashley N. Della, Kim, Eui Tae, Garcia, Benjamin A., & Weitzman, Matthew D. (2017). Time-resolved Global and Chromatin Proteomics during Herpes Simplex Virus Type 1 (HSV-1) Infection. *Molecular & Cellular Proteomics*, *16*(4 suppl 1), S92–S107. https://doi.org/10.1074/mcp.m116.065987

Kustatscher, Georg, Hothorn, Michael, Pugieux, Céline, Scheffzek, Klaus, & Ladurner, Andreas G. (2005). Splicing regulates NAD metabolite binding to histone macroH2A. *Nature Structural & Molecular Biology*, *12*(7), 624–625. https://doi.org/10.1038/nsmb956

Kwiatkowski, Dacia L., Thompson, Hilary W., & Bloom, David C. (2009). The Polycomb Group Protein Bmi1 Binds to the Herpes Simplex Virus 1 Latent Genome and Maintains Repressive Histone Marks during Latency ▿ . *Journal of Virology*, *83*(16), 8173–8181. https://doi.org/10.1128/jvi.00686-09

Kwong, A. D., Kruper, J. A., & Frenkel, N. (1988). Herpes simplex virus virion host shutoff function. *Journal of Virology*, *62*(3), 912–921. https://doi.org/10.1128/jvi.62.3.912-921.1988

Lacasse, Jonathan J., & Schang, Luis M. (2010). During Lytic Infections, Herpes Simplex Virus Type 1 DNA Is in Complexes with the Properties of Unstable Nucleosomes. *Journal of Virology*, *84*(4), 1920–1933. https://doi.org/10.1128/jvi.01934-09

Lai, J. S., & Herr, W. (1997). Interdigitated residues within a small region of VP16 interact with Oct-1, HCF, and DNA. *Molecular and Cellular Biology*, *17*(7), 3937–3946. https://doi.org/10.1128/mcb.17.7.3937

Lanfranca, Mirna Perusina, Mostafa, Heba H., & Davido, David J. (2014). HSV-1 ICP0: An E3 Ubiquitin Ligase That Counteracts Host Intrinsic and Innate Immunity. *Cells*, *3*(2), 438–454. https://doi.org/10.3390/cells3020438

Lavigne, Matthieu D., Vatsellas, Giannis, Polyzos, Alexander, Mantouvalou, Evangelia, Sianidis, George, Maraziotis, Ioannis, Agelopoulos, Marios, & Thanos, Dimitris. (2015). Composite macroH2A/NRF-1 Nucleosomes Suppress Noise and Generate Robustness in Gene Expression. *Cell Reports*, *11*(7), 1090–1101. https://doi.org/10.1016/j.celrep.2015.04.022

Lawrence, Michael, Huber, Wolfgang, Pagès, Hervé, Aboyoun, Patrick, Carlson, Marc, Gentleman, Robert, Morgan, Martin T., & Carey, Vincent J. (2013). Software for Computing and Annotating Genomic Ranges. *PLoS Computational Biology*, *9*(8), e1003118. https://doi.org/10.1371/journal.pcbi.1003118

Leach, Natalie, Bjerke, Susan L., Christensen, Desire K., Bouchard, Jacques M., Mou, Fan, Park, Richard, Baines, Joel, Haraguchi, Tokuko, & Roller, Richard J. (2007). Emerin Is Hyperphosphorylated and Redistributed in Herpes Simplex Virus Type 1-Infected Cells in a Manner Dependent on both UL34 and US3. *Journal of Virology*, *81*(19), 10792–10803. https://doi.org/10.1128/jvi.00196-07

Lee, Jennifer S., Raja, Priya, & Knipe, David M. (2016). Herpesviral ICP0 Protein Promotes Two Waves of Heterochromatin Removal on an Early Viral Promoter during Lytic Infection. *MBio*, *7*(1), e02007-15. https://doi.org/10.1128/mbio.02007-15

Lee, Jennifer S., Raja, Priya, Pan, Dongli, Pesola, Jean M., Coen, Donald M., & Knipe, David M. (2018). CCCTC-Binding Factor Acts as a Heterochromatin Barrier on Herpes Simplex Viral Latent Chromatin and Contributes to Poised Latent Infection. *MBio*, *9*(1), e02372-17. https://doi.org/10.1128/mbio.02372-17

Leinbach, S. S., & Summers, W. C. (1980). The structure of herpes simplex virus type 1 DNA as probed by micrococcal nuclease digestion. *The Journal of General Virology*, *51*(Pt 1), 45–59. https://doi.org/10.1099/0022-1317-51-1-45

Li, Feng, Yi, Ping, Pi, Jingnan, Li, Lanfang, Hui, Jingyi, Wang, Fang, Liang, Aihua, & Yu, Jia. (2015). QKI5-mediated alternative splicing of the histone variant macroH2A1 regulates gastric carcinogenesis. *Oncotarget*, *7*(22), 32821–32834. https://doi.org/10.18632/oncotarget.8739

Li, Gang, Nguyen, Christopher C., Ryckman, Brent J., Britt, William J., & Kamil, Jeremy P. (2015). A viral regulator of glycoprotein complexes contributes to human cytomegalovirus cell tropism. *Proceedings of the National Academy of Sciences*, *112*(14), 4471–4476. https://doi.org/10.1073/pnas.1419875112

Li, Zhuan, Yamauchi, Yohei, Kamakura, Maki, Murayama, Tsugiya, Goshima, Fumi, Kimura, Hiroshi, & Nishiyama, Yukihiro. (2012). Herpes Simplex Virus Requires Poly(ADP-Ribose) Polymerase Activity for Efficient Replication and Induces Extracellular Signal-Related Kinase-Dependent Phosphorylation and ICP0-Dependent Nuclear Localization of Tankyrase 1. *Journal of Virology*, *86*(1), 492–503. https://doi.org/10.1128/jvi.05897-11

Liang, Yu, Quenelle, Debra, Vogel, Jodi L., Mascaro, Cristina, Ortega, Alberto, & Kristie, Thomas M. (2013). A Novel Selective LSD1/KDM1A Inhibitor Epigenetically Blocks Herpes Simplex Virus Lytic Replication and Reactivation from Latency. *MBio*, *4*(1), e00558-12. https://doi.org/10.1128/mbio.00558-12

Liang, Yu, Vogel, Jodi L., Arbuckle, Jesse H., Rai, Ganesha, Jadhav, Ajit, Simeonov, Anton, Maloney, David J., & Kristie, Thomas M. (2013). Targeting the JMJD2 Histone Demethylases to Epigenetically Control Herpesvirus Infection and Reactivation from Latency. *Science Translational Medicine*, *5*(167), 167ra5. https://doi.org/10.1126/scitranslmed.3005145

Liang, Yu, Vogel, Jodi L., Narayanan, Aarthi, Peng, Hua, & Kristie, Thomas M. (2009). Inhibition of the histone demethylase LSD1 blocks α-herpesvirus lytic replication and reactivation from latency. *Nature Medicine*, *15*(11), 1312–1317. https://doi.org/10.1038/nm.2051

Lieberman-Aiden, Erez, Berkum, Nynke L. van, Williams, Louise, Imakaev, Maxim, Ragoczy, Tobias, Telling, Agnes, Amit, Ido, Lajoie, Bryan R., Sabo, Peter J., Dorschner, Michael O., Sandstrom, Richard, Bernstein, Bradley, Bender, M. A., Groudine, Mark, Gnirke, Andreas, Stamatoyannopoulos, John, Mirny, Leonid A., Lander, Eric S., & Dekker, Job. (2009). Comprehensive Mapping of Long-Range Interactions Reveals Folding Principles of the Human Genome. *Science*, *326*(5950), 289–293. https://doi.org/10.1126/science.1181369

Lilley, Caroline E., Carson, Christian T., Muotri, Alysson R., Gage, Fred H., & Weitzman, Matthew D. (2005). DNA repair proteins affect the lifecycle of herpes simplex virus 1. *Proceedings of the National Academy of Sciences*, *102*(16), 5844–5849. https://doi.org/10.1073/pnas.0501916102

Lilley, Caroline E., Chaurushiya, Mira S., & Weitzman, Matthew D. (2010). Chromatin at the intersection of viral infection and DNA damage. *Biochimica et Biophysica Acta (BBA) - Gene Regulatory Mechanisms*, *1799*(3–4), 319–327. https://doi.org/10.1016/j.bbagrm.2009.06.007

Lima-de-Faria, A., & Jaworska, Halina. (1968). Late DNA Synthesis in Heterochromatin. *Nature*, *217*(5124), 138–142. https://doi.org/10.1038/217138a0

Lin, Daniel H., & Hoelz, André. (2019). The Structure of the Nuclear Pore Complex (An Update). *Annual Review of Biochemistry*, *88*(1), 1–59. https://doi.org/10.1146/annurev-biochem-062917-011901

Looker, Katharine J., Elmes, Jocelyn A. R., Gottlieb, Sami L., Schiffer, Joshua T., Vickerman, Peter, Turner, Katherine M. E., & Boily, Marie-Claude. (2017). Effect of HSV-2 infection on subsequent HIV acquisition: an updated systematic review and meta-analysis. *The Lancet Infectious Diseases*, *17*(12), 1303–1316. https://doi.org/10.1016/s1473-3099(17)30405-x

Lorentzen, E. U., Eing, B. R., Hafezi, W., Manservigi, R., & Kühn, J. E. (2001). Replication-Competent Herpes simplex Virus Type 1 Mutant Expressing an Autofluorescent Glycoprotein H Fusion Protein. *Intervirology*, *44*(4), 232–242. https://doi.org/10.1159/000050053

Luger, Karolin, Mäder, Armin W., Richmond, Robin K., Sargent, David F., & Richmond, Timothy J. (1997). Crystal structure of the nucleosome core particle at 2.8 Å resolution. *Nature*, *389*(6648), 251–260. https://doi.org/10.1038/38444

Lynch, Kelsey L., Dillon, Melanie R., Bat-Erdene, Mongoljin, Lewis, Hannah C., Kaai, Robin J., Arnold, Edward A., & Avgousti, Daphne C. (2021). A viral histone-like protein exploits antagonism between linker histones and HMGB proteins to obstruct the cell cycle. *Current Biology*, *31*(23), 5227-5237.e7. https://doi.org/10.1016/j.cub.2021.09.050

Maeshima, Kazuhiro, Ide, Satoru, & Babokhov, Michael. (2019). Dynamic chromatin organization without the 30-nm fiber. *Current Opinion in Cell Biology*, *58*, 95–104. https://doi.org/10.1016/j.ceb.2019.02.003

Marjanović, Melanija Posavec, Hurtado-Bagès, Sarah, Lassi, Maximilian, Valero, Vanesa, Malinverni, Roberto, Delage, Hélène, Navarro, Miriam, Corujo, David, Guberovic, Iva, Douet, Julien, Gama-Perez, Pau, Garcia-Roves, Pablo M., Ahel, Ivan, Ladurner, Andreas G., Yanes, Oscar, Bouvet, Philippe, Suelves, Mònica, Teperino, Raffaele, Pospisilik, J. Andrew, & Buschbeck, Marcus. (2017). MacroH2A1.1 regulates mitochondrial respiration by limiting nuclear NAD+ consumption. *Nature Structural & Molecular Biology*, *24*(11), 902–910. https://doi.org/10.1038/nsmb.3481

McFarlane, Steven, Orr, Anne, Roberts, Ashley P. E., Conn, Kristen L., Iliev, Victor, Loney, Colin, Filipe, Ana da Silva, Smollett, Katherine, Gu, Quan, Robertson, Neil, Adams, Peter D., Rai, Taranjit Singh, & Boutell, Chris. (2019). The histone chaperone HIRA promotes the induction of host innate immune defences in response to HSV-1 infection. *PLOS Pathogens*, *15*(3), e1007667. https://doi.org/10.1371/journal.ppat.1007667

McGeoch, Duncan J., Rixon, Frazer J., & Davison, Andrew J. (2006). Topics in herpesvirus genomics and evolution. *Virus Research*, *117*(1), 90–104. https://doi.org/10.1016/j.virusres.2006.01.002

McQuillan, Geraldine, Kruszon-Moran, Deanna, Flagg, Elaine W., & Paulose-Ram, Ryne. (2018). Prevalence of Herpes Simplex Virus Type 1 and Type 2 in Persons Aged 14-49: United States, 2015-2016. *NCHS Data Brief*, *304*, 1–8.

Mermoud, Jacqueline E., Costanzi, Carl, Pehrson, John R., & Brockdorff, Neil. (1999). Histone Macroh2a1.2 Relocates to the Inactive X Chromosome after Initiation and Propagation of X-

Inactivation. *The Journal of Cell Biology*, *147*(7), 1399–1408. https://doi.org/10.1083/jcb.147.7.1399

Messer, Harald G. P., Jacobs, Derek, Dhummakupt, Adit, & Bloom, David C. (2015). Inhibition of H3K27me3-Specific Histone Demethylases JMJD3 and UTX Blocks Reactivation of Herpes Simplex Virus 1 in Trigeminal Ganglion Neurons. *Journal of Virology*, *89*(6), 3417–3420. https://doi.org/10.1128/jvi.03052-14

Mettenleiter, Thomas C. (2016). Breaching the Barrier—The Nuclear Envelope in Virus Infection. *Journal of Molecular Biology*, *428*(10), 1949–1961. https://doi.org/10.1016/j.jmb.2015.10.001

Millán-Zambrano, Gonzalo, Burton, Adam, Bannister, Andrew J., & Schneider, Robert. (2022). Histone post-translational modifications — cause and consequence of genome function. *Nature Reviews Genetics*, *23*(9), 563–580. https://doi.org/10.1038/s41576-022-00468-7

Miranda-Saksena, Monica, Denes, Christopher E., Diefenbach, Russell J., & Cunningham, Anthony L. (2018). Infection and Transport of Herpes Simplex Virus Type 1 in Neurons: Role of the Cytoskeleton. *Viruses*, *10*(2), 92. https://doi.org/10.3390/v10020092

Monier, Karine, Armas, Juan Carlos González, Etteldorf, Susanne, Ghazal, Peter, & Sullivan, Kevin F. (2000). Annexation of the interchromosomal space during viral infection. *Nature Cell Biology*, *2*(9), 661–665. https://doi.org/10.1038/35023615

Montgomery, Rebecca I., Warner, Morgyn S., Lum, Brian J., & Spear, Patricia G. (1996). Herpes Simplex Virus-1 Entry into Cells Mediated by a Novel Member of the TNF/NGF Receptor Family. *Cell*, *87*(3), 427–436. https://doi.org/10.1016/s0092-8674(00)81363-x

Morris, James B., Hofemeister, Helmut, & O'Hare, Peter. (2007). Herpes Simplex Virus Infection Induces Phosphorylation and Delocalization of Emerin, a Key Inner Nuclear Membrane Protein. *Journal of Virology*, *81*(9), 4429–4437. https://doi.org/10.1128/jvi.02354-06

Muggeridge, M. I., & Fraser, N. W. (1986). Chromosomal organization of the herpes simplex virus genome during acute infection of the mouse central nervous system. *Journal of Virology*, *59*(3), 764–767. https://doi.org/10.1128/jvi.59.3.764-767.1986

Mühlbauer, Dirk, Dzieciolowski, Julia, Hardt, Martin, Hocke, Andreas, Schierhorn, Kristina L., Mostafa, Ahmed, Müller, Christin, Wisskirchen, Christian, Herold, Susanne, Wolff, Thorsten, Ziebuhr, John, & Pleschka, Stephan. (2015). Influenza Virus-Induced Caspase-Dependent Enlargement of Nuclear Pores Promotes Nuclear Export of Viral Ribonucleoprotein Complexes. *Journal of Virology*, *89*(11), 6009–6021. https://doi.org/10.1128/jvi.03531-14

Muylaert, Isabella, & Elias, Per. (2007). Knockdown of DNA Ligase IV/XRCC4 by RNA Interference Inhibits Herpes Simplex Virus Type I DNA Replication*. *Journal of Biological Chemistry*, *282*(15), 10865–10872. https://doi.org/10.1074/jbc.m611834200

Myllys, Markko, Ruokolainen, Visa, Aho, Vesa, Smith, Elizabeth A., Hakanen, Satu, Peri, Piritta, Salvetti, Anna, Timonen, Jussi, Hukkanen, Veijo, Larabell, Carolyn A., & Vihinen-Ranta, Maija. (2016). Herpes simplex virus 1 induces egress channels through marginalized host chromatin. *Scientific Reports*, *6*(1), 28844. https://doi.org/10.1038/srep28844

Naldinho-Souto, Raquel, Browne, Helena, & Minson, Tony. (2006). Herpes Simplex Virus Tegument Protein VP16 Is a Component of Primary Enveloped Virions. *Journal of Virology*, *80*(5), 2582–2584. https://doi.org/10.1128/jvi.80.5.2582-2584.2006

Narita, Masashi, Nuñez, Sabrina, Heard, Edith, Narita, Masako, Lin, Athena W., Hearn, Stephen A., Spector, David L., Hannon, Gregory J., & Lowe, Scott W. (2003). Rb-Mediated Heterochromatin Formation and Silencing of E2F Target Genes during Cellular Senescence. *Cell*, *113*(6), 703–716. https://doi.org/10.1016/s0092-8674(03)00401-x

Naumova, Natalia, Imakaev, Maxim, Fudenberg, Geoffrey, Zhan, Ye, Lajoie, Bryan R., Mirny, Leonid A., & Dekker, Job. (2013). Organization of the Mitotic Chromosome. *Science*, *342*(6161), 948–953. https://doi.org/10.1126/science.1236083

Ni, Kai, & Muegge, Kathrin. (2021). LSH catalyzes ATP-driven exchange of histone variants macroH2A1 and macroH2A2. *Nucleic Acids Research*, gkab588-. https://doi.org/10.1093/nar/gkab588

Ni, Kai, Ren, Jianke, Xu, Xiaoping, He, Yafeng, Finney, Richard, Braun, Simon M. G., Hathaway, Nathaniel A., Crabtree, Gerald R., & Muegge, Kathrin. (2020). LSH mediates gene repression through macroH2A deposition. *Nature Communications*, *11*(1), 5647. https://doi.org/10.1038/s41467-020-19159-0

Nicholson, P., Addison, C., Cross, A. M., Kennard, J., Preston, V. G., & Rixon, F. J. (1994). Localization of the Herpes Simplex Virus Type 1 Major Capsid Protein VP5 to the Cell Nucleus Requires the Abundant Scaffolding Protein VP22a. *Journal of General Virology*, *75*(5), 1091–1099. https://doi.org/10.1099/0022-1317-75-5-1091

Nicola, Anthony V., McEvoy, Anna M., & Straus, Stephen E. (2003). Roles for Endocytosis and Low pH in Herpes Simplex Virus Entry into HeLa and Chinese Hamster Ovary Cells. *Journal of Virology*, *77*(9), 5324–5332. https://doi.org/10.1128/jvi.77.9.5324-5332.2003

Nicoll, Michael P., Hann, William, Shivkumar, Maitreyi, Harman, Laura E. R., Connor, Viv, Coleman, Heather M., Proença, João T., & Efstathiou, Stacey. (2016). The HSV-1 Latency-Associated Transcript Functions to Repress Latent Phase Lytic Gene Expression and Suppress Virus Reactivation from Latently Infected Neurons. *PLoS Pathogens*, *12*(4), e1005539. https://doi.org/10.1371/journal.ppat.1005539

Novikov, Leonid, Park, Jong Woo, Chen, Hongshan, Klerman, Hadassa, Jalloh, Abubakar S., & Gamble, Matthew J. (2011). QKI-Mediated Alternative Splicing of the Histone Variant MacroH2A1 Regulates Cancer Cell Proliferation. *Molecular and Cellular Biology*, *31*(20), 4244–4255. https://doi.org/10.1128/mcb.05244-11

Nusinow, Dmitri A., Sharp, Judith A., Morris, Alana, Salas, Sonia, Plath, Kathrin, & Panning, Barbara. (2007). The Histone Domain of macroH2A1 Contains Several Dispersed Elements that Are Each Sufficient to Direct Enrichment on the Inactive X Chromosome. *Journal of Molecular Biology*, *371*(1), 11–18. https://doi.org/10.1016/j.jmb.2007.05.063

Ogawa, Y., Ono, T., Wakata, Y., Okawa, K., Tagami, H., & Shibahara, K-i. (2005). Histone variant macroH2A1.2 is mono-ubiquitinated at its histone domain. *Biochemical and*

Biophysical Research Communications, *336*(1), 204–209. https://doi.org/10.1016/j.bbrc.2005.08.046

Oh, Jaewook, & Fraser, Nigel W. (2008). Temporal Association of the Herpes Simplex Virus Genome with Histone Proteins during a Lytic Infection ▿ . *Journal of Virology*, *82*(7), 3530–3537. https://doi.org/10.1128/jvi.00586-07

Oh, Jaewook, Sanders, Iryna F., Chen, Eric Z., Li, Hongzhe, Tobias, John W., Isett, R. Benjamin, Penubarthi, Sindura, Sun, Hao, Baldwin, Don A., & Fraser, Nigel W. (2015). Genome Wide Nucleosome Mapping for HSV-1 Shows Nucleosomes Are Deposited at Preferred Positions during Lytic Infection. *PLOS ONE*, *10*(2), e0117471. https://doi.org/10.1371/journal.pone.0117471

Olins, Ada L., & Olins, Donald E. (1974). Spheroid Chromatin Units (v Bodies). *Science*, *183*(4122), 330–332. https://doi.org/10.1126/science.183.4122.330

Ouararhni, Khalid, Hadj-Slimane, Réda, Ait-Si-Ali, Slimane, Robin, Philippe, Mietton, Flore, Harel-Bellan, Annick, Dimitrov, Stefan, & Hamiche, Ali. (2006). The histone variant mH2A1.1 interferes with transcription by down-regulating PARP-1 enzymatic activity. *Genes & Development*, *20*(23), 3324–3336. https://doi.org/10.1101/gad.396106

Park, Richard, & Baines, Joel D. (2006). Herpes Simplex Virus Type 1 Infection Induces Activation and Recruitment of Protein Kinase C to the Nuclear Membrane and Increased Phosphorylation of Lamin B. *Journal of Virology*, *80*(1), 494–504. https://doi.org/10.1128/jvi.80.1.494-504.2006

Park, S. J., Shim, J. W., Park, H. S., Eum, D. Y., Park, M. T., Yi, J. Mi, Choi, S. H., Kim, S. D., Son, T. G., Lu, W., Kim, N. D., Yang, K., & Heo, K. (2016). MacroH2A1 downregulation enhances the stem-like properties of bladder cancer cells by transactivation of Lin28B. *Oncogene*, *35*(10), 1292–1301. https://doi.org/10.1038/onc.2015.187

Pasque, Vincent, Radzisheuskaya, Aliaksandra, Gillich, Astrid, Halley-Stott, Richard P., Panamarova, Maryna, Zernicka-Goetz, Magdalena, Surani, M. Azim, & Silva, José C. R. (2012). Histone variant macroH2A marks embryonic differentiation in vivo and acts as an epigenetic barrier to induced pluripotency. *Journal of Cell Science*, *125*(24), 6094–6104. https://doi.org/10.1242/jcs.113019

Pehrson, & Fried, VA. (1992). MacroH2A, a core histone containing a large nonhistone region. *Science*, *257*(5075), 1398–1400. https://doi.org/10.1126/science.1529340

Pehrson, John R., Changolkar, Lakshmi N., Costanzi, Carl, & Leu, N. Adrian. (2014). Mice without MacroH2A Histone Variants. *Molecular and Cellular Biology*, *34*(24), 4523–4533. https://doi.org/10.1128/mcb.00794-14

Pehrson, John R., Costanzi, Carl, & Dharia, Chhaya. (1997). Developmental and tissue expression patterns of histone macroH2A1 subtypes. *Journal of Cellular Biochemistry*, *65*(1), 107–113. https://doi.org/10.1002/(sici)1097-4644(199704)65:1<107::aid-jcb11>3.0.co;2-h

Pehrson, John R., & Fuji, Reina N. (1998). Evolutionary conservation of histone macroH2A subtypes and domains. *Nucleic Acids Research*, *26*(12), 2837–2842. https://doi.org/10.1093/nar/26.12.2837

Peters, Antoine H. F. M., O'Carroll, Dónal, Scherthan, Harry, Mechtler, Karl, Sauer, Stephan, Schöfer, Christian, Weipoltshammer, Klara, Pagani, Michaela, Lachner, Monika, Kohlmaier, Alexander, Opravil, Susanne, Doyle, Michael, Sibilia, Maria, & Jenuwein, Thomas. (2001). Loss of the Suv39h Histone Methyltransferases Impairs Mammalian Heterochromatin and Genome Stability. *Cell*, *107*(3), 323–337. https://doi.org/10.1016/s0092-8674(01)00542-6

Phelan, A., Dunlop, J., Patel, A. H., Stow, N. D., & Clements, J. B. (1997). Nuclear sites of herpes simplex virus type 1 DNA replication and transcription colocalize at early times postinfection and are largely distinct from RNA processing factors. *Journal of Virology*, *71*(2), 1124–1132. https://doi.org/10.1128/jvi.71.2.1124-1132.1997

Pignatti, P. F., & Cassai, E. (1980). Analysis of herpes simplex virus nucleoprotein complexes extracted from infected cells. *Journal of Virology*, *36*(3), 816–828. https://doi.org/10.1128/jvi.36.3.816-828.1980

Placek, Brandon J., Huang, Jing, Kent, Jennifer R., Dorsey, Jean, Rice, Lyndi, Fraser, Nigel W., & Berger, Shelley L. (2009). The Histone Variant H3.3 Regulates Gene Expression during Lytic Infection with Herpes Simplex Virus Type 1 ▿. *Journal of Virology*, *83*(3), 1416–1421. https://doi.org/10.1128/jvi.01276-08

Plotkin, S. A., Furukawa, T., Zygraich, N., & Huygelen, C. (1975). Candidate cytomegalovirus strain for human vaccination. *Infection and Immunity*, *12*(3), 521–527. https://doi.org/10.1128/iai.12.3.521-527.1975

Popa, Mirela, Ruzsics, Zsolt, Lötzerich, Mark, Dölken, Lars, Buser, Christopher, Walther, Paul, & Koszinowski, Ulrich H. (2010). Dominant Negative Mutants of the Murine Cytomegalovirus M53 Gene Block Nuclear Egress and Inhibit Capsid Maturation. *Journal of Virology*, *84*(18), 9035–9046. https://doi.org/10.1128/jvi.00681-10

Procter, Dean J., Furey, Colleen, Garza-Gongora, Arturo G., Kosak, Steven T., & Walsh, Derek. (2020). Cytoplasmic control of intranuclear polarity by human cytomegalovirus. *Nature*, *587*(7832), 109–114. https://doi.org/10.1038/s41586-020-2714-x

Quinlan, Aaron R., & Hall, Ira M. (2010). BEDTools: a flexible suite of utilities for comparing genomic features. *Bioinformatics*, *26*(6), 841–842. https://doi.org/10.1093/bioinformatics/btq033

Quinodoz, Sofia A., Ollikainen, Noah, Tabak, Barbara, Palla, Ali, Schmidt, Jan Marten, Detmar, Elizabeth, Lai, Mason M., Shishkin, Alexander A., Bhat, Prashant, Takei, Yodai, Trinh, Vickie, Aznauryan, Erik, Russell, Pamela, Cheng, Christine, Jovanovic, Marko, Chow, Amy, Cai, Long, McDonel, Patrick, Garber, Manuel, & Guttman, Mitchell. (2018). Higher-Order Inter-chromosomal Hubs Shape 3D Genome Organization in the Nucleus. *Cell*, *174*(3), 744-757.e24. https://doi.org/10.1016/j.cell.2018.05.024

Rack, Johannes Gregor Matthias, Perina, Dragutin, & Ahel, Ivan. (2015). Macrodomains: Structure, Function, Evolution, and Catalytic Activities. *Annual Review of Biochemistry*, *85*(1), 1–24. https://doi.org/10.1146/annurev-biochem-060815-014935

Rai, Taranjit Singh, Glass, Mandy, Cole, John J., Rather, Mohammad I., Marsden, Morgan, Neilson, Matthew, Brock, Claire, Humphreys, Ian R., Everett, Roger D., & Adams, Peter D. (2017). Histone chaperone HIRA deposits histone H3.3 onto foreign viral DNA and contributes to anti-viral intrinsic immunity. *Nucleic Acids Research*, *45*(20), gkx771. https://doi.org/10.1093/nar/gkx771

Raja, Priya, Lee, Jennifer S., Pan, Dongli, Pesola, Jean M., Coen, Donald M., & Knipe, David M. (2016). A Herpesviral Lytic Protein Regulates the Structure of Latent Viral Chromatin. *MBio*, *7*(3), e00633-16. https://doi.org/10.1128/mbio.00633-16

Rakus, Krzysztof, Ouyang, Ping, Boutier, Maxime, Ronsmans, Maygane, Reschner, Anca, Vancsok, Catherine, Jazowiecka-Rakus, Joanna, & Vanderplasschen, Alain. (2013). Cyprinid herpesvirus 3: an interesting virus for applied and fundamental research. *Veterinary Research*, *44*(1), 85. https://doi.org/10.1186/1297-9716-44-85

Rao, Suhas S. P., Huntley, Miriam H., Durand, Neva C., Stamenova, Elena K., Bochkov, Ivan D., Robinson, James T., Sanborn, Adrian L., Machol, Ido, Omer, Arina D., Lander, Eric S., & Aiden, Erez Lieberman. (2014). A 3D Map of the Human Genome at Kilobase Resolution Reveals Principles of Chromatin Looping. *Cell*, *159*(7), 1665–1680. https://doi.org/10.1016/j.cell.2014.11.021

Rappa, Francesca, Greco, Azzura, Podrini, Christine, Cappello, Francesco, Foti, Michelangelo, Bourgoin, Lucie, Peyrou, Marion, Marino, Arianna, Scibetta, Nunzia, Williams, Roger, Mazzoccoli, Gianluigi, Federici, Massimo, Pazienza, Valerio, & Vinciguerra, Manlio. (2013). Immunopositivity for Histone MacroH2A1 Isoforms Marks Steatosis-Associated Hepatocellular Carcinoma. *PLoS ONE*, *8*(1), e54458. https://doi.org/10.1371/journal.pone.0054458

Rasmussen, Theodore P., Mastrangelo, Mary-Ann, Eden, Amir, Pehrson, John R., & Jaenisch, Rudolf. (2000). Dynamic Relocalization of Histone Macroh2a1 from Centrosomes to Inactive X Chromosomes during X Inactivation. *The Journal of Cell Biology*, *150*(5), 1189–1198. https://doi.org/10.1083/jcb.150.5.1189

Ratnakumar, Kajan, Duarte, Luis F., LeRoy, Gary, Hasson, Dan, Smeets, Daniel, Vardabasso, Chiara, Bönisch, Clemens, Zeng, Tianying, Xiang, Bin, Zhang, David Y., Li, Haitao, Wang, Xiaowo, Hake, Sandra B., Schermelleh, Lothar, Garcia, Benjamin A., & Bernstein, Emily. (2012). ATRX-mediated chromatin association of histone variant macroH2A1 regulates α-globin expression. *Genes & Development*, *26*(5), 433–438. https://doi.org/10.1101/gad.179416.111

Ray-Gallet, Dominique, Woolfe, Adam, Vassias, Isabelle, Pellentz, Céline, Lacoste, Nicolas, Puri, Aastha, Schultz, David C., Pchelintsev, Nikolay A., Adams, Peter D., Jansen, Lars E. T., & Almouzni, Geneviève. (2011). Dynamics of Histone H3 Deposition In Vivo Reveal a Nucleosome Gap-Filling Mechanism for H3.3 to Maintain Chromatin Integrity. *Molecular Cell*, *44*(6), 928–941. https://doi.org/10.1016/j.molcel.2011.12.006

Recoules, Ludmila, Heurteau, Alexandre, Raynal, Flavien, Karasu, Nezih, Moutahir, Fatima, Bejjani, Fabienne, Jariel-Encontre, Isabelle, Cuvier, Olivier, Sexton, Thomas, Lavigne, Anne-Claire, & Bystricky, Kerstin. (2022). The histone variant macroH2A1.1 regulates RNA Polymerase II paused genes within defined chromatin interaction landscapes. *Journal of Cell Science*, *135*(7), jcs259456. https://doi.org/10.1242/jcs.259456

Reynolds, Ashley E., Liang, Li, & Baines, Joel D. (2004). Conformational Changes in the Nuclear Lamina Induced by Herpes Simplex Virus Type 1 Require Genes U L 31 and U L 34. *Journal of Virology*, *78*(11), 5564–5575. https://doi.org/10.1128/jvi.78.11.5564-5575.2004

Reynolds, Ashley E., Ryckman, Brent J., Baines, Joel D., Zhou, Yuping, Liang, Li, & Roller, Richard J. (2001). U L 31 and U L 34 Proteins of Herpes Simplex Virus Type 1 Form a Complex That Accumulates at the Nuclear Rim and Is Required for Envelopment of Nucleocapsids. *Journal of Virology*, *75*(18), 8803–8817. https://doi.org/10.1128/jvi.75.18.8803-8817.2001

Ricci, Maria Aurelia, Manzo, Carlo, García-Parajo, María Filomena, Lakadamyali, Melike, & Cosma, Maria Pia. (2015). Chromatin Fibers Are Formed by Heterogeneous Groups of Nucleosomes In Vivo. *Cell*, *160*(6), 1145–1158. https://doi.org/10.1016/j.cell.2015.01.054

Rivera-Casas, Ciro, Gonzalez-Romero, Rodrigo, Cheema, Manjinder S., Ausió, Juan, & Eirín-López, José M. (2016). The characterization of macroH2A beyond vertebrates supports an ancestral origin and conserved role for histone variants in chromatin. *Epigenetics*, *11*(6), 415–425. https://doi.org/10.1080/15592294.2016.1172161

Robinson, Mark D., McCarthy, Davis J., & Smyth, Gordon K. (2010). edgeR: a Bioconductor package for differential expression analysis of digital gene expression data. *Bioinformatics*, *26*(1), 139–140. https://doi.org/10.1093/bioinformatics/btp616

Roizman, Bernard, Knipe, David M., & Whitley, Richard J. (2013). Herpes Simplex Viruses. In David KnipePeter Howley & Peter Howley (Eds.), *Fields Virology* (6th ed.). Lippincott Williams & Wilkins.

Roller, Richard J., Zhou, Yuping, Schnetzer, Renee, Ferguson, John, & DeSalvo, Diana. (2000). Herpes Simplex Virus Type 1 U L 34 Gene Product Is Required for Viral Envelopment. *Journal of Virology*, *74*(1), 117–129. https://doi.org/10.1128/jvi.74.1.117-129.2000

Ruiz, Penelope D., & Gamble, Matthew J. (2018). MacroH2A1 chromatin specification requires its docking domain and acetylation of H2B lysine 20. *Nature Communications*, *9*(1), 5143. https://doi.org/10.1038/s41467-018-07189-8

Ruiz, Penelope D., Hamilton, Gregory A., Park, Jong Woo, & Gamble, Matthew J. (2019). MacroH2A1 Regulation of Poly(ADP-Ribose) Synthesis and Stability Prevents Necrosis and Promotes DNA Repair. *Molecular and Cellular Biology*, *40*(1). https://doi.org/10.1128/mcb.00230-19

Rutkowski, Andrzej J., Erhard, Florian, L'Hernault, Anne, Bonfert, Thomas, Schilhabel, Markus, Crump, Colin, Rosenstiel, Philip, Efstathiou, Stacey, Zimmer, Ralf, Friedel, Caroline C., & Dölken, Lars. (2015). Widespread disruption of host transcription termination in HSV-1 infection. *Nature Communications*, *6*(1), 7126. https://doi.org/10.1038/ncomms8126

Sacks, W. R., Greene, C. C., Aschman, D. P., & Schaffer, P. A. (1985). Herpes simplex virus type 1 ICP27 is an essential regulatory protein. *Journal of Virology*, *55*(3), 796–805. https://doi.org/10.1128/jvi.55.3.796-805.1985

Saitoh, Tatsuya, Komano, Jun, Saitoh, Yasunori, Misawa, Takuma, Takahama, Michihiro, Kozaki, Tatsuya, Uehata, Takuya, Iwasaki, Hidenori, Omori, Hiroko, Yamaoka, Shoji, Yamamoto, Naoki, & Akira, Shizuo. (2012). Neutrophil Extracellular Traps Mediate a Host Defense Response to Human Immunodeficiency Virus-1. *Cell Host & Microbe*, *12*(1), 109–116. https://doi.org/10.1016/j.chom.2012.05.015

Saksouk, Nehmé, Simboeck, Elisabeth, & Déjardin, Jérôme. (2015). Constitutive heterochromatin formation and transcription in mammals. *Epigenetics & Chromatin*, *8*(1), 3. https://doi.org/10.1186/1756-8935-8-3

Sawtell, N. M., & Thompson, R. L. (1992). Rapid in vivo reactivation of herpes simplex virus in latently infected murine ganglionic neurons after transient hyperthermia. *Journal of Virology*, *66*(4), 2150–2156. https://doi.org/10.1128/jvi.66.4.2150-2156.1992

Schreiber, Katherine H., & Kennedy, Brian K. (2013). When Lamins Go Bad: Nuclear Structure and Disease. *Cell*, *152*(6), 1365–1375. https://doi.org/10.1016/j.cell.2013.02.015

Schultz, Jack. (1936). Variegation in Drosophila and the Inert Chromosome Regions. *Proceedings of the National Academy of Sciences*, *22*(1), 27–33. https://doi.org/10.1073/pnas.22.1.27

Sebastian, Robin, Hosogane, Eri K., Sun, Eric G., Tran, Andy D., Reinhold, William C., Burkett, Sandra, Sturgill, David M., Gudla, Prabhakar R., Pommier, Yves, Aladjem, Mirit I., & Oberdoerffer, Philipp. (2020). Epigenetic Regulation of DNA Repair Pathway Choice by MacroH2A1 Splice Variants Ensures Genome Stability. *Molecular Cell*. https://doi.org/10.1016/j.molcel.2020.06.028

Sedlak, Ruth Hall, Cook, Linda, Cheng, Anqi, Magaret, Amalia, & Jerome, Keith R. (2014). Clinical Utility of Droplet Digital PCR for Human Cytomegalovirus. *Journal of Clinical Microbiology*, *52*(8), 2844–2848. https://doi.org/10.1128/jcm.00803-14

Severini, A., Scraba, D. G., & Tyrrell, D. L. (1996). Branched structures in the intracellular DNA of herpes simplex virus type 1. *Journal of Virology*, *70*(5), 3169–3175. https://doi.org/10.1128/jvi.70.5.3169-3175.1996

Sherry, Maxwell R., Hay, Thomas J. M., Gulak, Michael A., Nassiri, Arash, Finnen, Renée L., & Banfield, Bruce W. (2017). The Herpesvirus Nuclear Egress Complex Component, UL31, Can Be Recruited to Sites of DNA Damage Through Poly-ADP Ribose Binding. *Scientific Reports*, *7*(1), 1882. https://doi.org/10.1038/s41598-017-02109-0

Shukla, Deepak, Liu, Jian, Blaiklock, Peter, Shworak, Nicholas W., Bai, Xiaomei, Esko, Jeffrey D., Cohen, Gary H., Eisenberg, Roselyn J., Rosenberg, Robert D., & Spear, Patricia G. (1999). A Novel Role for 3-O-Sulfated Heparan Sulfate in Herpes Simplex Virus 1 Entry. *Cell*, *99*(1), 13–22. https://doi.org/10.1016/s0092-8674(00)80058-6

Silva, Lindsey, Cliffe, Anna, Chang, Lynne, & Knipe, David M. (2008). Role for A-Type Lamins in Herpesviral DNA Targeting and Heterochromatin Modulation. *PLoS Pathogens*, *4*(5), e1000071. https://doi.org/10.1371/journal.ppat.1000071

Silva, Lindsey, Oh, Hyung Suk, Chang, Lynne, Yan, Zhipeng, Triezenberg, Steven J., & Knipe, David M. (2012). Roles of the Nuclear Lamina in Stable Nuclear Association and Assembly of a Herpesviral Transactivator Complex on Viral Immediate-Early Genes. *MBio*, *3*(1), e00300-11. https://doi.org/10.1128/mbio.00300-11

Simpson-Holley, Martha, Baines, Joel, Roller, Richard, & Knipe, David M. (2004). Herpes Simplex Virus 1 UL31 and UL34 Gene Products Promote the Late Maturation of Viral Replication Compartments to the Nuclear Periphery. *Journal of Virology*, *78*(11), 5591–5600. https://doi.org/10.1128/jvi.78.11.5591-5600.2004

Smith, Corey L., & Peterson, Craig L. (2005). ATP-dependent chromatin remodeling. *Current Topics in Developmental Biology*, *65*, 115–148. https://doi.org/10.1016/s0070-2153(04)65004-6

Smith, Samantha, & Weller, Sandra K. (2015). HSV-I and the cellular DNA damage response. *Future Virology*, *10*(4), 383–397. https://doi.org/10.2217/fvl.15.18

Solovei, Irina, Wang, Audrey S., Thanisch, Katharina, Schmidt, Christine S., Krebs, Stefan, Zwerger, Monika, Cohen, Tatiana V., Devys, Didier, Foisner, Roland, Peichl, Leo, Herrmann, Harald, Blum, Helmut, Engelkamp, Dieter, Stewart, Colin L., Leonhardt, Heinrich, & Joffe, Boris. (2013). LBR and Lamin A/C Sequentially Tether Peripheral Heterochromatin and Inversely Regulate Differentiation. *Cell*, *152*(3), 584–598. https://doi.org/10.1016/j.cell.2013.01.009

Spear, Patricia G. (2004). Herpes simplex virus: receptors and ligands for cell entry. *Cellular Microbiology*, *6*(5), 401–410. https://doi.org/10.1111/j.1462-5822.2004.00389.x

Speese, Sean D., Ashley, James, Jokhi, Vahbiz, Nunnari, John, Barria, Romina, Li, Yihang, Ataman, Bulent, Koon, Alex, Chang, Young-Tae, Li, Qian, Moore, Melissa J., & Budnik, Vivian. (2012). Nuclear Envelope Budding Enables Large Ribonucleoprotein Particle Export during Synaptic Wnt Signaling. *Cell*, *149*(4), 832–846. https://doi.org/10.1016/j.cell.2012.03.032

Sporn, J C, Kustatscher, G., Hothorn, T., Collado, M., Serrano, M., Muley, T., Schnabel, P., & Ladurner, A. G. (2009). Histone macroH2A isoforms predict the risk of lung cancer recurrence. *Oncogene*, *28*(38), 3423–3428. https://doi.org/10.1038/onc.2009.26

Sporn, Judith C., & Jung, Barbara. (2012). Differential Regulation and Predictive Potential of MacroH2A1 Isoforms in Colon Cancer. *The American Journal of Pathology*, *180*(6), 2516–2526. https://doi.org/10.1016/j.ajpath.2012.02.027

Sullivan, K. F., Hechenberger, M., & Masri, K. (1994). Human CENP-A contains a histone H3 related histone fold domain that is required for targeting to the centromere. *The Journal of Cell Biology*, *127*(3), 581–592. https://doi.org/10.1083/jcb.127.3.581

Sun, Zhen, Filipescu, Dan, Andrade, Joshua, Gaspar-Maia, Alexandre, Ueberheide, Beatrix, & Bernstein, Emily. (2018). Transcription-associated histone pruning demarcates macroH2A chromatin domains. *Nature Structural & Molecular Biology*, *25*(10), 958–970. https://doi.org/10.1038/s41594-018-0134-5

Suzich, Jon B., Cuddy, Sean R., Baidas, Hiam, Dochnal, Sara, Ke, Eugene, Schinlever, Austin R., Babnis, Aleksandra, Boutell, Chris, & Cliffe, Anna R. (2021). PML-NB-dependent type I interferon memory results in a restricted form of HSV latency. *EMBO Reports*, *22*(9), e52547. https://doi.org/10.15252/embr.202152547

Talbert, Paul B., & Henikoff, Steven. (2014). Environmental responses mediated by histone variants. *Trends in Cell Biology*, *24*(11), 642–650. https://doi.org/10.1016/j.tcb.2014.07.006

Talbert, Paul B., & Henikoff, Steven. (2017). Histone variants on the move: substrates for chromatin dynamics. *Nature Reviews Molecular Cell Biology*, *18*(2), 115–126. https://doi.org/10.1038/nrm.2016.148

Talbert, Paul B., & Henikoff, Steven. (2021). Histone variants at a glance. *Journal of Cell Science*, *134*(6), jcs244749. https://doi.org/10.1242/jcs.244749

Tanasijevic, Borko, & Rasmussen, Theodore P. (2011). X Chromosome Inactivation and Differentiation Occur Readily in ES Cells Doubly-Deficient for MacroH2A1 and MacroH2A2. *PLoS ONE*, *6*(6), e21512. https://doi.org/10.1371/journal.pone.0021512

Timinszky, Gyula, Till, Susanne, Hassa, Paul O., Hothorn, Michael, Kustatscher, Georg, Nijmeijer, Bianca, Colombelli, Julien, Altmeyer, Matthias, Stelzer, Ernst H. K., Scheffzek, Klaus, Hottiger, Michael O., & Ladurner, Andreas G. (2009). A macrodomain-containing histone rearranges chromatin upon sensing PARP1 activation. *Nature Structural & Molecular Biology*, *16*(9), 923–929. https://doi.org/10.1038/nsmb.1664

TOPP, KIMBERLY S., ROTHMAN, ALANA L., & LAVAIL, JENNIFER H. (1997). Herpes Virus Infection of RPE and MDCK Cells: Polarity of Infection. *Experimental Eye Research*, *64*(3), 343–354. https://doi.org/10.1006/exer.1996.0209

Trojer, Patrick, & Reinberg, Danny. (2007). Facultative Heterochromatin: Is There a Distinctive Molecular Signature? *Molecular Cell*, *28*(1), 1–13. https://doi.org/10.1016/j.molcel.2007.09.011

Turan, Aykut, Grosche, Linda, Krawczyk, Adalbert, Mühl-Zürbes, Petra, Drassner, Christina, Düthorn, Alexandra, Kummer, Mirko, Hasenberg, Mike, Voortmann, Sylvia, Jastrow, Holger, Dörrie, Jan, Schaft, Niels, Kraner, Max, Döhner, Katinka, Sodeik, Beate, Steinkasserer, Alexander, & Heilingloh, Christiane Silke. (2019). Autophagic degradation of lamins facilitates the nuclear egress of herpes simplex virus type 1. *The Journal of Cell Biology*, *218*(2), 508–523. https://doi.org/10.1083/jcb.201801151

Uprichard, S. L., & Knipe, D. M. (1996). Herpes simplex ICP27 mutant viruses exhibit reduced expression of specific DNA replication genes. *Journal of Virology*, *70*(3), 1969–1980. https://doi.org/10.1128/jvi.70.3.1969-1980.1996

Vastag, Livia, Koyuncu, Emre, Grady, Sarah L., Shenk, Thomas E., & Rabinowitz, Joshua D. (2011). Divergent Effects of Human Cytomegalovirus and Herpes Simplex Virus-1 on Cellular Metabolism. *PLoS Pathogens*, *7*(7), e1002124. https://doi.org/10.1371/journal.ppat.1002124

Vieira-Silva, Tânia Soraia, Monteiro-Reis, Sara, Barros-Silva, Daniela, Ramalho-Carvalho, João, Graça, Inês, Carneiro, Isa, Martins, Ana Teresa, Oliveira, Jorge, Antunes, Luis, Hurtado-Bagès, Sarah, Buschbeck, Marcus, Henrique, Rui, & Jerónimo, Carmen. (2019). Histone variant MacroH2A1 is downregulated in prostate cancer and influences malignant cell phenotype. *Cancer Cell International*, *19*(1), 112. https://doi.org/10.1186/s12935-019-0835-9

Waddington, C. H. (2012). The Epigenotype. *International Journal of Epidemiology*, *41*(1), 10–13. https://doi.org/10.1093/ije/dyr184

Wang, Fei, Zhao, Mengmeng, Chang, Boran, Zhou, Yilong, Wu, Xiangyang, Ma, Mingtong, Liu, Siyu, Cao, Yajuan, Zheng, Mengge, Dang, Yifang, Xu, Junfang, Chen, Li, Liu, Tianhao, Tang, Fen, Ren, Yefei, Xu, Zhu, Mao, Zhiyong, Huang, Kai, Luo, Minhua, … Ge, Baoxue. (2022). Cytoplasmic PARP1 links the genome instability to the inhibition of antiviral immunity through PARylating cGAS. *Molecular Cell*, *82*(11), 2032-2049.e7. https://doi.org/10.1016/j.molcel.2022.03.034

Wang, Liguo, Wang, Shengqin, & Li, Wei. (2012). RSeQC: quality control of RNA-seq experiments. *Bioinformatics*, *28*(16), 2184–2185. https://doi.org/10.1093/bioinformatics/bts356

Wang, Qing-Yin, Zhou, Changhong, Johnson, Karen E., Colgrove, Robert C., Coen, Donald M., & Knipe, David M. (2005). Herpesviral latency-associated transcript gene promotes assembly of heterochromatin on viral lytic-gene promoters in latent infection. *Proceedings of the National Academy of Sciences*, *102*(44), 16055–16059. https://doi.org/10.1073/pnas.0505850102

Wang, Yu, Yang, Yin, Wu, Songfang, Pan, Shuang, Zhou, Chaodong, Ma, Yijie, Ru, Yongxin, Dong, Shuxu, He, Bin, Zhang, Cuizhu, & Cao, Youjia. (2014). p32 Is a Novel Target for Viral Protein ICP34.5 of Herpes Simplex Virus Type 1 and Facilitates Viral Nuclear Egress*. *Journal of Biological Chemistry*, *289*(52), 35795–35805. https://doi.org/10.1074/jbc.m114.603845

Washington, Shannan D., Musarrat, Farhana, Ertel, Monica K., Backes, Gregory L., & Neumann, Donna M. (2018). CTCF Binding Sites in the Herpes Simplex Virus 1 Genome Display Site-Specific CTCF Occupation, Protein Recruitment, and Insulator Function. *Journal of Virology*, *92*(8). https://doi.org/10.1128/jvi.00156-18

Wertheim, Joel O., Smith, Martin D., Smith, Davey M., Scheffler, Konrad, & Pond, Sergei L. Kosakovsky. (2014). Evolutionary Origins of Human Herpes Simplex Viruses 1 and 2. *Molecular Biology and Evolution*, *31*(9), 2356–2364. https://doi.org/10.1093/molbev/msu185

Whitford, Abigail L., & Cliffe, Anna R. (2022). Key questions on the epigenetics of herpes simplex virus latency. *PLoS Pathogens*, *18*(6), e1010587. https://doi.org/10.1371/journal.ppat.1010587

Whitford, Abigail L., Clinton, Corinne A., Kennedy, E. B. Lane, Dochnal, Sara A., Suzich, Jon B., & Cliffe, Anna R. (2022). Ex Vivo Herpes Simplex Virus Reactivation Involves a Dual Leucine Zipper Kinase-Dependent Wave of Lytic Gene Expression That Is Independent of Histone Demethylase Activity and Viral Genome Synthesis. *Journal of Virology*, *96*(12), e00475-22. https://doi.org/10.1128/jvi.00475-22

Wiles, Elizabeth T., & Selker, Eric U. (2017). H3K27 methylation: a promiscuous repressive chromatin mark. *Current Opinion in Genetics & Development*, *43*, 31–37. https://doi.org/10.1016/j.gde.2016.11.001

Zhang, Rugang, Poustovoitov, Maxim V., Ye, Xiaofen, Santos, Hidelita A., Chen, Wei, Daganzo, Sally M., Erzberger, Jan P., Serebriiskii, Ilya G., Canutescu, Adrian A., Dunbrack, Roland L., Pehrson, John R., Berger, James M., Kaufman, Paul D., & Adams, Peter D. (2005). Formation of MacroH2A-Containing Senescence-Associated Heterochromatin Foci and Senescence Driven by ASF1a and HIRA. *Developmental Cell*, *8*(1), 19–30. https://doi.org/10.1016/j.devcel.2004.10.019

Zhou, Bing-Rui, Jiang, Jiansheng, Feng, Hanqiao, Ghirlando, Rodolfo, Xiao, T. Sam, & Bai, Yawen. (2015). Structural Mechanisms of Nucleosome Recognition by Linker Histones. *Molecular Cell*, *59*(4), 628–638. https://doi.org/10.1016/j.molcel.2015.06.025

Zwaagstra, John, Ghiasi, Homayon, Nesburn, Anthony B., & Wechsler, Steven L. (1989). In vitro Promoter Activity Associated with the Latency-associated Transcript Gene of Herpes Simplex Virus Type 1. *Journal of General Virology*, *70*(8), 2163–2169. https://doi.org/10.1099/0022-1317-70-8-2163